2008

Effect of Adding a Regenerator to Kornhauser's MIT "Two-Space" Test Rig

Praveen Gidugu
Cleveland State University

EFFECT OF ADDING A REGENERATOR TO KORNHAUSER'S MIT "TWO-SPACE" TEST RIG

PRAVEEN GIDUGU

Bachelor of Mechanical Engineering

Andhra University

May 2005.

Submitted in partial fulfillment of requirements for the degree

MASTER OF SCIENCE IN MECHANICAL ENGINEERING

at the

CLEVELAND STATE UNIVERSITY

May 2008

This thesis has been approved

for the Department of **MECHANICAL ENGINEERING**

and the College of Graduate Studies by

Thesis Committee Chairperson, Dr. Asuquo Ebiana

Department/Date

Thesis Committee Co-Chairperson, Dr. Roy Tew

Department/Date

Dr. Rama Gorla

Department/Date

Dr. Majid Rashidi

Department/Date

ACKNOWLEDGEMENT

My first and foremost words of appreciation go to my esteemed academic advisor, Dr. Asuquo Ebiana. I have continuously benefited from his outstanding expertise and enormous source of knowledge in both theoretical and practical matters for the past two and half years. I am truly privileged to be blessed with such a rare opportunity, to observe and hopefully learn his unique approach to analyzing problems, entertaining and structuring new ideas, developing viable solutions and putting them to practice. I would like to thank him for all his guidance in my study.

I am highly honored, to have Dr. Roy.C.Tew in my thesis committee, I would like to express my sincere gratitude to him for his guidance, financial support through research grants and also thank him for taking time and patiently reviewing my thesis and giving valuable suggestions.

I also would like to thank my other thesis committee members, Dr. Rama Gorla and Dr. Majid Rashidi for reviewing my thesis, providing me with valuable suggestions and also for taking time to attend my thesis presentation.

I thank my department of Mechanical Engineering, Cleveland State University for giving me the opportunity to pursue my Master's in Mechanical Engineering. I thank Dr. Paul.P.Lin ex-chairman of our department and also Dr. William Atherton chairman for their financial support through department. I also thank Ms. Angie Langford,

Mechanical Engineering, department secretary, for her warm and friendly cooperation. I also thank my senior Mr. Rupesh.T.Savadekar for his help during my program of study.

I would like to thank my parents, my sister for their support and encouragement in every phase of my life. I also would like to thank all my friends for their good wishes in pursuing my degree.

EFFECT OF ADDING A REGENERATOR TO KORNHAUSER'S MIT "TWO-SPACE" TEST RIG

PRAVEEN GIDUGU

ABSTRACT

A "3-space" solution domain (gas spring + heat exchanger + regenerator) is adapted from the "2-space" solution domain (gas spring + heat exchanger) in Kornhauser's MIT test rig [25] by modifying the heat exchanger space to include a porous regenerator system. A thermal non-equilibrium porous-media model is employed for the regenerator. Extensive numerical simulations of the fluid flow and heat transfer phenomena under conditions of oscillating pressure and oscillating fluid flow inside the "3-space" solution domain were performed using 1-D Sage and 2-D Fluent numerical codes. "3-space" results of temperature, pressure and surface heat transfer variations, pressure-volume diagrams, energy conservation and thermodynamic losses are compared with "2-space" results in order to observe the effect of the regenerator and with results obtained from the literature. An important and primary objective of this study is the development of an entropy-based thermodynamic loss post-processor to characterize the major thermodynamic losses inside the "3-space" model. It is anticipated that the experience gained from this can be extrapolated to more complex systems like the Stirling engine with a view towards improving the optimization capability of Stirling engine analysis codes through better understanding of the heat transfer and power losses. It is also anticipated that the incorporation of a successful thermal non-equilibrium model of the regenerator in Stirling engine analysis codes, will improve our ability to accurately model Stirling regenerators relative to current thermal-equilibrium porous-media model.

TABLE OF CONTENTS

LIST OF TABLES

Page

LIST OF FIGURES

NOMENCLATURE

Latin letters

A	Amplitude, Control surface
AE	Available energy
AEfric	AE(due to friction)
AEQ_w	AE(due to surface heat flow)
AEQ_x	AE(axial heat flow)
AEDiscr	Discrepancy (AE_{int} vs. AE_{ext})
c	Specific heat
c_1,c_2	Constants
D/Dt	Total derivative
h	Enthalpy
$\tilde{I}$	Identity vector
k	Thermal conductivity
N_k	Axial conductivity enhancement
n_α	Unit normal vector
p	Pressure
Pr	Prandtl number
$\vec{q}$	Heat flux vector
r_v	Volume ratio
S	Piston stroke
s	Mass specific entropy
s'''	Volumetric entropy gen. rate

T	Temperature
#tspc	Number of time steps per cycle
t	Time
Δt	Time step
u	Internal energy
$\hat{u}$	Specific internal energy
$\vec{u}$	Velocity vector
V	Volume, Averaging volume
H	Convective heat transfer coeff
v	Mass specific volume
$\wedge$	Spatial deviation quantity
$\langle\ \rangle$	Volume average quantity
W	Work
x	Position vector
x,y,z	Cartesian coordinates

Greek letters

α_v	Surface area per unit volume
ε	Volume fraction or porosity
∇	Gradient
μ	Viscous coefficient
Φ	Dissipation function
$\Phi_{i,,}\ \overline{\Phi}$	Instantaneous, mean data values (temperature or pressure)
φ	Phase angle
ρ	Density

θ	Crank angle
$\vec{\Omega}$	Vorticity vector

Subscripts

α	Fluid phase
β	Solid phase
cond	Conductive
e	Exit
ext	Extenal
gen	Generation
i	Inlet; Index; Instantaneous, Irreversible
int	Internal
k	Conductivity
L	Low
o	Outflow
p	Pressure
r	Region, Reversible
sys	system
th	Thermal
v	Volume
visc	Viscous
m,n	Positive constants

Abbreviations

BDC	Bottom Dead Center
CFD	Computational Fluid Dynamics

CAD	Computer Aided Design
CAE	Computer Aided Engineering.
COP	Coefficient of Performance
DTF	Database Template File
GRC	Glenn Research Center
MIT	Mass. Institute of Technology
NASA	National Aeronautics & Space Administration.
n-D	(n = 1,2,3) Dimension
RMS	Root Mean Square
SRG	Stirling Radioisotope Generator
TDC	Top Dead Center
TFE	Teflon

CHAPTER I

BACKGROUND

1.1 Introduction

Under the auspices of NASA's Nuclear Power Radioisotope System Development program, multiple efforts are currently underway, both in-house at NASA GRC and under various grants and contracts, to develop a high-efficiency Stirling Radioisotope Generator (SRG) for possible use on future NASA Space Science Missions. The SRG is being developed for multi-mission use including providing electric power for unmanned Mars rovers and deep space missions in environments with and without atmospheres. One of the multiple efforts underway includes the development of a multi-dimensional Stirling computational fluid dynamics code, including second law analysis post-processing to separate various thermodynamic losses [44,42] in Stirling engines. The work documented in this thesis is sponsored by NASA grant NNC05AA24A and supports the second law loss analysis effort.

Stirling engines, like other heat engines, convert heat to useful work. This conversion process is inherently irreversible due to the non-ideal nature of power systems. Internal

system irreversibilities resulting from viscous friction, heat transfer and non-equilibrium processes destroy part of the available work of a system resulting in thermodynamic losses which impact engine thermodynamic performance adversely. In order to improve the engine thermodynamic performance, it is necessary to identify and minimize the features guilty of the available energy loss within the system. Thermo-fluid system loss analysis and management is clearly an area of study that is generating a great deal of interest.

Optimal engine performance requires good heat transfer to and from the working fluid and maximum conversion of the input heat to useful work by reducing thermodynamic losses as mentioned above. Since engine geometry changes that reduce viscous losses often decrease heat transfer (thereby increasing heat transfer thermodynamic losses)—it is valuable for the designer to know the details of the trade-off between viscous-flow and heat-transfer thermodynamic losses. Until recently the heat transfer estimates used in reciprocating heat engines have been based on extrapolation of expressions that were developed for steady-pressure, steady-flow conditions. Because the ordinary, steady-state convective model contains no term to account for the oscillatory effect in variable volumes, designs of these equipment are nowhere near optimum. Using two Massachusetts Institute of Technology (MIT) test rigs (gas spring and gas spring+heat exchanger) Kornhauser [25] confirmed experimentally that there was a fundamental difference between steady and oscillatory flow heat transfer in the variable cylinder volumes of the MIT test rigs. Building on the work done by Lee, Smith, Faulkner, and Chafe, [27,16,9], Kornhauser started the development of expressions suitable for oscillating pressure and oscillating flow conditions. He closely integrated

experiment with analysis to achieve useful results with good qualitative but limited quantitative success.

In this study, entropy-based second law post-processing analysis is employed to characterize the various thermodynamic losses inside a "3-space" solution domain (gas spring + heat exchanger + regenerator) operating under conditions of oscillating pressure and oscillating flow. The "3-space" solution domain was adapted from the "2-space" solution domain (gas spring+heat exchanger) in Kornhauser's test rig [25] by modifying the heat exchanger space to include a porous regenerator system. A thermal non-equilibrium model which assumes that the regenerator porous matrix and gas average temperatures can differ by several degrees at a given axial location and time during the cycle is employed. A survey of the porous-media literature supports the need for thermal non-equilibrium porous-media models for Stirling regenerators [7, 2-38].

A valuable tool in the design of a high performance engine is a numerical code with multi-dimensional modeling capability and an ability to closely simulate the thermal-fluid processes inside the engine and account for all the thermodynamic losses. This study utilized a 1-D Sage and 2-D Fluent commercial numerical codes to model, analyze and post-process the thermal-fluid phenomena inside the "3-space" domain.

Fluent is a computational fluid dynamics (CFD) software package with comprehensive and flexible physical modeling and multi-physics capabilities for simulating fluid flow and heat transfer problems. The Fluent package includes the solver (FLUENT), the preprocessor (GAMBIT) for geometry modeling and mesh generation, and an additional preprocessor (TGrid,) that can generate volume meshes from existing boundary meshes and filters (translators) for import of surface and volume meshes from a

variety of CAD/CAE packages. All functions (specifying problem type and numerical technique, setting boundary and initial conditions, defining fluid properties, etc.) required to compute a solution and display the results are accessible in FLUENT through an interactive, menu-driven interface.

Sage is a 1D, multi-variable thermodynamic modeling package that supports simulation and optimization of spring-mass-damper resonant systems and Stirling-cycle coolers and engines. In the Sage code, an engineering system is built up from component parts obtained from component palettes. The components function as a whole by virtue of their connections which could be due to gas flow, heat flow, pressure, density, etc. Sage calculations are performed via its solver and optimizer routines.

1.2 Motivation and Objectives

This study supports the efforts underway in the Stirling research community to develop a high efficiency Stirling engine for use on future NASA space missions. There are two major design objectives for space-power applications of reciprocating heat engines like the Stirling engine: (1) To maximize performance by minimizing thermodynamic losses due to viscous flow, heat transfer and non-equilibrium processes — in order to minimize fuel requirements (expensive radioisotopes for example), and (2) To minimize system mass — in order to minimize propulsion fuel requirements.

An important and primary objective of this study is the development and application of a thermodynamic loss post-processor to characterize the major thermodynamic losses inside the “3-space” model. It is anticipated that the experience gained from thermodynamic loss analysis of the simple “3-space” model will be extrapolated to more complex systems like the Stirling engine. It is hoped that a

successful development of the loss post-processors will facilitate the improvement of the optimization capability of Stirling engine analysis codes through better understanding of the heat transfer and power losses [42]. It is also anticipated that a thermal non-equilibrium model of the regenerator such as that presented here, when incorporated in Stirling engine analysis codes, will improve our ability to accurately model Stirling regenerators relative to current thermal-equilibrium porous-media models.

1.3 Literature Survey

Typically neglected and often viewed as superfluous, the second law of thermodynamics remains an esoteric and mysterious subject [20] particularly in computational analysis of thermo-fluid systems. The methods of exergy analysis, entropy generation minimization and thermo-economics are the most established analysis that have taken place during the past three decades [6-7]. Entropy generation destroys the part of available work of a system and is associated with thermodynamic irreversibilities related to pressure drop, finite heat transfer, friction, mixing, leakages, and other nonidealities within systems. Second law analyses focusing on entropy generation and its minimization has been playing a dominant role in recent times to understand the irreversibility in applied engineering and transport processes [12]. Past studies have described various analytical and empirical techniques for entropy-based optimization of engineering systems. Bejan [3,5,7] has focused on the different mechanisms behind entropy generation in applied thermal engineering. Numerous other investigations (mostly numerical) have been performed to determine the entropy generation and irreversibility profiles for different geometric configurations, flow situations, and thermal boundary conditions [31,32,36].

1.4 Chapter Organization

Chapter 1 has provided the background information on the research problem, the motivation for the research and a brief literature survey of related previous investigations. The plan of the rest of the thesis is as follows: Chapter 2 presents a brief description of the Stirling engine structure and operation in order to provide a clear context for the study. Chapter 3 presents a description of the 1-D and 2-D computer modeling techniques for the "3-space" solution domain using the Sage and Fluent numerical codes respectively. In Chapter 4, the effects of incorporating a regenerator in Kornhauser's "2-space" solution domain are explored via parametric studies using Sage. Chapter 5 presents a discussion of the numerical simulation techniques and results of the simulation of the thermal-fluid processes (temperature, velocity and pressure variations, surface heat transfer, etc.). In Chapter 6 the governing conservation equations are united with the 2nd Law of thermodynamics to derive a complete set of entropy generation equations appropriate for 2-D thermodynamic loss modeling. Using the loss models derived in Chapter 4, the numerical simulation results are post-processed for the thermodynamic losses in the "3-space" model and the results are presented in Chapter 6. Conclusions and recommendations for future studies are presented in Chapters 7.

CHAPTER II

OVERVIEW OF THE STIRLING ENGINE

In order to fully understand the fundamental objective of this research effort, it is necessary to provide an overview of the Stirling engine. The Stirling Technology Demonstration Convertor (TDC) (shown in Figure 1) is a 55-watt space power Stirling engine prototype developed by Infinia Corporation (formerly, STC or Stirling technology corp.). It is essentially a free piston machine that generates electric power from a thermal energy input. The convertor is of the gamma type, gas-coupled, and single-acting. It can be divided into two basic subsystems – electro-mechanical and thermo-fluid.

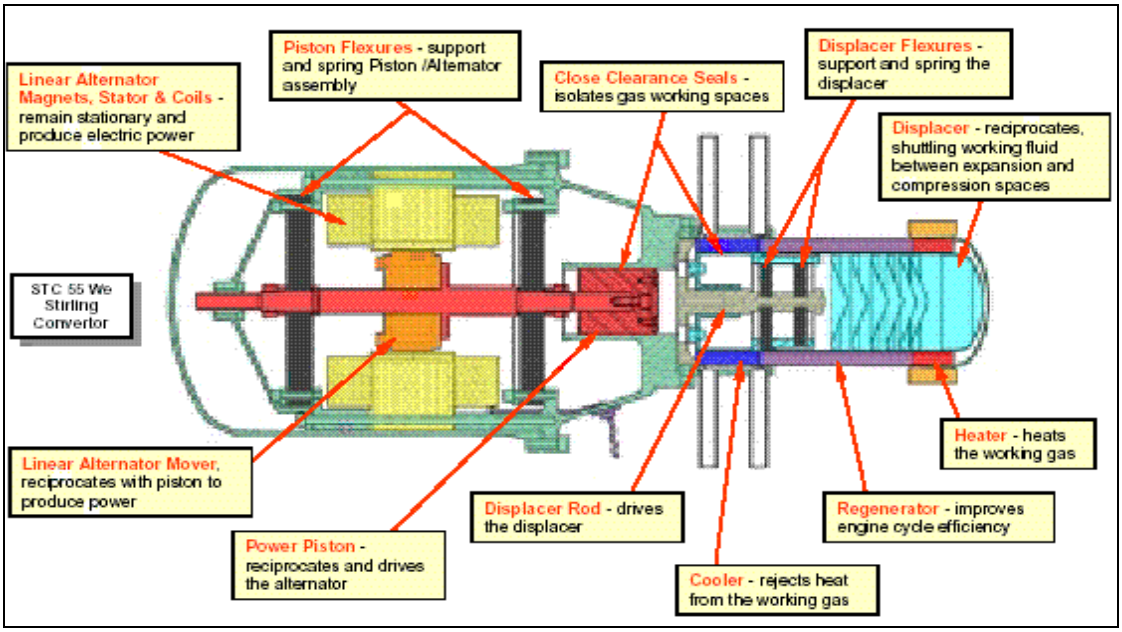

Figure 1. Schematic of STC's Stirling Convertor [Courtesy: www.nasa.gov].

2.1 The electro-mechanical subsystem

The electro-mechanical subsystem consists of a pressure vessel containing a flexurally supported power piston/linear alternator assembly. The power piston separates the thermodynamic working space in the thermo-fluid subsystem to the right of the piston from the "bounce" space, a weak but measurable gas spring between the piston and the casing. The pressure developed by the thermodynamic cycle created in the thermo-fluid subsystem acts on the top and under sides of the piston and drives the piston, alternately compressing and expanding the gas. The piston oscillations produced by the expanding and compressing gas drives the power piston through the alternator's magnetic field to produce electric power.

2.2 The thermo-fluid subsystem

The thermo-fluid subsystem can be considered to have two distinct fluid circuits (internal and external) for most applications.

The Internal Circuit

The internal engine thermodynamic circuit is filled with working fluid at an elevated pressure and is comprised of a flexurally supported displacer/rod assembly, two variable compression and expansion volumes and three heat exchangers in series: the heater, the regenerator and the cooler.

The working fluid

Unlike internal combustion engines, Stirling engines are adaptable to different working fluids (usually a gas: air, helium or hydrogen). The working fluid (helium is used for this study) does not change phase, is retained in the working parts of the engine rather than being ejected and replaced during each cycle and is subjected to a wide range of pressures in the variable compression space formed by the action of both the power piston and the displacer and the variable expansion space formed by the action of the displacer (and in the non-swept, or "dead", volume in the working space). By suitable choice of the working fluid, desirable factors such as heat transfer capability can be maximized while efficiency-robbing process such flow losses can be minimized. Hydrogen and helium combine low density and viscosity with good heat transfer properties. Hydrogen is superior for maximizing power to weight ratio (specific power). Helium can be used with a small penalty in efficiency or specific power output [28]. Air is used where low cost and ease of maintenance are the major design goals, and increased engine volume and mass are not major concerns.

The displacer/rod assembly

The displacer is hollow and contains working space gas (with a tiny communication channel to the working space to maintain the cyclic-mean working space pressure level)

and baffles or “radiation shields” to reduce thermal convection and radiation. Since the two variable volumes are coupled through the three heat exchangers in series, there is a substantial temperature difference across the displacer length. Its walls are relatively thin and long in order to reduce the thermal conduction losses along the walls. The displacer rod provides slightly different areas on the two ends of the displacer and therefore produces enough work to overcome pressure drop losses.

Variable expansion and compression volumes

Two variable working spaces can be identified inside the thermo-fluid subsystem, the cold compression space formed by the action of both the power piston and the displacer and the hot expansion space formed by the action of the displacer. Forming moving boundaries for the compression and expansion spaces, the power piston and displacer act to compress and expand the working fluid (power piston) and to displacer/ transfer the fluid between the variable space (displacer). The piston motion lags the displacer motion [21]. The two variable volumes are coupled through three heat exchangers in series: the cooler, the regenerator and the heater.

The heat exchangers

The cooler, in contact with a heat sink, extracts excess heat from the compression space providing a cold-sink temperature of ~80^{o}C. The heater head channels the thermal energy from an external heat source (see external circuit below) into the heater and the expansion space and heats the working fluid to a temperature of about 650^{o}C. The heater and cooler thus provide the hot and cold-sink temperatures for the engine. The regenerator is a duct packed with some large scale porous matrix (solid containing

interconnected pores that can transmit the flow of fluids). It is often made by stacking together a number of fine wire mesh screens, random fibers (for the TDC), foam metal plugs, perforated disks or felts to form a kind of metallic heat sponge. The inclusion of an effective regenerator results in a substantial increase in Stirling engine efficiency and is necessary for the stirling engine to be of practical use.

The external circuit

The external circuit (not shown in Figure 1) provides the thermal energy load which could come from just about any thermal energy source, which is available at a sufficiently high temperature. Stirling engines have been run on concentrated solar energy, thermal energy storage batteries, metal combustion, isotope nuclear energy, as well as a variety of liquid and solid fuels (oil, coal, gas, etc.). The TDC's heat source is an electric heater. Radioisotopes are the planned heat source for space applications. Cooling is achieved via a water circuit in the TDC, but will be achieved by solid conduction to a radiator for space power applications.

2.3 Clearance seals/Convertor material

Clearance seals used for the power piston and displacer isolate the gas working spaces. The radially-stiff flexures make tight clearance seals possible. The convertor uses hot-end materials capable of operating at the hot-end temperature over the planned life of the machine.

2.4 Stirling TDC Operation

The TDC receives thermal load via the heater head from an external heat source (radioisotopes are the planned heat source for space application) and operates in a closed

regenerative thermodynamic cycle created in the thermo-fluid subsystem. During each working cycle, the power piston and the displacer reciprocate in a coordinated almost sinusoidal fashion (with the power piston motion lagging the displacer motion [21]), shuttling the gas at different temperature levels through the heat exchangers between the expansion and compression spaces. Pressures acting on each end of the displacer are only slightly different, relative to the mean pressure level. On the other hand, the relatively large "bounce" space to the left of the power piston (see Figure 1), compared to the working space volume (compression space), ensures that the pressure excursions in the bounce space will be substantially less than inside the engine working spaces. Therefore the power piston extracts net power from the working space gas due to the larger pressure excursions on that side. The power piston's attached alternator parts oscillate within the alternator's magnetic field to produce electric power. The oscillating gas pressures within the working spaces, the spring-mass-damper systems of the piston & displacer, and the oscillating load on the piston produced by interaction with the alternator, all interact to produce sustained oscillating motion of the piston and displacer—when engine geometries, piston and displacer masses and heat sources and sinks are appropriately chosen.

The regenerator action

The action of the Stirling engine regenerator is most easily understood by first imagining the gas behavior without a regenerator. In the absence of the regenerator, hot gas would be transferred by the action of the displacer directly from the expansion space/heater into the cooler/compression space, where it would have to be cooled. The heat extracted during the cooling would be rejected and lost. When the gas is

subsequently returned to the expansion space, it would have to be reheated drawing more heat from the heat source. Extra heat would therefore be added and rejected during the cycle, with a consequence of loss of efficiency.

The regenerator experiences a large axial temperature gradient. As the gas passes from the hot end to the cold end, the gas gets cooled gradually by giving up the heat to the regenerator solid matrix and therefore gas leaves the regenerator already cooled, minimizing the heat to be rejected in the cold space. On the return journey, the gas is gradually heated up as it moves up the temperature gradient towards the expansion space, by picking up heat from the solid matrix that was deposited during the previous cycle. Thus the gas emerges into the heater with considerable heat already added, minimizing the heat to be added by the external source [31]. The regenerator thus serves as an economizer for storing heat during one part of the engine cycle and for re-use during another part.

Extensive efforts have been focused on improvement in regenerator technology. These efforts have been categorized into areas of materials and geometry, numerical modeling, and experimental measurement [22,30,37,41]. A NASA regenerator research grant effort led by Cleveland State University, with subcontractor assistance from the University of Minnesota, Gedeon Associates, and Sunpower Inc. has been providing computational and experimental results to support definition of various empirical parameters and "closure" relations needed in defining a thermal, non-equilibrium, macroscopic, porous-media model for use in multi-D Stirling codes for regenerator simulation [43].

CHAPTER III

"THREE-SPACE" SOLUTION DOMAIN
(Kornhauser's MIT "2-space" Solution Domain Modified).

A description of Kornhauser's MIT "2-space" Test Rig is first presented below in order to provide the proper context for the "3-space" solution domain used in this study.

3.1 Kornhauser's MIT "2-space" Test Rig

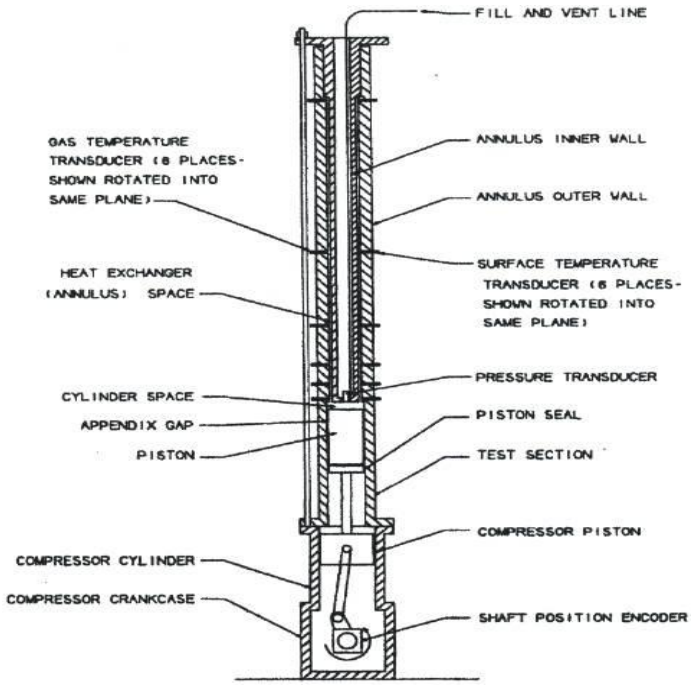

Figure 2. Kornhau ser's MIT Cylinder + HXer Test Rig.

Table 1. Gas Spring + Heat Exchanger Dimensions[3]

Cylinder Bore (Diameter)	50.80 mm (2.0 in)
Piston Stroke	76.2 mm (3.0 in)
Volume Ratio	2.0
Annulus Outside Diameter	44.5 mm (1.75 in)
Annulus Inside Diameter	39.4 mm (1.55 in)
Annulus Wall-to-Wall Distance	2.5 mm (0.10 in)
Annulus Length	445 mm (17.5 in)
Min. Cyl.-Head to Piston Clearance	2.9 mm (0.11 in)

Figure 2 shows a schematic representation of Kornhauser's piston-cylinder-heat exchanger test rig. A piston-cylinder device is mounted on a compressor base. The compressor piston drives the piston in the 50.8 mm (2.00 in.) diameter cylinder. The piston is sealed to the cylinder with a buna-n O-ring located more than a stroke's length from the piston face so that frictional heating of the cylinder wall would only affect results minimally. The piston top surface is brass, while the cylinder wall and head are made of steel. The fixed cylinder head has an annular opening leading into an annular dead-ended heat exchanger space such that flow can continuously pass between the heat exchanger and cylinder as the cylinder piston expands and compresses the gas spring (the volume of gas confined by the fixed cylinder and the moving piston) more like in a Stirling machine cylinder. The test section consists of the gas spring + heat exchanger space. A piston stroke length of 76.2 mm (3.00 in.) and volume ratio of 2.0 are used in this study. A volume ratio is defined to be the maximum cylinder volume (piston at "bottom-dead-center" (BDC)) over the minimum cylinder volume (piston at "top-dead-center" (TDC)).

The heat exchanger annulus is 44.5 mm (1.75 in) outside diameter and 39.4 mm (1.55 in) inside diameter, for a wall-to-wall distance of 2.5 mm (0.10 in). The annulus is 445 mm (17.5 in) long, so that a volume ratio of 2.0 for the combined cylinder and heat exchanger resulted in a very small cylinder clearance volume; the cylinder-head distance is nominally 2.9 mm (0.11 in) at top center position. The heat exchanger entrance has the same cross-sectional dimensions as the heat exchanger itself, the entrance corners being as sharp as could easily be machined. The inner wall of the heat exchanger space is made of steel. The outer wall of the heat exchanger space is steel lined with a 1.98 mm (0.078

in) layer of bronze-filled TFE (Teflon). This lining was chosen for thermal properties matching those of the Pyrex glass substrate of the surface temperature transducers. Because of the extended heat transfer surface in the annular heat exchanger, the energy flows are more complicated than in a simple gas spring.

The apparatus is belt driven by a D.C. motor to allow speed adjustment. The apparatus fill line is a capillary tube of negligible volume. The gas spring + heat exchanger dimensions are tabulated in Table 1.

The "3-space" solution domain (gas spring + heat exchanger + regenerator) will be adapted from the "2-space" solution domain (gas spring+heat exchanger) in Kornhauser's "2-space" test rig (Figure 2) by modifying the heat exchanger space to include a porous regenerator matrix. The flow dynamics in the "3-space" solution domain is expected to mimic the flow dynamics in the Stirling engine thermo-fluid subsystem. 1-D Sage and 2-D Fluent commercial numerical codes are used to model, analyze and post-process the thermal-fluid phenomena inside the "3-space" domain. The modeling procedures using Sage and Fluent are presented in Sections 3.2 and 3.3 below. Note that in Figures 3 (Sage model) and 4 (Fluent model), the regenerator is shown located at the heat exchanger end opposite from the end adjacent to the cylinder. The justification for this is discussed in Chapter 4. Note also that this "3-space" device is different from the usual Stirling engine/cooler, which contains a two-variable volume on each side of the cooler-regenerator-heater heat-exchanger circuit.

3.2 Sage "3-space" Model (1-D)

Figure 3 is a representation of the Sage graphical interface illustrating the 1-D model of the "3-space" solution domain.

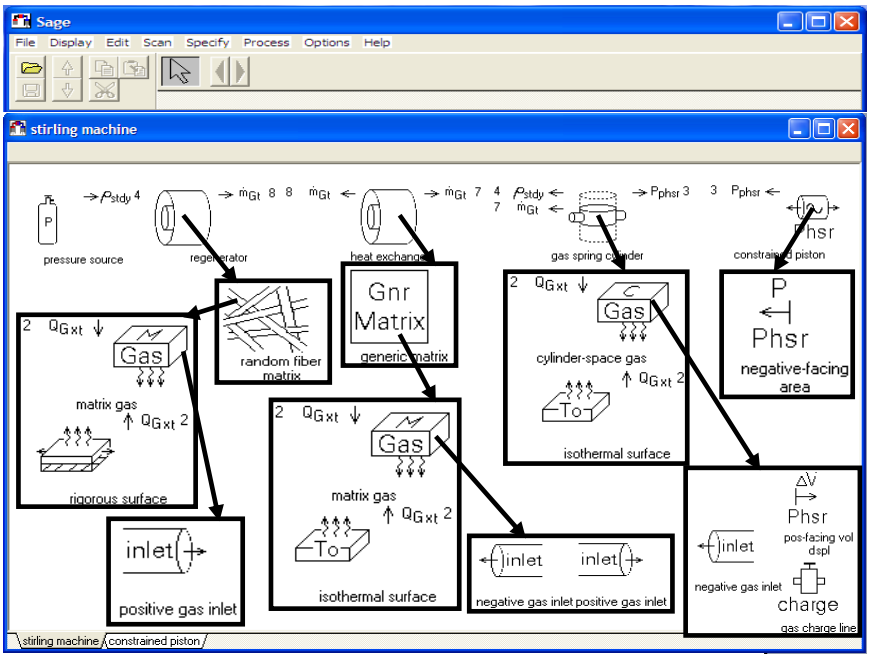

Figure 3. Sage Model of the "3-space" Solution Domain.

Sage provides 8 menus – File, Display, Edit, Scan, Specify, Process, Options, and Help – each with self-explanatory commands and graphical edit windows with model-component palettes. When "show window" in the edit menu is activated, the highest level graphical edit window (Stirling machine window) and its model-component palette appear. Each model-component palette contains buttons arranged in tab-selected pages corresponding to different categories of model components. Figure 3 shows the Stirling machine window with six Stirling engine model component palettes - "Basic", "Canisters", "Heat Exchanger", "Phasr Moving Parts", "Gt Moving Parts" and "Composite". A Sage model is a collection of component parts assembled in a graphical edit window by clicking and dragging the components into the window and connected in a particular way to form a complete system. Model components are organized in a hierarchical structure. The root model component contains a number of sub-components

which may themselves contain sub-sub-components. Child (sub) models are accessed by double-clicking on parent models. The labeled arrows sticking out of the sides of components are boundary connectors. They are joined together as matched pairs with numbers (2, 3, 4, etc.) identifying the match. The labels are meant to suggest what information is transferred across the connection between components. Sage is also able to perform such functions as open and save files, increase/decrease connector level, copy, cut and paste components.

The "3-space" solution domain (gas spring + heat exchanger + regenerator) is modeled using Sage's Stirling machine model component palettes. The variable volume cylinder space in Fig. 3 and the charge pressure inside it are modeled in the Sage code using a generic cylinder (renamed "gas spring cylinder" in Fig. 3) and a pressure source both obtained from the "Basic" component palette in the Stirling machine level. The pressure source comes with a built in steady state density connection (ρ_{stdy}) and acts as an isobaric gas reservoir in that the density in the gas domain adapts itself so that the time average pressure is continuous across the connection. The cylinder-space gas and isothermal surface, child models of the gas spring cylinder, are obtained from the "Gas Domain" and "Cylinder Walls" component palettes respectively in the gas spring cylinder level. The arrows labeled 2 in the gas spring edit window indicate a space-time varying heat flow connection Q_{Gxt} between the z-face of the cylinder-space gas and the isothermal surface. The positive-facing volume displacement phasor and gas charge line, both child models of the cylinder-space gas, are moved up to the Stirling machine level for pressure connections (P_{phsr}) to the constrained piston (label 3) and density connections (ρ_{stdy}) to the pressure source (label 4) respectively. The positive-facing volume

displacement phasor represents the volume change of the gas space due to the motion of the piston. The negative gas inlet, also a child model for the cylinder-space gas, is obtained from the “Charge/Inlet” component palette in the cylinder-space gas level and represents the gas flowing from the gas spring cylinder into the annular canister (heat exchanger). The mass flow connection arrow is moved up to the Stirling machine level for connection there to the annular canister (label 7).

The piston in Fig. 3 is modeled using the constrained piston obtained from the “Phsr Moving Parts” component palette in the Stirling machine level. Its child model, the negative facing-area phasor, is obtained from the “Mechanical Attachment” component palette in the constrained piston level. Its pressure connection arrow is moved up to the Stirling machine level for connection there to the gas spring cylinder (label 3).

The annular canister in Figure 3 is used to model the heat exchanger and the regenerator. It is obtained from the “Canisters” component palette in the Stirling machine level. The generic matrix, child model of the heat exchanger, represents the internal structure of the heat exchanger. It is obtained from the “Matrices” component palette in the annular canister level. The matrix gas and isothermal surface, child models of the generic matrix, are obtained from the “Gas Domain” and “Matrix Solids” component palettes respectively in the generic matrix level. The arrows labeled 2 in the generic matrix edit form indicate a heat flow connection between the matrix gas and the isothermal surface. The negative and positive gas inlets, child models of the matrix gas, model the gas flowing from the heat exchanger into the regenerator and gas spring cylinder. They are obtained from the “Charge/Inlet” component palette in the matrix gas level. The mass flow connection arrows from the negative (label 8) and positive gas

(label 7) inlets are moved up to the Stirling machine level for connection there to the gas spring cylinder (label 7) and regenerator (label 8). The regenerator is modeled in a similar manner as for the heat exchanger except for the requirement of a rigorous surface child model for the surface condition of the random fiber matrix representing the internal structure of the regenerator. The positive gas inlet, child model of the matrix gas, models the gas flowing from the regenerator into the heat exchanger (label 8). We see from Figure 3 and the foregoing descriptions that the "3-space" model components communicate with each other using density (ρ_{stdy}), mass flow ($\dot{m}_{Gt}$), heat flow (Q_{Gxt}) and pressure (P_{phsr}) boundary connections.

Once a model structure is created in Sage, numerical inputs for the model component are either specified or modified. Sometimes user-defined variables (special output variables) can be added to model components. Sage numerical simulation is initiated after initializing component and overall model parameters. Sage calculations are performed via its solver and optimizer routines.

3.3 Fluent "3-space" Model (2-D)

The optimum linear dimension of the regenerator was determined via a systematic parametric analysis using the Sage code.

The Fluent code exploits the symmetry of the problem domain to model only one-half of the domain (see Figure 4 below). The physical domain of interest is represented within GAMBIT using fundamental geometric entities (points, lines, curves, and surfaces) which can be manipulated (translated, rotated, projected, split, joined, etc.) as desired.

Grid generation, the process of discretizing the problem domain with individual cells over which the flow equations are integrated, follows the geometric representation of the

domain of interest. The locations of the corner points of these cells constitute the "grid" or "mesh" which is stored in a data base. Three grid distribution types are available: Power Law, Hyperbolic Tangent and Geometric. The power law grid distribution type is used to obtain a finer grid at the boundaries for more accurate resolution of the flow features. Structured and unstructured grids and different grid sizes can be generated. Different grid sizes (e.g., 100x20, 125x30, 147x46, 150X53, 160X70) were generated for parameter optimization study. The baseline grid size 100x20 is presented in Figure 4 for illustration.

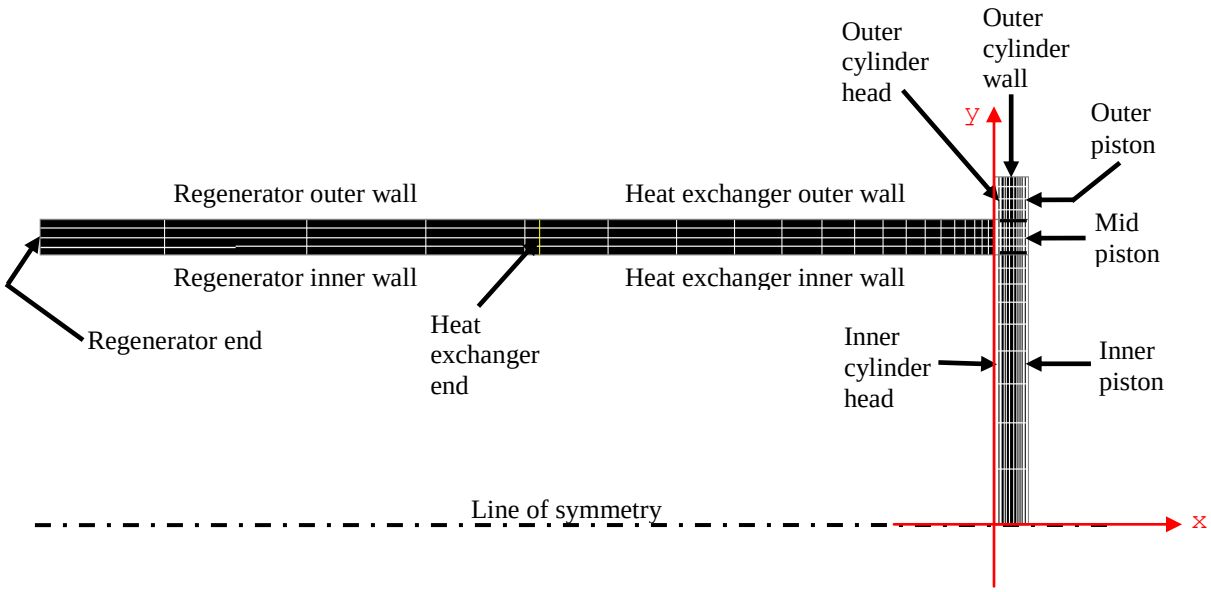

Figure 4. Fluent Model of the "3-space" Solution Domain.

After modeling is completed, the problem is formulated using FLUENT through an interactive, menu-driven interface that allows complete formulation of the problem. Problem formulation involves specifying the problem type, model options, volume conditions, boundary conditions, initial conditions and the numerical technique needed to solve the flow equations.

After problem formulation, simulation is performed using the FLUENT flow solver module. The GUI files created by the FLUENT flow solver are loaded directly into FLUENT, an interactive graphics program with many tools to visualize the flow physics, animate transient data sets, as well as to extract data for post processing the numerical results. Tools such as point, line, rake and surface are used to obtain the data of required parameters.

CHAPTER IV

REGENERATOR EFFECT ON SAGE "2-SPACE" TO "3-SPACE" MODELING

The results of a prior study [13] of a Sage model of the MIT "2-space" solution domain (Figure 4(a)) indicated a cylinder-cooling effect, with heat being drawn from the environment through the cylinder walls into the cylinder volume and pumped from the heat exchanger gas volume through the heat exchanger cylinder walls into the environment. Since the "3-space" solution domain used in this study was adapted from the MIT "2-space" solution domain by modifying the heat exchanger space to include a porous regenerator system, it was decided to investigate the impact of the regenerator on the cylinder-cooling effect using the Sage code. Table I summarizes the results of the investigation.

The second row of Table 1 shows results obtained using a Sage model of the original MIT "2-space" solution domain. This model assumed isothermal wall temperatures of 294 K for both the heat exchanger and the cylinder. Since the purpose of a "real cooler" is to reduce the temperature of the cooled area relative to the environment, the temperature of the cylinder walls was reduced (with everything else remaining the same) over a range of temperatures below 294 K, in order to obtain a temperature below which

no cooling results. The effects of changing the cylinder wall temperature are shown in Runs 1 thorough 5 (Table 1). Based on these results, the cylinder temperature (289 K) was established in Run 3. Run 3 (now designated Run A) was thus chosen to be the reference "cooler" case for subsequent runs B through H.

Next, in preparation for converting part of the 44.5 cm long heat exchanger into a regenerator, the heat exchanger was first split arbitrarily into two parts (40 cm part and 4.5 cm part) such that of the 16 equilength cells in the 44.5 cm long heat exchanger(44.5/16 = 2.78125), 14 equilength cells are now contained in the 40 cm part (40/14 = 2.85714) and 2 equilength cells in the 4.5 cm part (4.5/2 = 2.25) sectioned out from the end of the heat exchanger opposite the cylinder for use as the regenerator. With no regenerator porous matrix added, Run B was then initiated with ensuing results essentially the same as for Run A. The slight differences may be due to the non identical equilength cells.

The 4.5 cm part of the heat exchanger was next converted into a regenerator resulting essentially in a "3-space" Sage model of the solution domain – cylinder, regenerator and heat exchanger. The regenerator matrix is modeled as either as a generic random-fiber or a "dedicated" random-fiber. The regenerator and heat exchanger walls are kept fixed at 294K. The regenerator position relative to the heat exchanger and cylinder is now varied for best possible location based on cooling performance. With the regenerator between the heat exchanger and the cylinder (Figure 4(b); Runs C and D, Table 1) the cooling effect of the device was completely "wiped out", apparently because the regenerator acted as a "heat dam" to prevent heat from moving from the cylinder to the heat exchanger. Runs C and D differ only in the representations of the 90% porosity

regenerator matrix (generic-matrix-based random-fiber model in Run C, and "dedicated" random-fiber model for Run D).

In Runs E and F (90% porosity generic-matrix-based random fiber model and dedicated 90% porosity random-fiber model, respectively), the regenerator was placed at the end of the heat exchanger away from the cylinder (Figure 4(c)). A significant improvement in cooling performance, relative to the performance of the original "2-space" Sage model (Run A) was noted. The coefficient of performance (COP) improved from ~0.145 to ~ 0.211. It is also observed that the switch from generic matrix based random fiber to "dedicated" random fiber matrix (Run C to Run D and Run E to Run F) has less effect with the regenerator on the heat exchanger end away from the cylinder (Runs E and F) than with the regenerator between the heat exchanger and the cylinder (Runs C and D) — perhaps because "less is going on" at heat exchanger end away from the cylinder.

In Run G, the impact of the 90% porosity matrix at the end of the heat exchanger opposite the cylinder was checked by removing the generic matrix based 90% porosity random fiber matrix. Very similar results to Runs A and B were obtained as anticipated.

In Run H, it was thought necessary to investigate if the improvements shown in Runs E and F – regenerator at end of heat exchanger away from cylinder — were due primarily to the 10% reduction in the volume produced by adding the 90% porosity random fiber. This investigation was done by simply cutting off 4.5 cm of the heat exchanger. Removing this 4.5 cm's "worth of volume" does improve the cooling performance relative to Runs A and B (from COP ~ 0.146 to COP ~ 0.153), but not nearly as much as putting a 90% porosity random fiber matrix in the 4.5 cm. part of the heat exchanger

away from the cylinder (COP ~ 0.146 to COP ~ 0.211). Thus the impact of the regenerator matrix on the cooling performance is significant but it is not presently clear why the addition of the regenerator matrix at this end improves the performance.

Table 2: Summary Results of Regenerator-Effect on Sage "2-Space"/"3-Space" Modeling

Run Description	Regenerator Description	Regen./HXer Wall Temp. (K)	Cylinder Temp.(K)	Total HXer Length (cm)	PV Power (W)	Q thru Cyl. (W)	Q thru HXer (W)	COP = Q_{cyl}/PV Power	Comments
Orig. 2-space Sage model	No Regen.	294	292	44.5	- 29.97	+ 12.69	- 42.66	0.423	Sage model of MIT's 2-space test rig. (Figure 6(a))
Next 5 runs: Reduce Cylinder Temperature									
1	No Regen.	294	292	44.5	- 29.96	+ 9.38	- 39.34	0.313	
2	No Regen.	294	290	44.5	- 29.95	+ 6.05	- 36.00	0.202	
3	No Regen.	294	289	44.5	- 29.94	+ 4.38	- 34.32	0.146	Run A (Reference)
4	No Regen.	294	284	44.5	- 29.92	- 4.10	- 25.82	No cooling	
5	No Regen.	294	274	44.5	- 29.85	- 21.57	- 8.28	No cooling	
Rest of runs involve splitting-off part of heat exchanger - to serve as regenerator, or not									
Run A = Run 3	No Regen.	294	289	44.5	- 29.94	+ 4.38	- 34.32	0.146	Serves as a reference case for runs B through H
Run B	No Regen.	294	289	44.5	- 29.93	+ 4.30	- 34.24	0.144	Essentially same result as Run A. Slight difference may be due to different equilength cell distribs.
Run C	4.5cm. Generic-matrix-based random fiber model (90% porosity).Regenerator placed between HXer and Cylinder.	294	289	40.0	- 34.25	- 34.92	+ 0.67	No cooling	Regenerator acts like a "heat dam". Most of heat goes out through the cylinder wall (Fig. 6(b))
Run D	4.5cm. "Dedicated" 90% porosity random-fiber model. Regenerator placed between HXer and Cyl.	294	289	40.0	- 39.29	- 40.06	+ 0.775	No cooling	Almost same results as for Run C. Slight differences due to differences in random fiber matrix model (Fig. 6(b)).
Run E	4.5cm. Generic-matrix-based random fiber model (90% porosity).Regen. placed at end of HXer away from Cyl.	294	289	40.0	- 25.88	5.44	- 31.32	0.210	The switch from generic to dedicated random fiber matrix has less effect with the regenerator at end of HXer away from the cylinder than with regenerator between HXer and cylinder (Fig. 6(c)).
Run F	4.5cm."Dedicated"90% porosity random-fiber model. Regenerator placed at end of HXer away from Cylinder.	294	289	40.0	- 25.83	5.44	- 31.27	0.211	Dramatic improvement in cooling performance – significant when compared to Runs A and B (Fig. 6(c)).
Run G	No Regen. 4.5cm. section of HXer is now between HXer and Cyl.	294	289	44.5	- 29.92	4.30	- 34.33	0.147	Results very similar to Runs A and B.
Run H	No Regenerator	294	289	40.0	- 33.13	5.07	-38.20	0.153	Removing this 4.5 cm's "worth of volume" does improve cooling performance relative to Runs A and B, but not nearly as much as for 90% porosity random fiber matrix in the 4.5 cm.

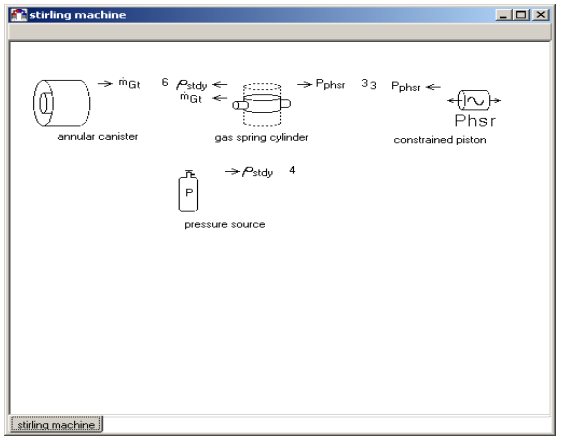

Figure 5(a): Sage model schematic of original "2-space" MIT test rig

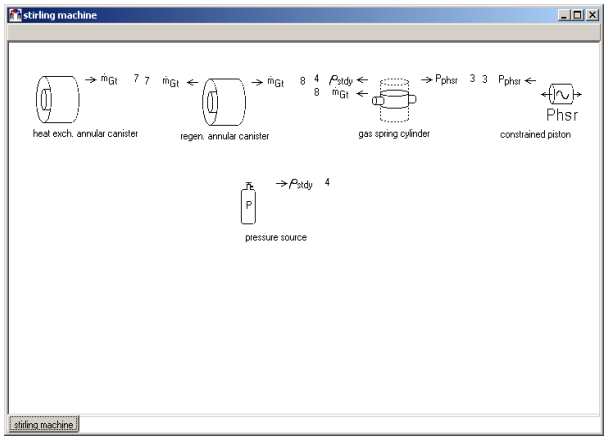

Figure 5(b): Sage model schematic corresponding to Runs C and D

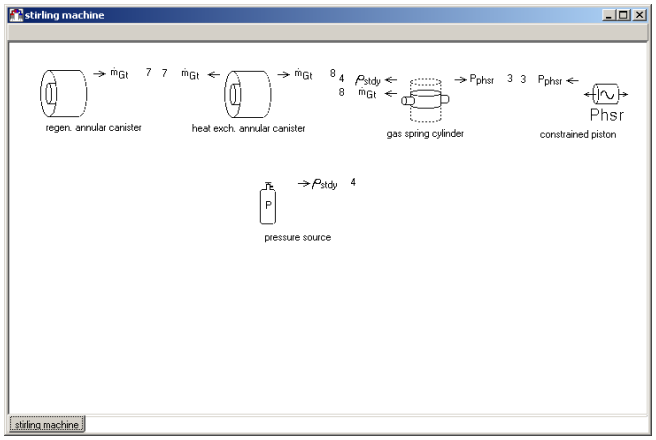

5(c): Sage model schematic corresponding to Runs E and F

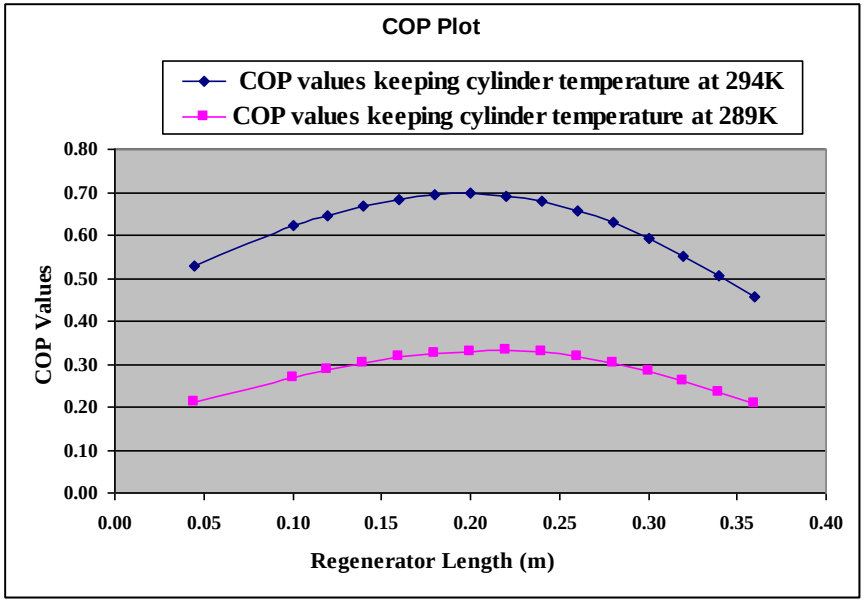

Figure 6: COP vs. Regenerator length (m)

With the "3-space" model configured as in Runs E and F, a series of parameter optimization studies can be designed and executed in an effort to obtain optimum values for regenerator parameters such as regenerator length, wire diameter, annulus diameter (inner and outer) and porosity with the objective being the maximization of the cylinder-cooling effect. The results of coefficient of performance (COP) values over a range of regenerator lengths which appear to be one of the safest optimizations to do are presented in graphical form in Figure 6. The variation in the regenerator length is made by increasing its length from 4.5 cm. while ensuring that the overall length of the regenerator-heat exchanger domain remains constant at 44.5 cm. From Figure 6, it is observed that the optimum cylinder-cooling effect is greater for the generic matrix-based random fiber regenerator model (COP = 0.44466) than for the "dedicated" random fiber regenerator model (COP = 0.33019). The optimum regenerator linear dimensions corresponding to the dedicated random fiber model 22 cm. respectively. It is suggested that other parameter optimization studies of the regenerator be investigated in a future study.

In order to observe the effect of the regenerator on the numerical simulation results of the original "2-space" model [13], the "3-space" model operating conditions, regenerator length optimization, were set to match those of the "2-space" model (201.7 RPM, 1.008 MPa., T_{wall} = 294 K). For this set-up, the optimum cylinder-cooling effect (COP = 0.69647) is observed at a regenerator length of 20 cm. as illustrated in Figure 6. The optimum linear dimension of the regenerator is thus set at 20 cm. for numerical simulations. A discussion of the effect of the regenerator on the numerical simulation results is presented in Chapter 6.

CHAPTER V

THEORETICAL BASIS FOR THERMODYNAMIC LOSS MODELING

5.1 Introduction

As in the Stirling convertor, the flow in the MIT test rig is highly compressible due mainly to the large internal volume changes. The competing effects of the heat transfer due to temperature gradients and flow friction in the "3-space" solution domain point to a loss model which requires coupling of the momentum and energy conservation equations. These coupling effects are united with the concept of entropy generation which relies on the second law of thermodynamics to develop the loss model.

The theoretical development of the loss model begins with the development of a generalized set of "local" or "microscopic" conserved equations of mass, momentum and energy for the two mechanically distinct phases, α (fluid) and β (solid) inside the non-porous regions of the "3-space" model. Because the flow geometry in the porous regenerator matrix is too complicated to allow for a direct application of the "local" or "microscopic" equations, the regenerator presents the need for volume-averaging, an analytical tool for describing the phenomena of compressible flow and heat transfer in a porous medium. The governing volume-averaged equations for use in the regenerator porous medium are discussed later in Section 5.3.

5.2 "Local" or "Microscopic" Equations

The "local" or "microscopic" equations of mass, momentum, energy and entropy that govern the flow in the non-porous regions of the "3-space" model are similar to those derived in any fluid mechanics text. The details of the derivations are presented in [14]. It is assumed that the α and β phases do not react chemically; that the density of the solid is constant and that the no-slip assumption at the fluid-solid interface is valid.

5.2.1 Conservation of Mass Equation

The conservation of mass equation, applicable only to the α-phase, is from [14]:

$$\frac{\partial \rho_\alpha}{\partial t} + \vec{\nabla} \cdot \left(\rho_\alpha \vec{u}_\alpha \right) = 0 \tag{5.1}$$

This equation is a scalar equation with 4 unknowns: the gas density ρ_α and three components of the gas velocity $\vec{u}_\alpha$.

5.2.2 Conservation of Momentum Equations

The conservation of momentum equations is also applicable only to the α-phase. The differential statement of the conservation of momentum for a Newtonian fluid with no body forces can be written as [14]:

$$\begin{aligned} \frac{\partial \left(\rho_\alpha \vec{u}_\alpha \right)}{\partial t} + \vec{\nabla} \cdot \left(\rho_\alpha \vec{u}_\alpha \vec{u}_\alpha \right) + \vec{\nabla} p_\alpha - \frac{1}{3} \vec{\nabla} \left(\mu_\alpha \vec{\nabla} \cdot \vec{u}_\alpha \right) - \left(\vec{\nabla} \cdot \mu_\alpha \vec{\nabla} \right) \vec{u}_\alpha \\ + \frac{2}{3} \left(\vec{\nabla} \mu_\alpha \right) \vec{\nabla} \cdot \vec{u}_\alpha - 2 \left(\vec{\nabla} \mu_\alpha \cdot \vec{\nabla} \right) \vec{u}_\alpha - \left(\vec{\nabla} \mu_\alpha \times \vec{\Omega}_\alpha \right) = 0 \end{aligned} \tag{5.2}$$

The parameter $\vec{\Omega}_\alpha$ is the vorticity vector. This equation is a vector equation with three components corresponding to the three components of velocity. The conservation of momentum equation produces 1 additional unknown, the fluid pressure, p_α. The fluid dynamic viscosity, μ_α, is a material property. For many fluids, μ_α depends significantly on

temperature and when appreciable temperature differences exist in the flow field, as in Stirling engines, it is necessary to regard μ_α as a function of position.

5.2.3 Conservation of Energy Equation

The energy equation is applicable to both the α and β phases. The different forms of the energy equation derived in [14] are shown below:

α-phase		β-phase	
$\frac{\partial(\rho_\alpha \hat{u}_\alpha)}{\partial t} + \vec{\nabla}\cdot\left(\rho_\alpha \vec{u}_\alpha h_\alpha - k_\alpha \vec{\nabla} T_\alpha\right) = 0$	(5.3a)	$(\rho c)_\beta \frac{\partial T_\beta}{\partial t} - \vec{\nabla}\cdot\left(k_\beta \vec{\nabla} T_\beta\right) = 0$	(5.3d)
$\frac{\partial(\rho_\alpha \hat{u}_\alpha)}{\partial t} + \vec{\nabla}\cdot(\rho_\alpha \vec{u}_\alpha \hat{u}_\alpha) = \vec{\nabla}\cdot\left(k_\alpha \vec{\nabla} T_\alpha\right) + \Phi_\alpha - p_\alpha \vec{\nabla}\cdot\vec{u}_\alpha$	(5.3b)		
$\rho_\alpha \frac{Dh_\alpha}{Dt} = \vec{\nabla}\cdot\left(k_\alpha \vec{\nabla} T_\alpha\right) + \Phi_\alpha + \frac{Dp_\alpha}{Dt}$	(5.3c)		

Eqs.(5.3a,b,c) are different forms of the conservation of energy equations for the α-phase. Eq.(5.3d) is the conservation of energy equation for the β-phase.

The energy equations introduce 3 additional unknowns; the fluid and solid temperatures (T_α and T_β), and the fluid specific internal energy $\hat{u}_\alpha$. The thermal conductivities k_α and k_β, like the viscous coefficient μ_α, are temperature dependent material properties. The parameters c_β, and $(\rho c)_\beta$, are the solid specific heat and heat capacity per unit volume respectively.

The gas enthalpy $h_\alpha = \hat{u}_\alpha + (p_\alpha/\rho_\alpha)$. Although not immediately obvious from Eq.(5.3a), it can be shown [14] that the gradient of the enthalpy flow term, $\vec{\nabla}\cdot(\rho_\alpha \vec{u}_\alpha h_\alpha) = \vec{\nabla}\cdot(\rho_\alpha \vec{u}_\alpha \hat{u}_\alpha) + p_\alpha \vec{\nabla}\cdot\vec{u}_\alpha - \Phi_\alpha$ where the viscous dissipation function Φ_α is defined as [19]:

$$\Phi_\alpha = -(2/3)\mu(\nabla\cdot\vec{u})^2 + 2\mu\left[\left(\frac{\partial u}{\partial x}\right)^2 + \left(\frac{\partial v}{\partial y}\right)^2 + \left(\frac{\partial w}{\partial z}\right)^2\right] + \mu\left[\left(\frac{\partial v}{\partial x} + \frac{\partial u}{\partial y}\right)^2 + \left(\frac{\partial w}{\partial y} + \frac{\partial v}{\partial z}\right)^2 + \left(\frac{\partial u}{\partial z} + \frac{\partial w}{\partial x}\right)^2\right] \quad (5.4)$$

5.2.4 Equations of State

Thus far, the system of six equations (mass, three components of momentum and the two phases of energy) containing eight unknowns (ρ_α, three components of $\vec{u}_\alpha$, p_α, T_α, T_β, $\hat{u}_\alpha$) requires two additional equations to close the problem. These equations are the thermodynamic equations of state which can be expressed generally as

$$p_\alpha = f_1(\rho_\alpha, \hat{u}_\alpha) \tag{5.5}$$

$$T_\alpha = f_2(\rho_\alpha, \hat{u}_\alpha) \tag{5.6}$$

The particular equations of state are arbitrary, in the sense that the particular forms do not affect the form of the governing equations. Ideal or real gas equations can be used.

5.2.5 Entropy Generation Equation

Optimization of thermo-fluid systems requires that the coupling effects of the mass, momentum and energy conservation equations be united with the concept of entropy generation which relies on the second law of thermodynamics. The differential statement of the second law of thermodynamics [4,14] is re-written in different forms for the α and β phases as:

α-phase	β-phase
$s'''_{gen,\alpha} = \frac{\partial(\rho_\alpha s_\alpha)}{\partial t} + \vec{\nabla}\cdot\left(\frac{\vec{q}_\alpha}{T_\alpha}\right) + \vec{\nabla}\cdot(\rho_\alpha s_\alpha \vec{u}_\alpha) \geq 0$ (4.7a)	$s'''_{gen,\beta} = \frac{\partial(\rho_\beta s_\beta)}{\partial t} + \vec{\nabla}\cdot\left(\frac{\vec{q}_\beta}{T_\beta}\right) \geq 0$ (4.7d)
$s'''_{gen,\alpha} = \rho_\alpha \frac{Ds_\alpha}{Dt} - \frac{\vec{q}_\alpha \cdot \vec{\nabla} T_\alpha}{T_\alpha^2} + \frac{\vec{\nabla}\cdot\vec{q}_\alpha}{T_\alpha} \geq 0$ (4.7b)	$s'''_{gen,\beta} = \rho_\beta \frac{\partial(s_\beta)}{\partial t} - \frac{\vec{q}_\beta \cdot \vec{\nabla} T_\beta}{T_\beta^2} + \frac{\vec{\nabla}\cdot\vec{q}_\beta}{T_\beta} \geq 0$ (4.7e)
$s'''_{gen,\alpha} = -\frac{\vec{q}_\alpha \cdot \vec{\nabla} T_\alpha}{T_\alpha^{\,2}} + \frac{\Phi_\alpha}{T_\alpha} \geq 0$ (4.7c)	$s'''_{gen,\beta} = -\frac{\vec{q}_\beta \cdot \vec{\nabla} T_\beta}{T_\beta^{\,2}} \geq 0$ (4.7f)

The entropy generation rate for the non-porous regions of the Stirling convector is thus:

$$s'''_{gen,\,sys(non\text{-}porous)} = s'''_{\alpha,\,gen} + s'''_{\beta,\,gen} \geq 0 \qquad (5.8)$$

The second law postulates the existence of entropy, s, a non-conserved thermodynamic property of state that can be created via a generation or production term, s'''_{gen}. The parameter $\vec{q}$ represents the heat flux vector. The inequality indicates that the entropy generation is always positive except for totally reversible processes, in which case, it is zero.

The foregoing equations represent the generalized, non-volume averaged, micro scale equations for a single fluid phase flowing and interacting with a stationary solid phase. As mentioned earlier, the flow geometry in a Stirling engine is far too complicated to allow for direct application of these equations for any large scale porous system such as the regenerator in the Stirling convertor. The flow in the regenerator is best analyzed in terms of volume-averaged quantities.

5.3 Volume-Averaged Equations

The Stirling regenerator porous medium under consideration is illustrated in Figure 7 where two mechanically distinct phases are identified as β (solid) and α (fluid). The physical process of interest is the compressible flow of a single fluid (gas) through the porous matrix. The parameter n_α is the unit normal vector on the α-β interface pointing into the β-phase and x is the position vector. The subscript on the position vector indicates the phase at that position. The porous matrix is assumed to be stationary and rigid with known thermal properties which are functions of temperature. The fluid phase is assumed to behave as a linearly viscous fluid (Newtonian) whose properties are known functions of temperature and pressure, or other combinations of state properties.

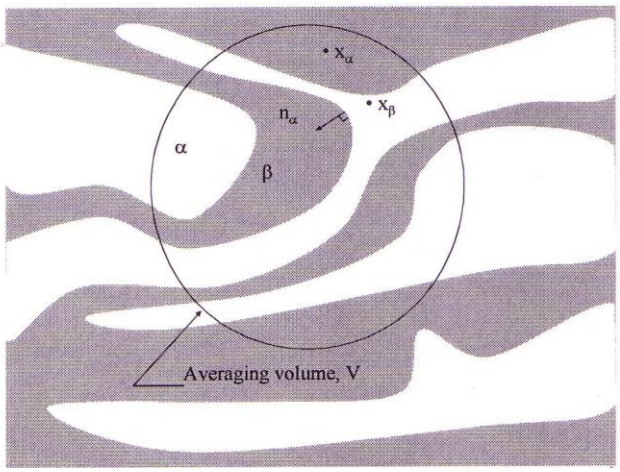

Figure 7. A two-phase model of a porous medium. The α-phase is a Newtonian fluid and the β-base is the solid part of the porous matrix. [Courtesy [23]].

The objective here is to derive the equations that govern the flow and heat transfer, in the average sense, in the α and β regions. In this regard, the "local" or "microscopic" conservation and entropy equations for the solid and fluid phases are volume averaged over a representative elementary volume to arrive at the corresponding "macroscopic" transport equations. The volume-averaging technique assumes that the velocity, pressure, temperature, and concentration can be represented in terms of a single large-scale averaged quantity in regions having significantly different mechanical, thermal, and chemical properties. This assumption provides the basis for the porous-media models available in two CFD codes, Fluent and CFD-ACE, used at GRC for modeling Infinia's Stirling TDC. The models assume that the porous matrix and the fluid are in local thermal equilibrium at each spatial interface between them. This is believed to be a poor assumption for the oscillating-flow environment within Stirling regenerators [37,41]. 1-D regenerator models, used in Stirling engine design, use thermal non-equilibrium models and suggest regenerator porous matrix and gas average temperatures can differ by several degrees at a given axial location and time during the cycle [43]. A survey of the porous-media literature

supports the need for thermal non-equilibrium porous-media models for thermal storage applications such as Stirling regenerators [7,2,29,30,38].

The details of the volume averaging method are discussed in [14] with guidance drawn largely from [23]. The resulting equations are shown below:

5.3.1 Conservation of Mass Equation

The volume-averaged conservation of mass equation is

$$\frac{\partial}{\partial t}\langle \rho_\alpha \rangle^\alpha + \nabla \cdot \left(\langle \rho_\alpha \rangle^\alpha \langle \vec{u}_\alpha \rangle^\alpha \right) + \frac{1}{\varepsilon_\alpha} \nabla \cdot \left\langle \hat{\rho}_\alpha \hat{\vec{u}}_\alpha \right\rangle = 0 \tag{5.9}$$

The parameter $\varepsilon_\alpha = V_\alpha / V$ is the gas phase volume fraction, or porosity. V_α is the gas phase volume and V is the arbitrary averaging volume containing the porous medium (see Figure 7 above). The notations $\langle\ \rangle$ and ^ indicate a volume average and a spatial deviation quantity respectively. Note that the terms in the original conservation of mass equation (5.1) have survived, except these terms are now in the form of volume-averaged quantities. The additional dispersive mass transport term results from the application of averaging theorems and principles. Under the assumption that the density deviation is small compared to the volume-averaged density [33], Eq.(5.9) becomes

$$\frac{\partial}{\partial t}\langle \rho_\alpha \rangle^\alpha + \nabla \cdot \left(\langle \rho_\alpha \rangle^\alpha \langle \vec{u}_\alpha \rangle^\alpha \right) = 0 \tag{5.10}$$

Note that this “macroscopic” conserved equation of mass is similar in form to the corresponding “microscopic” equation (Eq.(5.1)).

5.3.2 Conservation of Momentum Equations

The volume-averaged conservation of momentum is

$$\frac{\partial}{\partial t}\left(\langle\rho_\alpha\rangle^\alpha\langle\vec{u}_\alpha\rangle^\alpha\right) + \nabla\cdot\left(\langle\rho_\alpha\rangle^\alpha\langle\vec{u}_\alpha\rangle^\alpha\langle\vec{u}_\alpha\rangle^\alpha\right) + \nabla\langle p_\alpha\rangle^\alpha + \left[\frac{1}{3}\nabla\left(\mu_\alpha\nabla\cdot\langle\vec{u}_\alpha\rangle^\alpha\right) + \nabla\cdot\left(\mu_\alpha\nabla\langle\vec{u}_\alpha\rangle^\alpha\right)\right]$$
$$+ 2\varepsilon_\alpha\left(\vec{\nabla}\langle\mu_\alpha\rangle^\alpha\cdot\vec{\nabla}\right)\langle\vec{u}_\alpha\rangle^\alpha + \varepsilon_\alpha\left(\vec{\nabla}\langle\mu_\alpha\rangle^\alpha\right)x\left\langle\vec{\Omega}_\alpha\right\rangle^\alpha + \frac{1}{V_\alpha}\int_{A_{\alpha\beta}} n_\alpha\cdot\left[\tilde{\tilde{I}}\left(\hat{p}_\alpha + n_\alpha\frac{\mu_\alpha}{3}\nabla\cdot\hat{\vec{u}}_\alpha\right) + \mu_\alpha\nabla\hat{\vec{u}}_\alpha\right]dS$$
$$+ \frac{1}{\varepsilon_\alpha}\left[\frac{\partial}{\partial t}\left\langle\hat{\rho}_\alpha\hat{\vec{u}}_\alpha\right\rangle + \nabla\cdot\left(\langle\rho_\alpha\rangle^\alpha\left\langle\hat{\vec{u}}_\alpha\hat{\vec{u}}_\alpha\right\rangle\right) + \nabla\cdot\left(\langle\vec{u}_\alpha\rangle^\alpha\left\langle\hat{\rho}_\alpha\hat{\vec{u}}_\alpha\right\rangle\right) + \nabla\cdot\left(\left\langle\hat{\rho}_\alpha\hat{\vec{u}}_\alpha\right\rangle\langle\vec{u}_\alpha\rangle^\alpha\right) + \nabla\cdot\left\langle\hat{\rho}_\alpha\hat{\vec{u}}_\alpha\hat{\vec{u}}_\alpha\right\rangle\right]$$
$$+ \frac{2\varepsilon_\alpha}{3}\left(\vec{\nabla}\langle\mu_\alpha\rangle^\alpha\right)^2 = 0 \qquad (5.11)$$

The above Eq. (5.11) can be re-written in a weak conservation form as:

$$\langle\rho_\alpha\rangle^\alpha\frac{\partial}{\partial t}\langle\vec{u}_\alpha\rangle^\alpha + \langle\rho_\alpha\rangle^\alpha\langle\vec{u}_\alpha\rangle^\alpha\nabla\cdot\langle\vec{u}_\alpha\rangle^\alpha + \nabla\langle p_\alpha\rangle^\alpha + \left[\frac{1}{3}\nabla\left(\mu_\alpha\nabla\cdot\langle\vec{u}_\alpha\rangle^\alpha\right) + \nabla\cdot\left(\mu_\alpha\nabla\langle\vec{u}_\alpha\rangle^\alpha\right)\right]$$
$$+ 2\varepsilon_\alpha\left(\vec{\nabla}\langle\mu_\alpha\rangle^\alpha\cdot\vec{\nabla}\right)\langle\vec{u}_\alpha\rangle^\alpha + \varepsilon_\alpha\left(\vec{\nabla}\langle\mu_\alpha\rangle^\alpha\right)x\left\langle\vec{\Omega}_\alpha\right\rangle^\alpha + \frac{1}{V_\alpha}\int_{A_{\alpha\beta}} n_\alpha\cdot\left[\tilde{\tilde{I}}\left(\hat{p}_\alpha + n_\alpha\frac{\mu_\alpha}{3}\nabla\cdot\hat{\vec{u}}_\alpha\right) + \mu_\alpha\nabla\hat{\vec{u}}_\alpha\right]dS$$
$$+ \frac{1}{\varepsilon_\alpha}\left[\frac{\partial}{\partial t}\left\langle\hat{\rho}_\alpha\hat{\vec{u}}_\alpha\right\rangle + \nabla\cdot\left(\langle\rho_\alpha\rangle^\alpha\left\langle\hat{\vec{u}}_\alpha\hat{\vec{u}}_\alpha\right\rangle\right) + \nabla\cdot\left(\langle\vec{u}_\alpha\rangle^\alpha\left\langle\hat{\rho}_\alpha\hat{\vec{u}}_\alpha\right\rangle\right) + \left\langle\hat{\rho}_\alpha\hat{\vec{u}}_\alpha\right\rangle\cdot\nabla\langle\vec{u}_\alpha\rangle^\alpha + \nabla\cdot\left\langle\hat{\rho}_\alpha\hat{\vec{u}}_\alpha\hat{\vec{u}}_\alpha\right\rangle\right]$$
$$+ \frac{2\varepsilon_\alpha}{3}\left(\vec{\nabla}\langle\mu_\alpha\rangle^\alpha\right)^2 = 0 \qquad (5.12)$$

The terms in Eq.(5.12) additional to the standard conservation of momentum equations (Eq.(5.2)) result from the application of averaging theorems and principles. Whitaker [46] shows by scale analysis that the mechanical dispersion term and the Brinkman effect (effect of macroscopic shear) are generally negligible in comparison to the Darcy and Forchheimer effects (flow inertia effects). Since the density deviation is small, terms containing density deviation will be negligible also. The simplified momentum equation becomes

$$\frac{\partial}{\partial t}\left(\langle\rho_\alpha\rangle^\alpha\langle\vec{u}_\alpha\rangle^\alpha\right) + \nabla\cdot\left(\langle\rho_\alpha\rangle^\alpha\langle\vec{u}_\alpha\rangle^\alpha\langle\vec{u}_\alpha\rangle^\alpha\right) + \nabla\langle p_\alpha\rangle^\alpha + \frac{1}{V_\alpha}\int_{A_{\alpha\beta}} n_\alpha\cdot\left[\tilde{\tilde{I}}\left(\hat{p}_\alpha + n_\alpha\frac{\mu_\alpha}{3}\nabla\cdot\hat{\vec{u}}_\alpha\right) + \mu_\alpha\nabla\hat{\vec{u}}_\alpha\right]dS$$
$$+ \varepsilon_\alpha\left[2\left(\vec{\nabla}\langle\mu_\alpha\rangle^\alpha\cdot\vec{\nabla}\right)\langle\vec{u}_\alpha\rangle^\alpha + \left(\vec{\nabla}\langle\mu_\alpha\rangle^\alpha\right)x\left\langle\vec{\Omega}_\alpha\right\rangle^\alpha + \frac{2}{3}\left(\vec{\nabla}\langle\mu_\alpha\rangle^\alpha\right)^2\right] = 0 \qquad (5.13)$$

Or, in weak conservation form:

$$\langle\rho_\alpha\rangle^\alpha \frac{\partial}{\partial t}\langle\vec{u}_\alpha\rangle^\alpha + \langle\rho_\alpha\rangle^\alpha\langle\vec{u}_\alpha\rangle^\alpha\nabla\cdot\langle\vec{u}_\alpha\rangle^\alpha + \nabla\langle p_\alpha\rangle^\alpha + \frac{1}{V_\alpha}\int_{A_{\alpha\beta}} n_\alpha\cdot\left[\tilde{\bar{I}}\left(\hat{p}_\alpha + n_\alpha\frac{\mu_\alpha}{3}\nabla\cdot\hat{\vec{u}}_\alpha\right) + \mu_\alpha\nabla\hat{\vec{u}}_\alpha\right]dS$$

$$+ \varepsilon_\alpha\left[2\left(\vec{\nabla}\langle\mu_\alpha\rangle^\alpha\cdot\vec{\nabla}\right)\langle\vec{u}_\alpha\rangle^\alpha + \left(\vec{\nabla}\langle\mu_\alpha\rangle^\alpha\right)\times\langle\vec{\Omega}_\alpha\rangle + \frac{2}{3}\left(\vec{\nabla}\langle\mu_\alpha\rangle^\alpha\right)^2\right] = 0 \qquad (5.14)$$

5.3.3 Conservation of Energy Equation

The volume-averaged conservation of energy equations in α and β phases are

α-phase

$$\frac{\partial}{\partial t}\left(\langle\rho_\alpha\rangle^\alpha\langle\hat{u}_\alpha\rangle^\alpha\right) + \nabla\cdot\left(\langle\rho_\alpha\rangle^\alpha\langle\vec{u}_\alpha\rangle^\alpha\langle h_\alpha\rangle^\alpha\right)$$

$$- \nabla\cdot\left[k_\alpha\left(\nabla\langle T_\alpha\rangle^\alpha + \frac{1}{V_\alpha}\int_{A_{\alpha\beta}} n_\alpha\hat{T}_\alpha dS\right)\right] + \frac{1}{\varepsilon_\alpha}\nabla\cdot\left(\langle\rho_\alpha\rangle^\alpha\langle\hat{\vec{u}}_\alpha\hat{h}_\alpha\rangle\right)$$

$$- \frac{1}{V_\alpha}\int_{A_{\alpha\beta}} n_\alpha\cdot k_\alpha\nabla T_\alpha dS + \frac{1}{\varepsilon_\alpha}\frac{\partial\langle\hat{\rho}_\alpha\hat{\vec{u}}_\alpha\rangle}{\partial t} + \frac{1}{\varepsilon_\alpha}\nabla\cdot\left(\langle\hat{\rho}_\alpha\hat{\vec{u}}_\alpha\rangle\langle h_\alpha\rangle^\alpha\right)$$

$$\frac{1}{\varepsilon_\alpha}\nabla\cdot\left(\langle\hat{\rho}_\alpha\hat{h}_\alpha\rangle\langle\hat{\vec{u}}_\alpha\rangle^\alpha\right) + \frac{1}{\varepsilon_\alpha}\nabla\cdot\langle\hat{\rho}_\alpha\hat{\vec{u}}_\alpha\hat{h}_\alpha\rangle = 0 \qquad (5.15a)$$

β-phase

$$(\rho c)_\beta\frac{\partial\langle T_\beta\rangle^\beta}{\partial t} - \nabla\cdot\left[k_\beta\left(\nabla\langle T_\beta\rangle^\beta + \frac{1}{V_\beta}\int_{A_{\alpha\beta}} n_\beta\hat{T}_\beta dS\right)\right]$$

$$- \frac{1}{V_\beta}\int_{A_{\alpha\beta}} n_\beta\cdot k_\beta\nabla T_\beta dS = 0 \qquad (5.15b)$$

Again, the volume averaging has produced additional terms (many for the α-phase). The terms of the original energy equations (5.3a, 5.3b) are now in the form of volume-averaged quantities.

The sum of the terms in the α-phase energy equation representing molecular dispersion (molecular conduction + "thermal tortuosity" conduction) and thermal dispersion have been shown by Whitaker [47] to reduce to an overall effective gas conduction term $-\nabla\cdot\left(N_k k_\alpha\nabla\langle T_\alpha\rangle^\alpha\right)$. That is

$$-\nabla\cdot\left[k_\alpha\left(\nabla\langle T_\alpha\rangle^\alpha + \frac{1}{V_\alpha}\int_{A_{\alpha\beta}} n_\alpha\hat{T}_\alpha dS\right)\right] + \frac{1}{\varepsilon_\alpha}\nabla\cdot\left(\langle\rho_\alpha\rangle^\alpha\langle\hat{\vec{u}}_\alpha\hat{h}_\alpha\rangle\right) = -\nabla\cdot\left(N_k k_\alpha\nabla\langle T_\alpha\rangle^\alpha\right) \qquad (5.16)$$

Gedeon [17] recognized N_k, as axial conductivity enhancement due to thermal dispersion having a Peclet dependence of the form $(c_1 + c_2 Re^m Pr^n)$ where m and n are positive

constants. This functional form for the dispersion agrees with other empirical predictions [29].

With the terms containing density deviation negligible, the α-phase energy equation (5.15a) simplifies to

$$\frac{\partial}{\partial t}\left(\langle\rho_\alpha\rangle^\alpha\langle e_\alpha\rangle^\alpha\right) + \nabla\cdot\left(\langle\rho_\alpha\rangle^\alpha\langle\vec{u}_\alpha\rangle^\alpha\langle h_\alpha\rangle^\alpha - N_k k_\alpha\nabla\langle T_\alpha\rangle^\alpha\right) - \frac{1}{V_\alpha}\int_{A_{\alpha\beta}} n_\alpha\cdot k_\alpha\nabla T_\alpha dS = 0 \qquad (5.17)$$

In equations (5.15a,b), the surface integral terms containing the temperature gradients, each divided by the corresponding phase volume, represent the volumetric heat transfer between the two phases. Whitaker [47] has proposed that these integrals which are exactly of the same magnitude but opposite in sign be represented as

$$-\frac{\varepsilon_\beta}{\varepsilon_\alpha}\frac{1}{V_\beta}\int_{A_{\alpha\beta}} n_\beta\cdot k_\beta\nabla T_\beta\, dS = \frac{1}{V_\alpha}\int_{A_{\alpha\beta}} n_\alpha\cdot k_\alpha\nabla T_\alpha\, dS = \alpha_v H\left(\langle T_\beta\rangle^\beta - \langle T_\alpha\rangle^\alpha\right) \qquad (5.18)$$

The equivalence of the form of the integrals is ensured by noting that $[\varepsilon_\beta/(\varepsilon_\alpha V_\beta)] = 1/V_\alpha$. The parameter $\alpha_v H$ is the volumetric heat transfer coefficient.

The molecular dispersion term in the β-phase energy equation (5.15b) can be written as

$$\nabla\cdot\left[k_\beta\left(\nabla\langle T_\beta\rangle^\beta + \frac{1}{V_\beta}\int_{A_{\alpha\beta}} n_\beta\hat{T}_\beta dS\right)\right] = \nabla\cdot\left[k_\beta\left(\tilde{I} + \frac{1}{V_\beta}\int_{A_{\alpha\beta}} n_\beta\tilde{b}_\beta dS\right)\nabla\langle T_\beta\rangle^\beta\right] = \nabla\cdot\left[k_\beta\tau_\beta\nabla\langle T_\beta\rangle^\beta\right] \qquad (5.19)$$

The parameter $\tilde{b}_\beta$ is the closure variable that is solved for numerically and τ_β is referred to as the "tortuosity" by Gedeon [12]. There is no standard definition for tortuosity in the literature. Tortuosity in porous media is often defined as $\tau = L_e/L$ [2**,9***], where L_e and L are the actual length of the flow path and the straight-line distance between the ends of the flow path. With this definition, experiments have suggested that the tortuosity is greater than or equal to one. Tortuosity equal to one represents parallel path geometries such as tube bundles. Geometries such as wire mesh, felts, and sintered metals have tortuosities

greater than one. Unlike dispersion, the tortuosity is thought to be a function of geometry only, and not the flow field.

Substitution of Eq.(5.18) into Eq.(5.17) and Eqs. (5.18) and (5.19) into Eq.(5.15b) result in a simplified two-equation energy model

α-phase

$$\frac{\partial}{\partial t}\left(\langle\rho_\alpha\rangle^\alpha\langle\hat{u}_\alpha\rangle^\alpha\right)+\nabla\cdot\left(\langle\rho_\alpha\rangle^\alpha\langle\vec{u}_\alpha\rangle^\alpha\langle h_\alpha\rangle^\alpha-N_k k_\alpha\nabla\langle T_\alpha\rangle^\alpha\right)-\alpha_v H\left(\langle T_\beta\rangle^\beta-\langle T_\alpha\rangle^\alpha\right)=0 \quad (5.20a)$$

β-phase

$$(\rho c)_\beta\frac{\partial\langle T_\beta\rangle^\beta}{\partial t}-\nabla\cdot\left[k_\beta\tau_\beta\nabla\langle T_\beta\rangle^\beta\right]+\frac{\varepsilon_\alpha}{\varepsilon_\beta}\alpha_v H\left(\langle T_\beta\rangle^\beta-\langle T_\alpha\rangle^\alpha\right)=0 \quad (5.20b)$$

Volume averaging in this case results in the film heat transfer term, a term additional to the standard form of the α- and β-phase microscopic energy equations (5.3a, 5.3d).

5.3.4 Entropy Generation Equation

The volume-averaged entropy generation equations in α and β phases are from [14]

α-phase

$$\langle s'''_{\alpha,\text{gen}}\rangle^\alpha=\frac{\partial\left(\langle\rho_\alpha\rangle^\alpha\langle s_\alpha\rangle^\alpha\right)}{\partial t}+\nabla\cdot\left(\langle\rho_\alpha\rangle^\alpha\langle s_\alpha\rangle^\alpha\langle\vec{u}_\alpha\rangle^\alpha\right)-\frac{1}{\varepsilon_\alpha}\nabla\cdot\left[k_\alpha\left\langle\frac{\nabla T_\alpha}{T_\alpha}\right\rangle\right]+\frac{1}{\varepsilon_\alpha}\nabla\cdot\left(\langle\rho_\alpha\rangle^\alpha\langle\hat{s}_\alpha\hat{\vec{u}}_\alpha\rangle\right)-\frac{1}{V_\alpha}\int_{A_{\alpha\beta}}n_\alpha\cdot\frac{k_\alpha\nabla T_\alpha}{T_\alpha}dS+\frac{1}{\varepsilon_\alpha}\frac{\partial\left(\hat{\rho}_\alpha\hat{s}_\alpha\right)}{\partial t}+\frac{1}{\varepsilon_\alpha}\nabla\cdot\left(\langle\hat{\rho}_\alpha\hat{s}_\alpha\rangle\langle\vec{u}_\alpha\rangle^\alpha\right)+\frac{1}{\varepsilon_\alpha}\nabla\cdot\left(\langle\hat{\rho}_\alpha\hat{\vec{u}}_\alpha\rangle\langle s_\alpha\rangle^\alpha\right)+\frac{1}{\varepsilon_\alpha}\nabla\cdot\langle\hat{\rho}_\alpha\hat{s}_\alpha\hat{\vec{u}}_\alpha\rangle \quad (5.21a)$$

β-phase

$$\langle s'''_{\beta,\text{gen}}\rangle^\beta=\rho_\beta\frac{\partial\langle s_\beta\rangle^\beta}{\partial t}-\frac{1}{\varepsilon_\beta}\nabla\cdot\left[k_\beta\left\langle\frac{\nabla T_\beta}{T_\beta}\right\rangle\right]-\frac{1}{V_\beta}\int_{A_{\alpha\beta}}n_\beta\cdot\frac{k_\beta\nabla T_\beta}{T_\beta}dS \quad (5.21b)$$

The volume averaging has produced additional terms to the non-volume averaged terms of the original entropy equations (5.7a, 5.7d). For the α-phase, these include many terms involving density deviations and a fluid-solid heat transfer term. For the β-phase, the additional term is the fluid-solid heat transfer term.

The sum of the terms in the α-phase entropy equation representing molecular conduction and thermal dispersion has been shown to reduce to an overall effective conduction term [47] viz:

$$-\frac{1}{\varepsilon_\alpha}\nabla\cdot\left[k_\alpha\left\langle\frac{\nabla T_\alpha}{T_\alpha}\right\rangle^\alpha\right]+\frac{1}{\varepsilon_\alpha}\nabla\cdot\left(\left\langle\rho_\alpha\right\rangle^\alpha\left\langle\hat{s}_\alpha\hat{u}_\alpha\right\rangle\right)=-\nabla\cdot\left(\frac{N_k k_\alpha\nabla\left\langle T_\alpha\right\rangle^\alpha}{\left\langle T_\alpha\right\rangle^\alpha}\right) \tag{5.22}$$

Also, since the terms in Eq.(5.21a) containing density deviation are negligible, the simplified two-equation entropy model becomes

α-phase

$$\left\langle s'''_{\alpha,gen}\right\rangle^\alpha=\frac{\partial\left(\left\langle\rho_\alpha\right\rangle^\alpha\left\langle s_\alpha\right\rangle^\alpha\right)}{\partial t}+\nabla\cdot\left(\left\langle\rho_\alpha\right\rangle^\alpha\left\langle s_\alpha\right\rangle^\alpha\left\langle\vec{u}_\alpha\right\rangle^\alpha\right)-\nabla\cdot\left[\frac{N_k k_\alpha}{\left\langle T_\alpha\right\rangle^\alpha}\nabla\left\langle T_\alpha\right\rangle^\alpha\right]-\frac{1}{V_\alpha}\int_{A_{\alpha\beta}}n_\alpha\cdot\frac{k_\alpha\nabla T_\alpha}{T_\alpha}dS\geq 0 \tag{5.23a}$$

β-phase

$$\left\langle s'''_{\beta,gen}\right\rangle^\beta=\rho_\beta\frac{\partial\left\langle s_\beta\right\rangle^\beta}{\partial t}-\frac{1}{\varepsilon_\beta}\nabla\cdot\left[k_\beta\left\langle\frac{\nabla T_\beta}{T_\beta}\right\rangle^\beta\right]-\frac{1}{V_\beta}\int_{A_{\alpha\beta}}n_\beta\cdot\frac{k_\beta\nabla T_\beta}{T_\beta}dS \tag{5.23b}$$

As with the energy equation method, the integral terms representing entropy generation due to volumetric heat transfer between the two phases can be expressed as

α-phase

$$\frac{1}{V_\alpha}\int_{A_{\alpha\beta}}n_\alpha\cdot\frac{k_\alpha\nabla T_\alpha}{T_\alpha}dS=\frac{\alpha_v H}{\left\langle T_\beta\right\rangle^\beta}\left(\left\langle T_\beta\right\rangle^\beta-\left\langle T_\alpha\right\rangle^\alpha\right) \tag{5.24a}$$

β-phase

$$-\frac{1}{V_\beta}\int_{A_{\alpha\beta}}n_\beta\cdot\frac{k_\beta\nabla T_\beta}{T_\beta}dS=\frac{\varepsilon_\alpha\alpha_v H}{\varepsilon_\beta\left\langle T_\alpha\right\rangle^\alpha}\left(\left\langle T_\beta\right\rangle^\beta-\left\langle T_\alpha\right\rangle^\alpha\right) \tag{5.24b}$$

Substitution of the above equations (5.24a,b) into the two-equation entropy generation model, Eq.(5.23a,b), results in

α-phase

$$\left\langle s'''_{\alpha,gen}\right\rangle^\alpha=\frac{\partial\left(\left\langle\rho_\alpha\right\rangle^\alpha\left\langle s_\alpha\right\rangle^\alpha\right)}{\partial t}+\nabla\cdot\left(\left\langle\rho_\alpha\right\rangle^\alpha\left\langle s_\alpha\right\rangle^\alpha\left\langle\vec{u}_\alpha\right\rangle^\alpha\right)-\nabla\cdot\left[\frac{N_k k_\alpha}{\left\langle T_\alpha\right\rangle^\alpha}\nabla\left\langle T_\alpha\right\rangle^\alpha\right]-\frac{\alpha_v H}{\left\langle T_\beta\right\rangle^\beta}\left(\left\langle T_\beta\right\rangle^\beta-\left\langle T_\alpha\right\rangle^\alpha\right) \tag{5.25a}$$

β-phase

$$\left\langle s'''_{\beta,gen}\right\rangle^\beta=\rho_\beta\frac{\partial\left\langle s_\beta\right\rangle^\beta}{\partial t}-\frac{1}{\varepsilon_\beta}\nabla\cdot\left[k_\beta\left\langle\frac{\nabla T}{T_\beta}\right\rangle^\beta\right]+\frac{\varepsilon_\alpha\alpha_v H}{\varepsilon_\beta\left\langle T_\alpha\right\rangle^\alpha}\left(\left\langle T_\beta\right\rangle^\beta-\left\langle T_\alpha\right\rangle^\alpha\right) \tag{5.25b}$$

The Maxwell relation for a pure substance, written in a more convenient form as [4]

$$ds = \frac{1}{\rho T}\left(dE - h d\rho\right) \tag{5.26}$$

can be used to simplify the entropy generation equations for the gas and the matrix. After considerable simplification, using the energy and momentum equations, the entropy generation equations (5.25a, 5.25b) reduce to [23]:

α-phase

$$\left\langle s'''_{\alpha,gen}\right\rangle^{\alpha} = N_k k_\alpha \left(\frac{\nabla\langle T_\alpha\rangle^{\alpha}}{\langle T_\alpha\rangle^{\alpha}}\right)^2 + \frac{\alpha_v H}{\langle T_\alpha\rangle^{\alpha}\langle T_\beta\rangle^{\beta}}\left|\langle T_\beta\rangle^{\beta} - \langle T_\alpha\rangle^{\alpha}\right|^2 - \frac{\langle \bar{u}_\alpha\rangle^{\alpha}}{\langle T_\alpha\rangle^{\alpha}}\nabla\langle p_\alpha\rangle^{\alpha} \tag{5.27a}$$

β-phase

$$\left\langle s'''_{\beta,gen}\right\rangle^{\beta} = k_\beta \left(\frac{\nabla\langle T_\beta\rangle^{\beta}}{\langle T_\beta\rangle^{\beta}}\right)^2 + \frac{\varepsilon_\alpha \alpha_v H}{\varepsilon_\beta \langle T_\alpha\rangle^{\alpha}\langle T_\beta\rangle^{\beta}}\left|\langle T_\beta\rangle^{\beta} - \langle T_\alpha\rangle^{\alpha}\right|^2 \tag{5.27b}$$

It is now possible to write the entropy generation rate equation for the gas-matrix system as

$$s'''_{gen,sys} = \varepsilon_\alpha s'''_{\alpha,gen} + \varepsilon_\beta s'''_{\beta,gen} \geq 0 \tag{5.28}$$

Substituting Eqs.(5.27a and 5.27b) into Eq.(5.28) the system entropy generation equation can be written as

$$\left\langle s'''_{gen,sys}\right\rangle^{\alpha} = \underbrace{\varepsilon_\alpha N_k k_\alpha \left(\frac{\nabla\langle T_\alpha\rangle^{\alpha}}{\langle T_\alpha\rangle^{\alpha}}\right)^2}_{\text{Gas conduction}} + \underbrace{\varepsilon_\beta k_\beta \left(\frac{\nabla\langle T_\beta\rangle^{\beta}}{\langle T_\beta\rangle^{\beta}}\right)^2}_{\text{Matrix conduction}} + \underbrace{\frac{\varepsilon_\alpha \alpha_v H}{\langle T_\alpha\rangle^{\alpha}\langle T_\beta\rangle^{\beta}}\left|\langle T_\beta\rangle^{\beta} - \langle T_\alpha\rangle^{\alpha}\right|^2}_{\text{Film heat transfer}} - \underbrace{\varepsilon_\alpha \frac{\langle \bar{u}_\alpha\rangle^{\alpha}}{\langle T_\alpha\rangle^{\alpha}}\nabla\langle p_\alpha\rangle^{\alpha}}_{\text{viscous and inertial losses}} \geq 0 \tag{5.29}$$

Eq.(5.29) indicates that the sources of irreversibility are gas conduction, matrix conduction, film heat transfer and viscous and inertial losses.

5.4 Second Law Loss Model Development

The second law of thermodynamics has proven to be a useful tool in identifying the mechanisms and system components that are responsible for thermodynamic losses and for indicating how to minimize these losses in practical equipment in order to improve

performance. Five main approaches, developed over the last several decades and reported in the literature, form the basis of second-law analysis. These are, in order of decreasing comprehensiveness, exergy, physical-exergy, exergy-consumption, negentropy and entropy analyses. These second law analysis types can be grouped into two broad categories. The first (exergy and physical-exergy analyses) is more detailed, and examines systems in an analogous way to energy analysis. The second (exergy-consumption, negentropy and entropy analyses) is concerned mainly with losses due to internal irreversibilities. The entropy analysis concept is employed in this study.

Entropy generation destroys the available work of a system and is associated with internal system irreversibilities related to three fluid dynamic processes [11]: heat transfer across a non-zero temperature difference, viscous friction leading to pressure drop and non-equilibrium processes such as mixing of different streams of fluid, unrestrained expansion, non-quasi equilibrium compression and expansion and chemical reaction. These three fundamental mechanisms (heat transfer, viscous friction and non-equilibrium processes) that generate entropy within thermo-fluid systems are clearly evident in the derivations of the preceding sections 5.2.5 and 5.3.4 (e.g. Eq.(5.7c) and Eq.(5.25a)).

Entropy generation may be calculated in one of two ways: by entropy transfer accompanied by heat transfer and mass flow across the external boundaries of a system (external entropy generation) or by entropy generated by internal processes due to heat transfer, viscous friction and non-equilibrium processes (internal entropy generation). In principle, the two methods of accounting should give the same answer. Discrepancies which usually arise are often attributable to numerical errors (finite-difference truncation errors, round-off errors, interpolation errors, etc.).

5.4.1 External Entropy Generation

The external entropy calculation is made by integrating the heat transfer and mass flow over the surface between the internal calculation domain and the environment. In a reciprocating engine like the Stirling engine or the MIT test rig, the external entropy generation over each period is obtained via a cyclic integral.

5.4.1.1 Non-Porous Regions of the Stirling Convertor:

Substituting equations (5.7a) and (5.7d) in Eq.(5.8) gives

$$s'''_{gen,\,sys(non\text{-}porous)} = \left\{\frac{\partial(\rho_\alpha s_\alpha)}{\partial t} + \vec{\nabla}\cdot\left(\frac{\vec{q}_\alpha}{T_\alpha}\right) + \vec{\nabla}\cdot(\rho_\alpha \vec{u}_\alpha s_\alpha)\right\} + \left\{\frac{\partial(\rho_\alpha s_\alpha)}{\partial t} + \vec{\nabla}\cdot\left(\frac{\vec{q}_\alpha}{T_\alpha}\right)\right\} \geq 0 \tag{5.38}$$

Expressing Eq.(5.38) in integral form we get

$$\int_{cv} s'''_{\substack{gen,\,sys\\(non\text{-}porous)}}\, dV = \left\{\int_{cv}\frac{\partial(\rho_\alpha s_\alpha)}{\partial t}dV + \int_{cs}\frac{\vec{q}_\alpha}{T_\alpha}\cdot\hat{n}_\alpha dA + \int_{cs}\rho_\alpha \vec{u}_\alpha s_\alpha\cdot\hat{n}_\alpha\, dA\right\} + \left\{\int_{cv}\frac{\partial(\rho_\beta s_\beta)}{\partial t}dV + \int_{cs}\frac{\vec{q}_\beta}{T_\beta}\cdot\hat{n}_\beta dA\right\} \geq 0 \tag{5.39}$$

$$\dot{S}_{gen,sys(non\text{-}porous)} = \int_{cv}\left[\frac{\partial(\rho_\alpha s_\alpha)}{\partial t} + \frac{\partial(\rho_\beta s_\beta)}{\partial t}\right]dV + \int_{cs}\left[\left(\frac{\vec{q}_\alpha}{T_\alpha}\cdot\hat{n}_\alpha + \frac{\vec{q}_\beta}{T_\beta}\cdot\hat{n}_\beta\right) + \rho_\alpha \vec{u}_\alpha s_\alpha\cdot\hat{n}_\alpha\right]dA \tag{5.40}$$

Taking the cyclic integral of Eq.(5.40) over one period gives:

$$\oint_{period}\dot{S}_{\substack{gen,\,sys\\(non\text{-}porous)}}\, dt = \oint_{period}\left\{\int_{cv}\left[\frac{\partial(\rho_\alpha s_\alpha)}{\partial t} + \frac{\partial(\rho_\beta s_\beta)}{\partial t}\right]dV + \int_{cs}\left[\left(\frac{\vec{q}_\alpha}{T_\alpha}\cdot\hat{n}_\alpha + \frac{\vec{q}_\beta}{T_\beta}\cdot\hat{n}_\beta\right) + \rho_\alpha \vec{u}_\alpha s_\alpha\cdot\hat{n}_\alpha\right]dA\right\}dt \geq 0 \tag{5.41}$$

For the steady periodic process occurring in the "3-space" model, the first term in Eq.(5.41) goes to zero giving:

$$\dot{S}_{\substack{gen,\,sys,\,cyl(ext)\\(non\text{-}porous)}} = \oint_{period}\int_{cs}\left(\frac{\vec{q}_\alpha}{T_\alpha}\cdot\hat{n}_\alpha + \frac{\vec{q}_\beta}{T_\beta}\cdot\hat{n}_\beta\right)dA\,dt + \oint_{period}\int_{cs}\rho_\alpha \vec{u}_\alpha s_\alpha\cdot\hat{n}_\alpha\, dA\,dt \geq 0 \tag{5.42}$$

5.4.1.2 Porous Regions of the Stirling Convertor:

Substituting equations (5.25a and 5.25b) into Eq.(5.28) gives:

$$\left\langle s'''_{gen,sys}\right\rangle = \varepsilon_\alpha\left\{\frac{\partial\left(\left\langle\rho_\alpha\right\rangle^\alpha\left\langle s_\alpha\right\rangle^\alpha\right)}{\partial t}+\nabla\cdot\left(\left\langle\rho_\alpha\right\rangle^\alpha\left\langle s_\alpha\right\rangle^\alpha\left\langle\vec{u}_\alpha\right\rangle^\alpha\right)-\nabla\cdot\left[\frac{N_k k_\alpha}{\left\langle T_\alpha\right\rangle^\alpha}\nabla\left\langle T_\alpha\right\rangle^\alpha\right]-\frac{\alpha_v H}{\left\langle T_\beta\right\rangle^\beta}\left(\left\langle T_\beta\right\rangle^\beta-\left\langle T_\alpha\right\rangle^\alpha\right)\right\}+ \\ \varepsilon_\beta\left\{\rho_\beta\frac{\partial\left\langle s_\beta\right\rangle^\beta}{\partial t}-\frac{1}{\varepsilon_\beta}\nabla\cdot\left[k_\beta\left\langle\frac{\nabla T}{T_\beta}\right\rangle^\beta\right]+\frac{\varepsilon_\alpha\alpha_v H}{\varepsilon_\beta\left\langle T_\alpha\right\rangle^\alpha}\left(\left\langle T_\beta\right\rangle^\beta-\left\langle T_\alpha\right\rangle^\alpha\right)\right\}\geq 0 \tag{5.43}$$

Expressing Eq.(5.43) in integral form we get:

$$\int_{cv}\left\langle s'''_{gen,sys}\right\rangle_{porous}dV=\int_{cv}\varepsilon_\alpha\frac{\partial\left(\left\langle\rho_\alpha\right\rangle^\alpha\left\langle s_\alpha\right\rangle^\alpha\right)}{\partial t}dV+\int_{cs}\varepsilon_\alpha\left(\left\langle\rho_\alpha\right\rangle^\alpha\left\langle s_\alpha\right\rangle^\alpha\left\langle\vec{u}_\alpha\right\rangle^\alpha\right)\cdot\hat{n}\,dA-\int_{cs}\left[\frac{\varepsilon_\alpha N_k k_\alpha}{\left\langle T_\alpha\right\rangle^\alpha}\nabla\left\langle T_\alpha\right\rangle^\alpha\right]\cdot\hat{n}\,dA \\ -\int_{cs}\frac{\varepsilon_\alpha\alpha_v H}{\left\langle T_\beta\right\rangle^\beta}\left(\left\langle T_\beta\right\rangle^\beta-\left\langle T_\alpha\right\rangle^\alpha\right)dA+\int_{cv}\varepsilon_\beta\rho_\beta\frac{\partial\left\langle s_\beta\right\rangle^\beta}{\partial t}dV-\int_{cs}\left[k_\beta\left\langle\frac{\nabla T_\beta}{T_\beta}\right\rangle^\beta\right]\cdot\hat{n}\,dA+\int_{cs}\frac{\varepsilon_\alpha\alpha_v H}{\left\langle T_\alpha\right\rangle^\alpha}\left(\left\langle T_\beta\right\rangle^\beta-\left\langle T_\alpha\right\rangle^\alpha\right)dA\geq 0 \tag{5.44}$$

$$\dot{S}_{\substack{gen,sys\\porous}}=\int_{cv}\left[\varepsilon_\alpha\frac{\partial\left(\left\langle\rho_\alpha\right\rangle^\alpha\left\langle s_\alpha\right\rangle^\alpha\right)}{\partial t}+\varepsilon_\beta\rho_\beta\frac{\partial\left\langle s_\beta\right\rangle^\beta}{\partial t}\right]dV+\int_{cs}\varepsilon_\alpha\left(\left\langle\rho_\alpha\right\rangle^\alpha\left\langle s_\alpha\right\rangle^\alpha\left\langle\vec{u}_\alpha\right\rangle^\alpha\right)\cdot\hat{n}\,dA-\int_{cs}\left[\frac{\varepsilon_\alpha N_k k_\alpha}{\left\langle T_\alpha\right\rangle^\alpha}\nabla\left\langle T_\alpha\right\rangle^\alpha\right]\cdot\hat{n}\,dA \\ -\int_{cs}\left[\varepsilon_\beta k_\beta\left\langle\frac{\nabla T_\beta}{T_\beta}\right\rangle^\beta\right]\cdot\hat{n}\,dA\geq 0 \tag{5.45}$$

Taking the cyclic integral of Eq.(5.45) over one period gives:

$$\oint_{period}\dot{S}_{\substack{gen,sys\\porous}}dt=\oint_{period}\left\{\int_{cv}\left[\varepsilon_\alpha\frac{\partial\left(\left\langle\rho_\alpha\right\rangle^\alpha\left\langle s_\alpha\right\rangle^\alpha\right)}{\partial t}+\varepsilon_\beta\rho_\beta\frac{\partial\left\langle s_\beta\right\rangle^\beta}{\partial t}\right]dV+\int_{cs}\varepsilon_\alpha\left(\left\langle\rho_\alpha\right\rangle^\alpha\left\langle s_\alpha\right\rangle^\alpha\left\langle\vec{u}_\alpha\right\rangle^\alpha\right)\cdot\hat{n}_\alpha\,dA \\ -\int_{cs}\left[\frac{\varepsilon_\alpha N_k k_\alpha}{\left\langle T_\alpha\right\rangle^\alpha}\nabla\left\langle T_\alpha\right\rangle^\alpha\right]\cdot\hat{n}_\alpha\,dA-\int_{cs}\left[\varepsilon_\beta k_\beta\left\langle\frac{\nabla T_\beta}{T_\beta}\right\rangle^\beta\right]\cdot\hat{n}_\beta\,dA\right\}dt\geq 0 \tag{5.46}$$

$$\dot{S}_{\substack{gen,sys,cyl(ext)\\porous}}=\oint_{period}\int_{cs}\left\{\varepsilon_\alpha\left(\left\langle\rho_\alpha\right\rangle^\alpha\left\langle s_\alpha\right\rangle^\alpha\left\langle\vec{u}_\alpha\right\rangle^\alpha\right)\cdot\hat{n}_\alpha-\left[\frac{\varepsilon_\alpha N_k k_\alpha}{\left\langle T_\alpha\right\rangle^\alpha}\nabla\left\langle T_\alpha\right\rangle^\alpha\right]\cdot\hat{n}_\alpha-\left[\varepsilon_\beta k_\beta\left\langle\frac{\nabla T_\beta}{T_\beta}\right\rangle^\beta\right]\cdot\hat{n}_\beta\right\}dA\,dt\geq 0 \tag{5.47}$$

$$\dot{S}_{\substack{gen,sys,cyl(ext)\\porous}}=\oint_{period}\int_{cs}\left(\varepsilon_\alpha N_k\frac{\left\langle\vec{q}_\alpha\right\rangle^\alpha}{\left\langle T_\alpha\right\rangle^\alpha}\cdot\hat{n}_\alpha+\varepsilon_\beta\frac{\left\langle\vec{q}_\beta\right\rangle^\beta}{\left\langle T_\beta\right\rangle^\beta}\cdot\hat{n}_\beta\right)dA\,dt+\oint_{period}\int_{cs}\varepsilon_\alpha\left(\left\langle\rho_\alpha\right\rangle^\alpha\left\langle s_\alpha\right\rangle^\alpha\left\langle\vec{u}_\alpha\right\rangle^\alpha\right)\cdot\hat{n}_\beta\,dA\,dt\geq 0 \tag{5.48}$$

Eqs.(5.42 and 5.48) account for the net entropy transfer with heat and mass out of the control surface into the surrounding environment during each cycle of operation.

5.4.2 Internal Entropy Generation

Internal entropy generation can be accounted for by tallying up the individual entropy generations due to, heat transfer, viscous friction and non-equilibrium processes in all internal processes.

5.4.2.1 Non-Porous Regions of the Stirling Convertor:

Substituting equations (5.7c) and (5.7f) in Eq.(5.8) gives

$$s'''_{gen,sys} = -\frac{\vec{q}_\alpha \cdot \vec{\nabla} T_\alpha}{T_\alpha^{\,2}} + \frac{\Phi_\alpha}{T_\alpha} - \frac{\vec{q}_\beta \cdot \vec{\nabla} T_\beta}{T_\beta^{\,2}} \geq 0 \tag{5.49}$$

Expressing Eq.(5.49) in integral form we get

$$\int_{cv} s'''_{\substack{gen,sys \\ (non\text{-}porous)}} dV = -\int_{cv}\left(\frac{\vec{q}_\alpha \cdot \vec{\nabla} T_\alpha}{T_\alpha^{\,2}} + \frac{\vec{q}_\beta \cdot \vec{\nabla} T_\beta}{T_\beta^{\,2}}\right) dV + \int_{cv} \frac{\Phi_\alpha}{T_\alpha} dV \geq 0 \tag{5.50}$$

$$\dot{S}_{gen,sys(non\text{-}porous)} = -\int_{cv}\left(\frac{\vec{q}_\alpha \cdot \vec{\nabla} T_\alpha}{T_\alpha^{\,2}} + \frac{\vec{q}_\beta \cdot \vec{\nabla} T_\beta}{T_\beta^{\,2}}\right) dV + \int_{cv} \frac{\Phi_\alpha}{T_\alpha} dV \geq 0 \tag{5.51}$$

Taking the cyclic integral of Eq. (5.51) over one period gives:

$$\dot{S}_{gen,cyl(int)} = -\oint_{period}\int_{cv}\left(\frac{\vec{q}_\alpha \cdot \vec{\nabla} T_\alpha}{T_\alpha^{\,2}} + \frac{\vec{q}_\beta \cdot \vec{\nabla} T_\beta}{T_\beta^{\,2}}\right) dV\,dt + \oint_{period}\int_{cv} \frac{\Phi_\alpha}{T_\alpha} dV\,dt \geq 0 \tag{5.52}$$

Note that:

$$\frac{\vec{q}\cdot\vec{\nabla}T}{T^2} = \frac{k}{T^2}\left[\left(\frac{\partial T}{\partial x}\right)^2 + \left(\frac{\partial T}{\partial y}\right)^2 + \left(\frac{\partial T}{\partial z}\right)^2\right] \tag{5.53}$$

$$\frac{\Phi}{T} = \frac{1}{T}\left\{(-2/3)\mu\left(\vec{\nabla}\cdot\vec{u}\right)^2 + 2\mu\left[\left(\frac{\partial u}{\partial x}\right)^2 + \left(\frac{\partial v}{\partial y}\right)^2 + \left(\frac{\partial w}{\partial z}\right)^2\right] + \mu\left[\left(\frac{\partial v}{\partial x}+\frac{\partial u}{\partial y}\right)^2 + \left(\frac{\partial w}{\partial y}+\frac{\partial v}{\partial z}\right)^2 + \left(\frac{\partial u}{\partial z}+\frac{\partial w}{\partial x}\right)^2\right]\right\} \tag{5.54}$$

Eq.(5.52) accounts for the internal entropy generation in a reciprocating engine like the Stirling convertor or the MIT test rig. From Eqs.(5.53 and 5.54), we see that the first term on the right-hand side of Eq. (5.52) which involves the squares of the temperature gradients is the entropy generation due to conductive heat flow while the second term which involves the squares of the velocity gradients is the contribution due to viscous

dissipation which accounts for mixing loss in the flow field. Mixing loss is generated by mixing of the flow field due to the shear stress between fluid layers, vortices resulting from wall flow separation or shed vortices in the core of the fluid.

Equation (5.52) seems to imply that the internal thermodynamic losses can be minimized by minimizing the magnitude of these local temperature and velocity gradients and the sum of their squares, throughout the domain of interest. These measures are however difficult or impractical to implement. For example, it is not practical to reduce the fluid viscosity which would lead to a reduction of the velocity gradients at the wall and the boundary layer viscous losses. Also, it is not practical to increase the fluid thermal conductivity which would reduce the temperature gradients at the wall, and the conductive heat transfer loss.

A control volume approach can be used quite successfully to calculate the viscous dissipation term and hence the total mixing loss. Errors in the mixing loss are likely to be small, since all mixing processes obey the fundamental conservation equations that also govern the behavior of the numerical predictions. The difficulties found in using numerical predictions to estimate the mixing losses are thought to be due to false entropy due to numerical dissipation [10]. Although mixing is only a relatively short-lived phenomenon as the flow eventually mixes out completely, it is a major contributor to the total loss. This is especially true for turbulent flows where the effective viscosity is very large.

5.4.2.2 Porous Regions of the Stirling Convertor:

Expressing the system entropy generation equation, Eq.(5.29), in integral form gives

$$\int_{cv} \left\langle s'''_{gen,sys} \right\rangle^{\alpha} dV = \int_{cv} \left\{ \varepsilon_{\alpha} N_k k_{\alpha} \left(\frac{\nabla \langle T_{\alpha} \rangle^{\alpha}}{\langle T_{\alpha} \rangle^{\alpha}} \right)^2 + \varepsilon_{\beta} k_{\beta} \left(\frac{\nabla \langle T_{\beta} \rangle^{\beta}}{\langle T_{\beta} \rangle^{\beta}} \right)^2 \right\} dV + \int_{cv} \left(\frac{\varepsilon_{\alpha} \alpha_v H}{\langle T_{\alpha} \rangle^{\alpha} \langle T_{\beta} \rangle^{\beta}} \left| \langle T_{\beta} \rangle^{\beta} - \langle T_{\alpha} \rangle^{\alpha} \right|^2 \right) dV$$
$$- \int_{cv} \left(\varepsilon_{\alpha} \frac{\langle \vec{u}_{\alpha} \rangle^{\alpha}}{\langle T_{\alpha} \rangle^{\alpha}} \nabla \langle p_{\alpha} \rangle^{\alpha} \right) dV \geq 0 \qquad (5.55)$$

Taking the cyclic integral of Eq.(5.55) over one period gives:

$$\dot{S}_{gen,cyl\ (int)} = \oint_{period}\int_{cv}\left\{\varepsilon_\alpha N_k k_\alpha\left(\frac{\nabla\langle T_\alpha\rangle^\alpha}{\langle T_\alpha\rangle^\alpha}\right)^2 + \varepsilon_\beta k_\beta\left(\frac{\nabla\langle T_\beta\rangle^\beta}{\langle T_\beta\rangle^\beta}\right)^2\right\}dV\,dt + \oint_{period}\int_{cv}\left(\frac{\varepsilon_\alpha\alpha_v H}{\langle T_\alpha\rangle^\alpha\langle T_\beta\rangle^\beta}\left|\langle T_\beta\rangle^\beta - \langle T_\alpha\rangle^\alpha\right|^2\right)dV\,dt$$
$$- \oint_{period}\int_{cv}\left(\varepsilon_\alpha\frac{\langle\vec{u}_\alpha\rangle^\alpha}{\langle T_\alpha\rangle^\alpha}\nabla\langle p_\alpha\rangle^\alpha\right)dV\,dt \geq 0 \qquad (5.56)$$

For a multiport flow system's control volume the general entropy balance which is a statement of the second law can be written as [4]

$$\dot{S}_{gen} = \frac{dS}{dt} - \sum_r \dot{Q}_r / T_r + \sum_e \dot{m}_e s_e - \sum_i \dot{m}_i s_i \geq 0 \qquad (5.57)$$

The left-hand side of Eq. (5.30) represents the rate entropy is generated within the control volume while the right-hand side represents the rate of entropy accumulation inside the control volume minus entropy transfer rate into the control volume via heat transfer plus net entropy flow rate out of the control volume via mass flow. The second law stipulates that entropy generation must be non-negative in all thermo-physical processes. The parameters S, $\dot{Q}_r$, T_r, $\dot{m}$ and s denote, respectively, the total entropy, the rate at which heat is transferred into the system, the absolute temperature, the mass flow rate and the mass specific entropy. The subscripts i, e and r denote, respectively, inlet port, exit port and region on the system boundary across which heat is transferred.

5.4.3 Availability Energy Loss

All internal entropy generations can be characterized in terms of availability energy loss defined as [8]:

$$\text{Availability Loss} = W_{rev} - W_{irrev} \qquad (5.58)$$

where W_{rev} and W_{irrev} ($< W_{rev}$) are the net mechanical work available from reversible and irreversible heat engines respectively; both obtained from the same heat input $\dot{Q}_{in}$ and

operating between a high temperature reservoir at temperature T_H and a low temperature reservoir at temperature T_L.

The efficiency of an irreversible heat engine is defined as [8]

$$\eta_{th} = \frac{\dot{W}_{irrev}}{\dot{Q}_{in}} = 1 - \frac{\dot{Q}_{out,irrev}}{\dot{Q}_{in}} \tag{5.59}$$

From this definition, the net heat outflow for the irreversible heat engine $\dot{Q}_{out,irrev}$ should be greater than the net heat outflow for the reversible heat engine, $\dot{Q}_{out,rev}$.

For the reversible heat engine [8]

$$\eta_{th,rev} = \frac{\dot{W}_{rev}}{\dot{Q}_{in}} = 1 - \frac{T_L}{T_H} \tag{5.60}$$

where the Kelvin thermodynamic temperature scale $\left(\dot{Q}_{in}/\dot{Q}_{out}\right)_{rev} = T_H/T_L$ has been used [8].

Thus:
$$\dot{W}_{rev} = \dot{Q}_{in}\left(1 - \frac{T_L}{T_H}\right) \tag{5.61}$$

and
$$\dot{W}_{irrev} = \dot{Q}_{in}\left(1 - \frac{\dot{Q}_{out,irrev}}{\dot{Q}_{in}}\right) \tag{5.62}$$

Substituting Eqs. (5.34 and 5.35) in Eq. (5.31) gives, after simplification:

$$\text{Availability Loss} = -T_L\left(\frac{\dot{Q}_{in}}{T_H} - \frac{\dot{Q}_{out,irrev}}{T_L}\right) \tag{5.63}$$

For steady periodic process in a closed system, $\frac{dS}{dt} = 0$ and $\dot{m} = 0$. Substituting the simplified Eq. (5.30) in Eq. (5.36):

$$\text{Availability Loss} = T_L\dot{S}_{gen} \tag{5.64}$$

Evaluation of the external entropy generation equations (5.42 and 5.52) and internal entropy generation equations (5.48 and 5.56) enable the corresponding availability energy loss calculations using Equation (5.37). The availability-loss concept allows us to think about entropy generation in terms of the more concrete notion of lost mechanical work. A loss in availability equates to a decrease of PV power in an engine. For example, in turbo-machines that generate shaft power (turbines) or absorb power (pumps, compressors), the rate of power lost owing to irreversibilities is proportional to a loss in availability and thus to the rate of entropy generation. Increase in entropy gives a measure of the extent to which the energy of a system is lost or unavailable for work during a certain process. It is therefore desirable to study the various mechanisms responsible for entropy generation in order to minimize it in engineering equipment.

Loss analysis using entropy-generation rates due to heat, fluid flow and non-equilibrium processes is a relatively new technique for assessing component performance. It offers a deep insight into the flow phenomena, allows a more exact calculation of losses than is possible with traditional means involving the application of loss correlations and provides an effective tool for improving performance. Entropy generation maps of cumulative amounts of all losses computed locally in the flow domain can be produced and designers can use them to detect critical areas (locations in which entropy generation is higher than its integral average value over the entire flow field). The design emphasis would then be aimed at avoiding the critical areas or reducing the local values for entropy production in these critical areas by modifying design variables so as to maintain the required overall performance.

Our understanding of loss mechanisms is however far from complete. Although

numerical predictions are valuable in predicting the heat transfer and flow structure, there are difficulties in predicting the loss accurately. This is due to errors in predicting the boundary layers, transition as well as due to false entropy generation due to numerical dissipation. This work provides a point of reference for incorporation of loss post-processors into Stirling engine numerical codes. The incorporation of a loss post-processor in Stirling engine numerical codes, it is believed, will facilitate the optimization of Stirling engine performance.

5.5 Summary of Relevant Equations

The relevant equations are repeated here for convenience.

"Local or "Microscopic" Equations **Volume-Averaged Equations**

Conservation of Mass

$$\frac{\partial \rho_\alpha}{\partial t} + \nabla\cdot(\rho_\alpha \vec{u}_\alpha) = 0 \qquad (5.65)$$

$$\frac{\partial}{\partial t}\langle \rho_\alpha\rangle^\alpha + \nabla\cdot\left(\langle\rho_\alpha\rangle^\alpha\langle\vec{u}_\alpha\rangle^\alpha\right) = 0 \qquad (5.66)$$

Conservation of Momentum Equations

$$\frac{\partial(\rho_\alpha\vec{u}_\alpha)}{\partial t} + \vec{\nabla}\cdot(\rho_\alpha\vec{u}_\alpha\vec{u}_\alpha) + \vec{\nabla}p_\alpha - \frac{1}{3}\vec{\nabla}(\mu_\alpha\vec{\nabla}\cdot\vec{u}_\alpha) - (\vec{\nabla}\cdot\mu_\alpha\vec{\nabla})\vec{u}_\alpha + \frac{2}{3}(\vec{\nabla}\mu_\alpha)\vec{\nabla}\cdot\vec{u}_\alpha - 2(\vec{\nabla}\mu_\alpha\cdot\vec{\nabla})\vec{u}_\alpha - (\vec{\nabla}\mu_\alpha x\vec{\Omega}_\alpha) = 0 \qquad (5.67)$$

$$\frac{\partial}{\partial t}\left(\langle\rho_\alpha\rangle^\alpha\langle\vec{u}_\alpha\rangle^\alpha\right) + \nabla\cdot\left(\langle\rho_\alpha\rangle^\alpha\langle\vec{u}_\alpha\rangle^\alpha\langle\vec{u}_\alpha\rangle^\alpha\right) + \nabla\langle p_\alpha\rangle^\alpha + \frac{1}{V_\alpha}\int_{A_{\alpha\beta}} n_\alpha\cdot\left[\tilde{I}\left(\hat{p}_\alpha + n_\alpha\frac{\mu_\alpha}{3}\nabla\cdot\hat{u}_\alpha\right) + \mu_\alpha\nabla\hat{u}_\alpha\right]dS + \varepsilon_\alpha\left[2\left(\vec{\nabla}\langle\mu_\alpha\rangle^\alpha\cdot\vec{\nabla}\right)\langle\vec{u}_\alpha\rangle^\alpha + \left(\vec{\nabla}\langle\mu_\alpha\rangle^\alpha\right)x\langle\vec{\Omega}_\alpha\rangle^\alpha + \frac{2}{3}\left(\vec{\nabla}\langle\mu_\alpha\rangle^\alpha\right)^2\right] = 0 \qquad (5.68)$$

Or, in weak conservation form:

$$\langle\rho_\alpha\rangle^\alpha\frac{\partial}{\partial t}\langle\vec{u}_\alpha\rangle^\alpha + \langle\rho_\alpha\rangle^\alpha\langle\vec{u}_\alpha\rangle^\alpha\nabla\cdot\langle\vec{u}_\alpha\rangle^\alpha + \nabla\langle p_\alpha\rangle^\alpha + \frac{1}{V_\alpha}\int_{A_{\alpha\beta}} n_\alpha\cdot\left[\tilde{I}\left(\hat{p}_\alpha + n_\alpha\frac{\mu_\alpha}{3}\nabla\cdot\hat{u}_\alpha\right) + \mu_\alpha\nabla\hat{u}_\alpha\right]dS + \varepsilon_\alpha\left[2\left(\vec{\nabla}\langle\mu_\alpha\rangle^\alpha\cdot\vec{\nabla}\right)\langle\vec{u}_\alpha\rangle^\alpha + \left(\vec{\nabla}\langle\mu_\alpha\rangle^\alpha\right)x\langle\vec{\Omega}_\alpha\rangle + \frac{2}{3}\left(\vec{\nabla}\langle\mu_\alpha\rangle^\alpha\right)^2\right] = 0 \qquad (5.69)$$

Conservation of Energy Equations

α- phase

$$\frac{\partial(\rho_\alpha\hat{u}_\alpha)}{\partial t} + \vec{\nabla}\cdot\left(\rho_\alpha\vec{u}_\alpha h_\alpha - k_\alpha\vec{\nabla}T_\alpha\right) = 0 \qquad (5.70a)$$

$$\frac{\partial(\rho_\alpha\hat{u}_\alpha)}{\partial t} + \vec{\nabla}\cdot(\rho_\alpha\vec{u}_\alpha\hat{u}_\alpha) = \vec{\nabla}\cdot\left(k_\alpha\vec{\nabla}T_\alpha\right) + \Phi_\alpha - p_\alpha\vec{\nabla}\cdot\vec{u}_\alpha \qquad (5.70b)$$

$$\rho_\alpha\frac{Dh_\alpha}{Dt} = \vec{\nabla}\cdot\left(k_\alpha\vec{\nabla}T_\alpha\right) + \Phi_\alpha + \frac{Dp_\alpha}{Dt} \qquad (5.70c)$$

β- phase

$$(\rho c)_\beta\frac{\partial T_\beta}{\partial t} - \vec{\nabla}\cdot\left(k_\beta\vec{\nabla}T_\beta\right) = 0 \qquad (5.70d)$$

α-phase

$$\frac{\partial}{\partial t}\left(\langle\rho_\alpha\rangle^\alpha\langle\hat{u}_\alpha\rangle^\alpha\right) + \nabla\cdot\left(\langle\rho_\alpha\rangle^\alpha\langle\vec{u}_\alpha\rangle^\alpha\langle h_\alpha\rangle^\alpha - N_k k_\alpha\nabla\langle T_\alpha\rangle^\alpha\right) - a_v H\left(\langle T_\beta\rangle^\beta - \langle T_\alpha\rangle^\alpha\right) = 0 \qquad (5.71a)$$

β-phase

$$(\rho c)_\beta\frac{\partial\langle T_\beta\rangle^\beta}{\partial t} - \nabla\cdot\left[k_\beta\tau_\beta\nabla\langle T_\beta\rangle^\beta\right] + \frac{\varepsilon_\alpha}{\varepsilon_\beta}a_v H\left(\langle T_\beta\rangle^\beta - \langle T_\alpha\rangle^\alpha\right) = 0 \qquad (5.71b)$$

Equations of State:

$$p_\alpha = f_1(\rho_\alpha, \hat{u}_\alpha) \qquad (5.72)$$

$$T_\alpha = f_2(\rho_\alpha, \hat{u}_\alpha) \qquad (5.73)$$

Entropy Generation Equations

$$s'''_{gen,\alpha} = \frac{\partial(\rho_\alpha s_\alpha)}{\partial t} + \vec{\nabla}\cdot(\rho_\alpha s_\alpha \vec{u}_\alpha) + \vec{\nabla}\cdot\left(\frac{\vec{q}_\alpha}{T_\alpha}\right) \geq 0 \quad (5.74a)$$

$$s'''_{gen,\alpha} = \rho_\alpha \frac{Ds_\alpha}{Dt} - \frac{\vec{q}_\alpha\cdot\vec{\nabla}T_\alpha}{T_\alpha^2} + \frac{\vec{\nabla}\cdot\vec{q}_\alpha}{T_\alpha} \geq 0 \quad (5.74b)$$

$$s'''_{gen,\alpha} = -\frac{\vec{q}_\alpha\cdot\vec{\nabla}T_\alpha}{T_\alpha^2} + \frac{\Phi_\alpha}{T_\alpha} \geq 0 \quad (5.74c)$$

$$s'''_{gen,\beta} = \frac{\partial(\rho_\beta s_\beta)}{\partial t} + \vec{\nabla}\cdot\left(\frac{\vec{q}_\beta}{T_\beta}\right) \geq 0 \quad (5.74d)$$

$$s'''_{gen,\beta} = \rho_\beta\frac{\partial(s_\beta)}{\partial t} - \frac{\vec{q}_\beta\cdot\vec{\nabla}T_\beta}{T_\beta^2} + \frac{\vec{\nabla}\cdot\vec{q}_\beta}{T_\beta} \geq 0 \quad (5.74e)$$

$$s'''_{gen\beta} = -\frac{\vec{q}_\beta\cdot\vec{\nabla}T_\beta}{T_\beta^2} \geq 0 \quad (5.74f)$$

$$\langle s'''_{\alpha,gen}\rangle^\alpha = N_k k_\alpha\left(\frac{\nabla\langle T_\alpha\rangle^\alpha}{\langle T_\alpha\rangle^\alpha}\right)^2 + \frac{\alpha_v H}{\langle T_\alpha\rangle^\alpha\langle T_\beta\rangle^\beta}\left|\langle T_\beta\rangle^\beta - \langle T_\alpha\rangle^\alpha\right|^2 - \frac{\langle\vec{u}_\alpha\rangle^\alpha}{\langle T_\alpha\rangle^\alpha}\nabla\langle p_\alpha\rangle^\alpha \quad (5.74g)$$

$$\langle s'''_{\beta,gen}\rangle^\beta = k_\beta\left(\frac{\nabla\langle T_\beta\rangle^\beta}{\langle T_\beta\rangle^\beta}\right)^2 + \frac{\varepsilon_\alpha\alpha_v H}{\varepsilon_\alpha\langle T_\alpha\rangle^\alpha\langle T_\beta\rangle^\beta}\left|\langle T_\beta\rangle^\beta - \langle T_\alpha\rangle^\alpha\right|^2 \quad (5.74h)$$

Second Law Analysis via Entropy Generation

External Entropy Generation

Non-Porous Regions of the Stirling Convertor:

$$\dot{S}_{\substack{gen,sys,\,cyl(ext)\\(non\text{-}porous)}} = \oint_{period}\int_{cs}\left(\frac{\vec{q}_\alpha}{T_\alpha}\cdot\hat{n}_\alpha + \frac{\vec{q}_\beta}{T_\beta}\cdot\hat{n}_\beta\right)dA\,dt + \oint_{period}\int_{cs}\rho_\alpha\vec{u}_\alpha s_\alpha\cdot\hat{n}_\alpha\,dA\,dt \geq 0 \quad (5.75)$$

Porous Regions of the Stirling Convertor:

$$\dot{S}_{\substack{gen,sys,cyl(ext)\\porous}} = \oint_{period}\int_{cs}\left(\varepsilon_\alpha N_k\frac{\langle\vec{q}_\alpha\rangle^\alpha}{\langle T_\alpha\rangle^\alpha}\cdot\hat{n}_\alpha + \varepsilon_\beta\frac{\langle\vec{q}_\beta\rangle^\beta}{\langle T_\beta\rangle^\beta}\cdot\hat{n}_\beta\right)dA\,dt + \oint_{period}\int_{cs}\varepsilon_\alpha\left(\langle\rho_\alpha\rangle^\alpha\langle s_\alpha\rangle^\alpha\langle\vec{u}_\alpha\rangle^\alpha\right)\cdot\hat{n}_\beta\,dA\,dt \geq 0 \quad (5.76)$$

Internal Entropy Generation

Non-Porous Regions of the Stirling Convertor:

$$\dot{S}_{gen,cyl(int)} = -\oint_{period}\int_{cv}\left(\frac{\vec{q}_\alpha\cdot\vec{\nabla}T_\alpha}{T_\alpha^2} + \frac{\vec{q}_\beta\cdot\vec{\nabla}T_\beta}{T_\beta^2}\right)dV\,dt + \oint_{period}\int_{cv}\frac{\Phi_\alpha}{T_\alpha}dV\,dt \geq 0 \quad (5.77)$$

Note that: $\frac{\vec{q}\cdot\vec{\nabla}T}{T^2} = \frac{k}{T^2}\left[\left(\frac{\partial T}{\partial x}\right)^2 + \left(\frac{\partial T}{\partial y}\right)^2 + \left(\frac{\partial T}{\partial z}\right)^2\right]$; $\frac{\Phi}{T} = \frac{1}{T}\left\{(-2/3)\mu(\vec{\nabla}\cdot\vec{u})^2 + 2\mu\left[\left(\frac{\partial u}{\partial x}\right)^2 + \left(\frac{\partial v}{\partial y}\right)^2 + \left(\frac{\partial w}{\partial z}\right)^2\right] + \mu\left[\left(\frac{\partial v}{\partial x}+\frac{\partial u}{\partial y}\right)^2 + \left(\frac{\partial w}{\partial y}+\frac{\partial v}{\partial z}\right)^2 + \left(\frac{\partial u}{\partial z}+\frac{\partial w}{\partial x}\right)^2\right]\right\}$ (5.45) (5.78)

Porous Regions of the Stirling Convertor:

$$\dot{S}_{gen,cyl\,(int)} = \oint_{period}\int_{cv}\left\{\varepsilon_\alpha N_k k_\alpha\left(\frac{\nabla\langle T_\alpha\rangle^\alpha}{\langle T_\alpha\rangle^\alpha}\right)^2 + \varepsilon_\beta k_\beta\left(\frac{\nabla\langle T_\beta\rangle^\beta}{\langle T_\beta\rangle^\beta}\right)^2\right\}dV\,dt + \oint_{period}\int_{cv}\left(\frac{\varepsilon_\alpha\alpha_v H}{\langle T_\alpha\rangle^\alpha\langle T_\beta\rangle^\beta}\left|\langle T_\beta\rangle^\beta - \langle T_\alpha\rangle^\alpha\right|^2\right)dV\,dt - \oint_{period}\int_{cv}\left(\varepsilon_\alpha\frac{\langle\vec{u}_\alpha\rangle^\alpha}{\langle T_\alpha\rangle^\alpha}\nabla\langle p_\alpha\rangle^\alpha\right)dV\,dt \geq 0 \quad (5.79)$$

Eq. (5.30) in Eq. (5.36): $\text{Availability Loss} = T_L\dot{S}_{gen}$ (5.80)

CHAPTER VI

NUMERICAL SIMULATION RESULTS

6.1 Introduction

In the prior study cited above [13], extensive numerical simulations of the fluid flow and heat transfer phenomena (velocity, temperature, pressure, heat transfer rate, etc.) under conditions of oscillating pressure and oscillating fluid flow inside the original MIT "2-space" solution domain were performed using 1-D Sage and 2-D CFD-ACE+ numerical codes. In this study, similar numerical simulation results were obtained for a "3-space" solution domain using 1-D Sage and 2-D Fluent numerical codes in order to observe the effect of a regenerator. The Run F configuration of the "3-space" model (see Table 2) is used except that the cylinder wall temperature is reset to 294 K to match the cylinder wall temperature of the original "2-space" model. From Figure 6, optimum cylinder-cooling effect (COP = 0.69647) is observed at a regenerator length of 20 cm. The optimum linear dimension of the regenerator is thus set at 20 cm. (with a corresponding 24.5 cm heat exchanger length) for numerical simulations. Note that the numerical simulation results in the regenerator are obtained using the thermal non-equilibrium porous-media model discussed in Chapter 5.

In this study, energy conservation, temperature and pressure values (mean and crank angle dependent), pressure-volume diagrams and wall heat transfer rate for the "2-space" and "3-space" models are compared, noting the effect of the regenerator where possible. Also, results of heat exchanger surface heat fluxes, temperature differences between the gas temperature at the radial center of the heat exchanger and the heat exchanger wall, domain temperature contours and velocity vectors obtained in these models are compared with some results obtained from the literature [25, 34, 40]. Also entropy generation and availability loss results obtained from 2nd Law analysis post processing are presented and discussed.

Prior to performing the 2-D numerical simulations, the grid size (m x n) and number of cycles of piston motion N_{cycles} were optimized using three analysis techniques for purposes of comparison: line probe, root mean square (rms) and energy conservation and the time step Δt was chosen so that the Courant condition [24] was satisfied. A summary of the results for the optimum grid size, number of cycles and time step is shown on Table 3 below:

Table 3. Summary of Results for Optimum Grid size, Number of Cycles and Time step

Analysis Type	**Gas Spring+Heat Exchanger**† (Operating Conds.: 201.7 RPM, 1.008 MPa, T_{wall} = 294 K)			**Gas Spring+Heat Exchanger+Regenerator**‡ (Operating Conds.: 201.7 RPM, 1.008 MPa, T_{wall} = 294 K)		
	Optimum Values			**Optimum Values**		
	Grid size	Cycle	Δt s. (#tspc)	Grid size	Cycle	Δt s. (#tspc)
Line Probe	147 x 46	6	**6.19E-04 (480)**	147 x 46	6	**6.19E-04 (480)**
RMS	147 x 46	5		147 x 46	5	
Energy Conserv.	147 x 46	7		147 x 46	6	
AVG.	**147 x 46**	**6**		**147 x 46**	**6**	

† Using the CFD-ACE+ code; ‡ Using the Fluent code

The values in bold type are the optimum values for the control parameters (grid size, number of cycles of piston motion and time step (or number of time steps per cycle)) employed in the CFD-ACE+ and Fluent codes for the 2-D "2-space" and "3-space" numerical simulations respectively. The optimum values for the control parameters for the "2-space" and "3-space" domains are identical on the average. Details of the numerical optimization and simulation techniques that produced the "2-space" results shown on Table 3 are discussed in [13].

6.2 1-D Sage code vs. 2-D CFD code (CFD-ACE+ or Fluent) Results

Results of energy conservation, temperature and pressure values (mean and crank angle dependent), pressure-volume diagrams and wall heat transfer rate for the "2-space" and "3-space" models are compared. To ensure a common basis for comparison between Sage and CFD-ACE+/Fluent results, the begining point for the piston motion is taken at BDC moving toward TDC. The volume swept in one cycle of the piston motion starting from this reference position is calculated in Sage and CFD-ACE/Fluent and verified to be the same (617.8 m^3).

6.2.1. Energy Conservation

The energy conservation principle can be expressed per unit time for a closed system undergoing a cyclic process in differential form as follows:

$$\oint \delta \dot{Q} = \oint \delta \dot{W} \tag{6.1}$$

For our study, the mechanical work is associated with the expansion and compression of a gas in a piston-cylinder device. During this process, the inner face of the piston moves back and forth. Therefore, the expansion and compression work is a moving boundary work or PdV work. Strictly speaking, the pressure is the pressure at the inner surface of

the piston. It becomes equal to the pressure of the gas in the cylinder only if the process is quasi-equilibrium and thus the entire gas in the cylinder is at the same pressure at any given time. For non-quasi-equilibrium processes such as we have, the pressure at the inner face of the piston P_i is used for P. Thus the equation relevant to our study is

$$\frac{1}{T}\oint \delta Q = \frac{1}{T}\oint P_i dV \tag{6.2}$$

The parameter T is the period of the cycle. The Q and P_i output data files created using the surface monitor option in Fluent are exported to an Excel spread sheet where $\oint \delta Q/T$ is calculated by first summing the δQ data over the total number of time steps in the 6th cycle and then dividing the sum by the period T and $\int PdV/T$ is computed using Simpson's integration rule over the total number of time steps in the 6th cycle viz:

$$\frac{1}{T}\oint P_i dV = \frac{1}{T}\left[\sum_{n=1}^{\#tspc}\left(\frac{P_i^{\,n} + P_i^{\,n-1}}{2}\right)\left(V^n - V^{n-1}\right)\right] \tag{6.3}$$

The superscripts n and n-1 imply values at the current and previous time steps respectively. The volume V is calculated by multiplying the piston displacement during a given time step by the piston area. Sage output results provide mean values of the heat transfer rate and pressure which are equivalent to the integral parameters $\oint \delta Q/T$ and $\oint P_i dV/T$ respectively. The energy conservation results are shown in Table 3 below.

Table 4. Energy Conservation Results with the incorporation of the β weighting factor

Domain	**Gas Spring + Heat Exchanger** (Op. Conds.: 201.7 RPM, 1.008 MPa, T_{wall} = 294 K,)			**Gas Spring + Heat Exchanger + Regenerator** (Op. Conds.: 201.7 RPM, 1.008 MPa, T_{wall} = 294 K,)		
Code	$\oint \delta Q / T$ (W/K)	$\oint P_i dV / T$ (W/K)	% Diff.	$\oint \delta Q / T$ (W/K)	$\oint P_i dV / T$ (W/K)	% Diff.
Sage	-29.87680382	-29.9502915	0.2460	-22.37000440	-22.37000149	0.0000
CFD-ACE+/ Fluent‡	-53.28309808	-53.24190164	0.0773	-40.18477383	-40.188166053	0.0084
% Diff.	43.9282	43.7468		44.3321	44.3368	

‡ Grid size (m x n) = 147 x 46; N_{cycles} = 6, Δt = 6.19E-04 (#tspc = 480)

Sage and CFD-ACE+ numerical codes were employed for the "2-space" model (gas spring + heat exchanger) and Sage and Fluent codes for the "3-space" model (gas spring + heat exchanger + regenerator). Recktenwald [34] modified Eq.(6.3) by introducing the work term weighting factor β to reduce the error introduced by the discretization of the pressure-volume work term viz.:

$$\oint P_i dV = \sum_{n=1}^{\#tspc} \left[\beta P_i^{\,n} + (1-\beta) P_i^{\,n-1} \right] \left(V^n - V^{n-1} \right) \tag{6.4}$$

The discretization is controlled by adjusting β to obtain cycle energy balance. A β value of 1.49 was obtained for both the "2-space" and "3-space" models. The energy balance is significantly improved for the "3-space" model.

6.2.2 Mean Temperature and Pressure

Using the CFD-ACE+/Fluent code, mean fluid temperature and pressure values in the cylinder and heat-exchanger domains of the "2-space" model and in the cylinder, heat-

exchanger and regenerator domains of the "3-space" model are computed from the instantaneous temperatures and pressures obtained over a cycle of piston motion beginning at TDC. In the cylinder domain, a stationary point probe/rake is placed near the center of the inner face of the piston. In the heat exchanger and regenerator domains the probe/rake is placed at the domain center. Temperature and pressure data are exported to an Excel spreadsheet for calculation of mean values over the cycle. In Sage, mean temperature and pressure values for the domain of interest are obtained directly from the output results. The computed mean temperature and mean pressure values are illustrated in Table 5 below.

Table 5. Mean Temperature and Pressure Results

Parameter	Sage	CFD-ACE+	| % Diff. |
	Gas Spring + Heat Exchanger (Op. Conds.: 201.7 RPM, 1.008 MPa, T_{wall} =300/294K)		
	Cylinder Space		
Mean Temp. (K)	290.683845	277.8699639	4.6115
Mean Press. (Pa)	1007850.348	1022670.288	1.4491
	Heat Exchanger Space		
Mean Temp. (K)	294.798084	297.938805	1.0598
Mean Press. (Pa)	1008006.055	1022678.103	1.4347
Parameter	Sage	Fluent	| % Diff. |
	Gas Spring + Heat Exchanger + Regenerator (Op. Conds.: 201.7 RPM, 1.008 MPa, T_{wall} =300/294K)		
	Cylinder Space		
Mean Temp. (K)	289.400004	278.638365	3.7186
Mean Press. (Pa)	1007999.999	1008002.173	0.0002
	Heat Exchanger Space		
Mean Temp. (K)	294.900000	297.037220	0.7195
Mean Press. (Pa)	1008000.032	1008002.173	0.0002
	Regenerator Space		
Mean Temp. (K)	339.500000	296.68	12.61
Mean Press. (Pa)	1008000.032	1008012.185	0.0012

Note that T_{wall} was specified at 300 K and 294 K in Sage and CFD-ACE+/Fluent respectively. In the gas spring + heat exchanger model, the CFD-ACE+ predicted mean temperature in the cylinder was almost 5% lower than predicted by Sage, but in the heat exchanger was about 1.1% higher than predicted by Sage. The CFD-ACE+ mean pressure predictions indicate that the initial pressure in the cylinder and in the heat exchanger needed to be adjusted downward by about 1.5% in order to match the Sage predictions. In the gas spring + heat exchanger + regenerator model, 1-D Sage and Fluent mean temperature predictions are closest in agreement (~0.72% difference) in the heat exchanger space with the greatest divergence observed in the regenerator space (~12.61% difference). In the cylinder space, the Fluent predicted mean temperature is about 3.72% lower than predicted by Sage. The mean pressure predictions are essentially equivalent in each domain. The addition of the regenerator appears to improve the correspondence between Sage and Fluent temperature and pressure measurements in the cylinder and heat exchanger spaces, with essentially negligible difference in the pressure measurements.

6.2.3 Temperature and Pressure vs. Crank Angle

Temperature and pressure profiles in the "2-space" and "3-space" models over a cycle of piston motion, obtained using CFD-ACE+/Fluent and Sage codes, are illustrated in Figs. 8(a, b, c and d) as functions of crank angle, θ, calculated using:

$$\text{Crank Angle, } \theta = \left[(\omega t + 3\pi/2)\cdot 180/\pi + 270\right]/360 \tag{6.5}$$

The parameter ω is angular frequency and t is time. The use of crank angle enables comparison at the same piston position.

In CFD-ACE+/Fluent, instantaneous temperatures and pressures over a cycle of piston motion are obtained at specified points in the domain of interest and for two cases: with the

points stationary and with the points (grid points) moving with the piston motion. Temperature and pressure data are taken in the cylinder space for stationary and moving points and in the heat exchanger and regenerator spaces for stationary points only. The same initial x-y coordinates are assigned the stationary and moving points. The x=0 point of reference is the cylinder head, with the positive direction toward the piston (and the negative direction toward the closed end of the heat exchanger/regenerator for the "2-space"/"3-space" domain). The y=0 point of reference is the line of symmetry. Note that for the moving grid point, grid node numbers are used as coordinates to tag their locations.

In Sage, the equation

$$\Phi_i = \overline{\Phi} + \sum_{n=1}^{3} A_n \cos(n\omega t_i + \varphi), \quad i = 1,2,...,\#\text{tspc} \tag{6.6}$$

is used to calculate the instantaneous values, Φ_i, of the data of interest Φ (temperature or pressure) over the number of time steps per cycle (#tspc). Each of the instantaneous values Φ_i is equal to the sum of the mean value, $\overline{\Phi}$, and three Fourier cosine harmonics of the piston motion at each time step. The parameter A is the amplitude of Φ and φ is the phase angle. $\overline{\Phi}$, A and φ are obtained from Sage output results. Note that Sage values are spatially averaged values over the domain.

Sage and CFD-ACE+/Fluent pressure and temperature profiles in the "2-space" and "3-space" models as functions of the crank angle are shown in Figs. 8(a-l). The legends in the Figures show the x-coordinates (x-nodes) of the specified points. The y-coordinate (0.0132673 m) or y-node (9) is kept constant in each domain of interest.

The cylinder space temperature profiles for three stationary points and three moving grid points are illustrated in Figs. 8(a-d) below.

"2-space" model **"3-space" model**

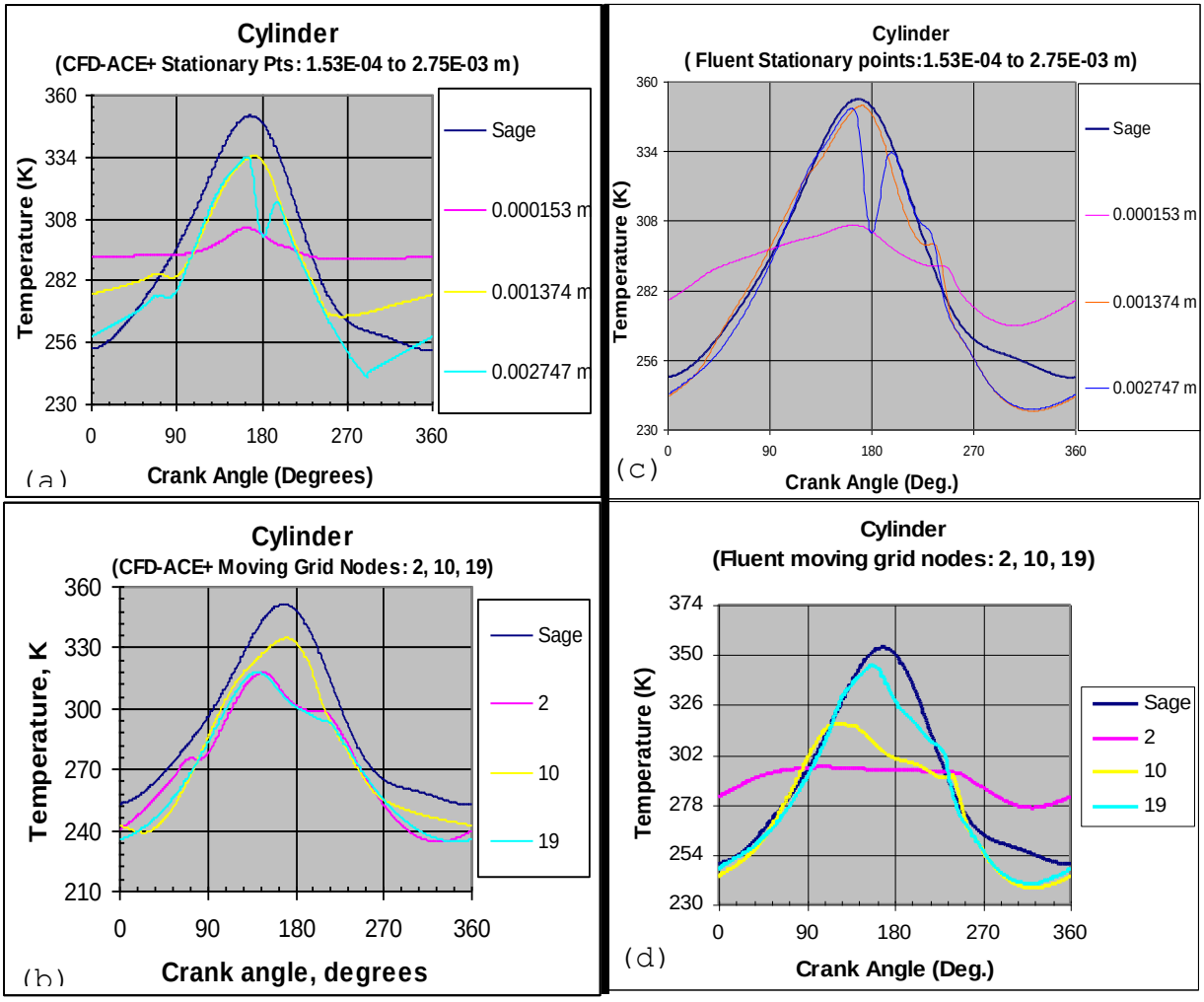

Figures 8(a-d). Temperature Profiles at Stationary and Moving Points in Cylinder Space
(Operating Conds.: 201.7 RPM, 1.008 MPa, T_{wall} = 294 K, #tspc = 480, Grid size = 147 x 46).

The cylinder space temperature profiles are observed to be dependent on point location and on whether the point is stationary or moving. The temperature profiles are more irregular for stationary points than for moving points. Profile irregularity is more pronounced for stationary points close to the midpoint of the cylinder clearance volume (x = 0.001374 m) and the piston top center position (x = 0.002747 m). The sudden dip in temperature at $\theta = 180^{o}$ for the stationary point at x = 0.002747 m. may possibly be due to

flow disturbance close to the piston top center position. The dip in temperature at $\theta = 180^{o}$ for moving grid points (x-nodes 2 and 19) are not as sudden as observed for the stationary point at x = 0.002747 m.

In general, temperature values are observed to increase with crank angle during the compression phase and decrease during the expansion phase of the cycle as expected. All the CFD-ACE+/Fluent generated peak temperatures for stationary and moving points are below Sage's peak temperature. Unlike the case for stationary points, all CFD-ACE+/Fluent temperature profiles for the moving grid points are below Sage's temperature profile at all crank angles. On the average, the highest temperature recorded by Sage exceeds the highest temperature recorded by CDF-ACE+/Fluent in the "2-space" model by ~ 16 K. In the "3-space" model the difference in the highest temperatures is minimal. Close to the cylinder head or entrance to the heat exchanger (x = 0.000153 m, x-node 2), the fluid in the cylinder space experiences an appreciable drop in the peak temperature since almost all the fluid is pushed into the heat exchanger at this point. Addition of the regenerator appears to elevate the cylinder space temperature especially for stationary points close to the midpoint of the cylinder clearance volume (x = 0.001374 m) and to the piston top center position (x = 0.002747 m).

Temperature profiles for the stationary points in the heat exchanger space are illustrated in Figs. 8(e,f) below. Five and three stationary points are specified for the "2-space" and "3-space" models, respectively. Three stationary points are specified in the heat exchanger space of the "3-space" model because of its reduced linear dimension due to the incorporation of the regenerator.

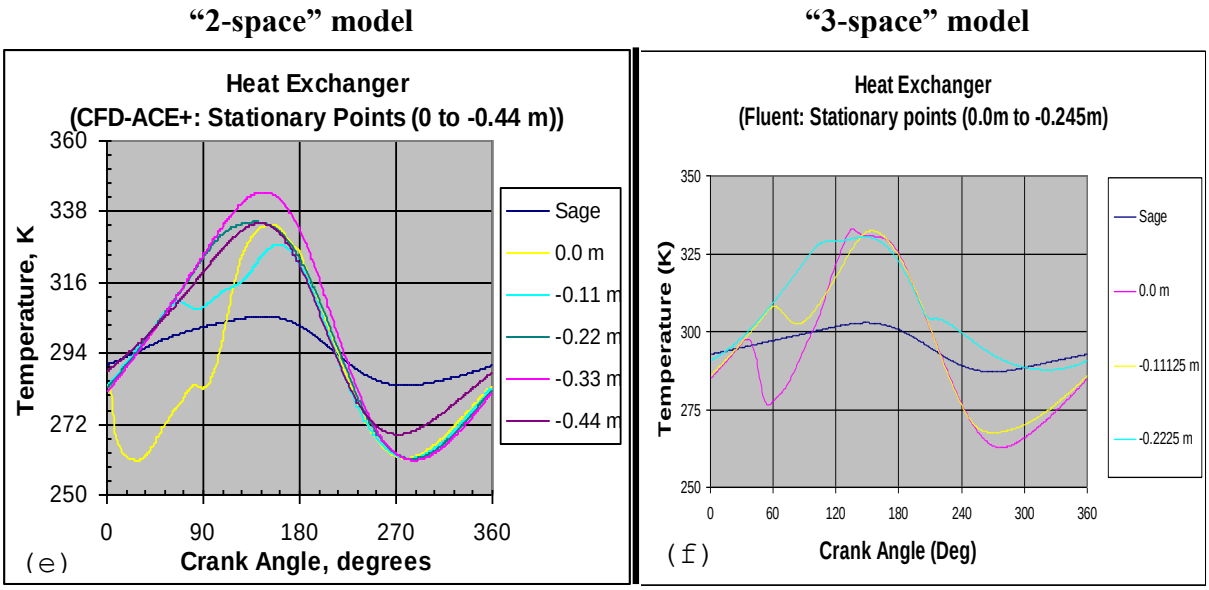

Figure 8(e-f). Temperature Profiles at Stationary Points.
(Operating Conds.: 201.7 RPM, 1.008 MPa, T_{wall} = 294 K, #tspc = 480, Grid size = 147 x 46).

Temperature profiles in the heat exchanger are more irregular especially during the compression part of the cycle for points at or close to the heat exchanger entrance (0.0 and -0.11 m). Unlike in the cylinder space, all CDF-ACE+/Fluent maximum temperatures in the heat exchanger are greater than Sage's maximum temperature (~ 304K @ θ ~ 148^o) and all CFD-ACE+/Fluent minimum temperatures in the heat exchanger are lower than Sage's minimum temperature (~ 286 K @ θ ~ 274^o). As expected, peak temperatures are recorded near the end of the compression process and the lowest temperatures are recorded close to the end of the expansion process. For the "2-space" model, the highest temperature (~ 344.1K @ θ = 146.3^o) and lowest temperature (~260.8K @ θ = 287.3^o) are recorded near the end of the heat exchanger (x = - 0.33 m) disregarding the anomaly near the heat exchanger entrance. For the "3-space" model, the highest temperature (~ 333.3 K @ θ = 148.5^o) and lowest temperature (~262.8K @ θ = 270^o) are recorded near the heat

exchanger entrance (x = 0 m). On the average, the highest temperature recorded by CDF-ACE+/Fluent in both the "2-space" and "3-space" models exceeds Sage's highest temperature by ~ 40 K and Sage's lowest temperature exceeds the lowest temperature recorded by CDF-ACE+/Fluent by ~ 24 K. The presence of the regenerator does appear to decrease the maximum temperature in the heat exchanger by ~ 11 K, increase the minimum temperature in the heat exchanger by ~ 2 K and to shift the maximum and minimum temperature values from near the end of the heat exchanger to near the heat exchanger entrance during a cycle.

The cylinder space and heat exchanger space pressure profiles are illustrated in Figs. 8(g-j). The pressure profiles in the cylinder and heat exchanger spaces are insensitive to stationary or moving spatial coordinates and are fairly symmetric over the crank angle range $0^o \le \theta \le 360^o$ with peak pressure values predictably occurring very close to the end of the compression phase of the cycle. Whereas the pressure profiles in the cylinder predicted by Fluent and Sage are in excellent agreement for the "3-space" model over the crank angle range $0^o \le \theta \le 360^o$, with maximum pressure 1.55E+06 N/m^2 occurring at $\theta \approx 175^o$, pressure profiles in the cylinder predicted by CFD-ACE+ and Sage for the "2-space" model are not in agreement over the crank angle range $90^o \le \theta \le 210^o$. At maximum compression CFD-ACE+'s peak pressure (1.55E+06 N/m^2 at $\theta \approx 173^o$) exceeds Sage's (1.49E+06 N/m^2 at θ = 174.75^o) by about 60.0 kPa with about 1.75^o crank angle lead. Also, it is observed that whereas the 2D peak pressure values predicted by Fluent in the "3-space" domains (cylinder and heat exchanger) are less than those predicted by CFD-ACE+ in the corresponding "2-space" domains, 1D peak pressure values predicted by Sage in cylinder and heat exchanger domains are higher in the "3-space" domains.

In the heat exchanger space of the "2-space" model there is a significant difference between CFD-ACE+ and Sage calculations of the pressure peak values. At maximum compression ($\theta \approx 175^{o}$), CFD-ACE+'s peak pressure (1.55E+06 N/m^2 at $\theta \approx 173^{o}$) exceeds

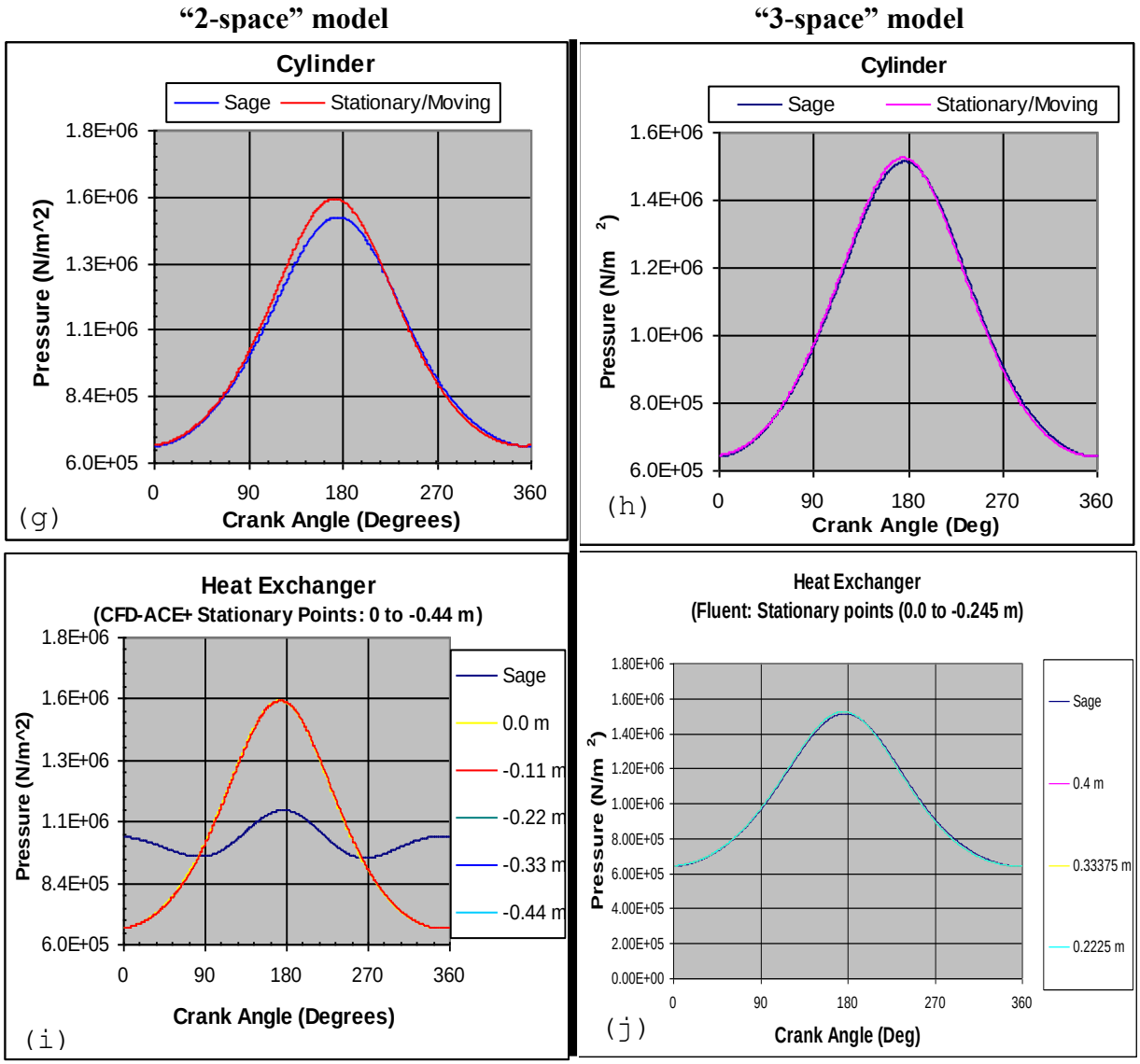

Figure 8(g-j). Pressure Profiles at Stationary and/or Moving Points.
(Operating Conds.: 201.7 RPM, 1.008 MPa, T_{wall} = 294 K, #tspc = 480, Grid size = 147 x 46).

Sage's (1.13E+06 N/m^2 at $\theta \approx 176.3^{o}$) by about 420.0 kPa with about 3.3^{o} crank angle lead. Note that in going from the cylinder space to the heat exchanger space, Sage predicts

a large pressure drop (~0.36E+06 N/m^2). CFD-ACE+/Fluent predicts no pressure drop. Perhaps the argument can be made that the regenerator helps to improve the pressure profile correspondence with Sage result in both the cylinder and heat exchanger spaces and to reduce the peak pressure values in both the cylinder and heat exchanger domains.

Temperature and pressure profiles in the regenerator predicted using Fluent and Sage are illustrated in Figures 8(k-l). The pressure profiles are in excellent agreement over the crank angle range $0^o \le \theta \le 360^o$, with maximum pressure ~ 1.5E+06 N/m^2 occurring at $\theta \approx 180^o$.

Regenerator in "3-space" domain

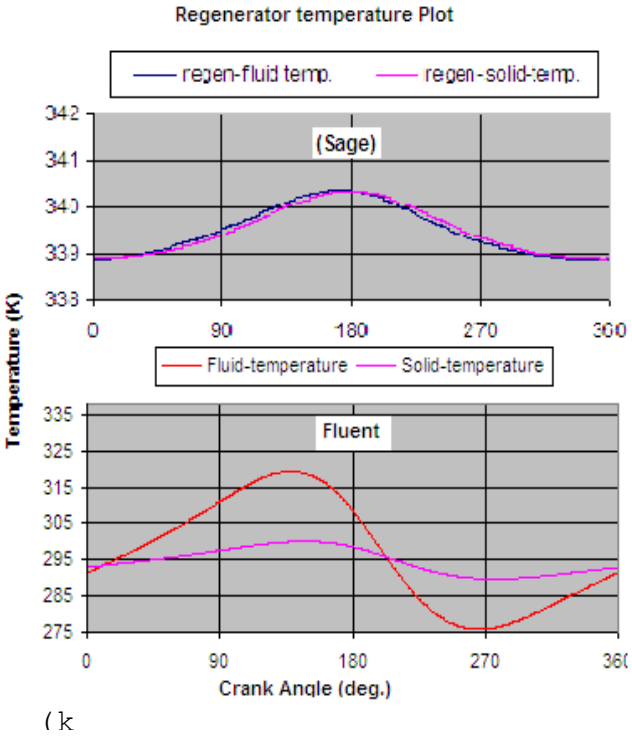

(k

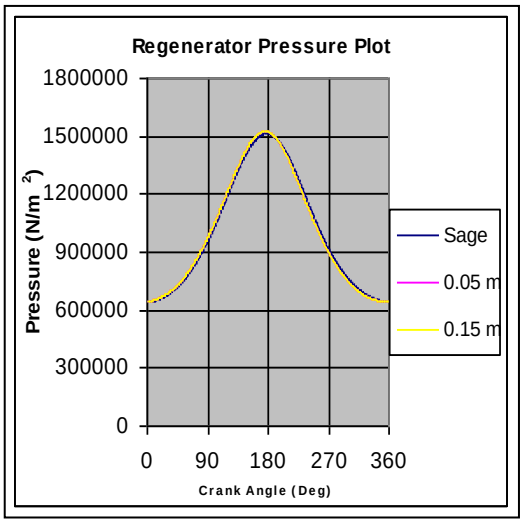

(l

Figure 8(k-l). Temperature and Pressure Profiles at Stationary Points.

(Operating Conds.: 201.7 RPM, 1.008 MPa, T_{wall} = 294 K, #tspc = 480, Grid size = 147 x 46).

The Sage code's temperature prediction at each crank angle of piston motion exceeds the Fluent code's predictions (fluid and solid temperatures) at corresponding crank angle. The arbitrariness of some of the prediction parameters (e.g., thermal conductivity of the solid matrix) introduced into the Fluent code may be responsible for this. As expected, the regenerator is seen to store heat during the compression phase of the cycle (during which the fluid temperature is higher than the temperature of the solid) and to release heat to the fluid during the expansion phase of the cycle (during which the fluid temperature is lower than the temperature of the solid).

6.2.4 Pressure-Volume Diagrams

Pressure-volume diagrams over a cycle in the cylinder space of the "2space" and "3-space" domains are illustrated in Figs. 9(a,b). The indicated operating pressure is arithmetic mean cycle pressure. Wall and piston-face temperature was a constant 294 K. It should be noted that the maximum cylinder volume (1.60E-04 m^3), the minimum cylinder volume (0.59E-04 m^3) and the swept volume (1.545E-04 m^3) are the same in both models.

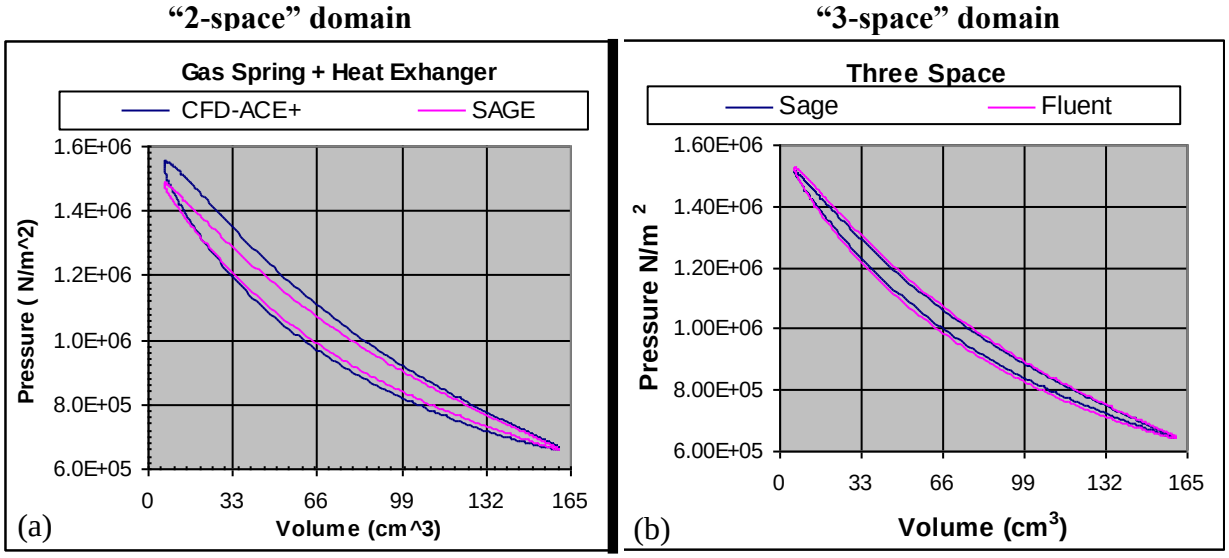

Figure 9. Pressure-Volume Diagram for the Cylinder Space in the (a) "2-space" and (b) "3-space" Domains. (Operating Conds.: 201.7 RPM, 1.008 MPa., 480 tspc, Grid size: 147 x 46).

Because Sage variable volume calculations are only limited to the cylinder space, CFD-ACE+/Fluent pressure-volume calculations were limited to the cylinder space too for comparison with Sage results. The pressure-volume diagrams appear qualitatively similar in both the "2-space" and "3-space" domains. Sage and Fluent calculations of maximum pressures at minimum compression volume compare better (~ 0.6% error) for the "3-space" model than for the "2-space" model (~ 4.3% error). On the other hand, the minimum pressures at maximum expansion volume are in better agreement for the "2-space" model (~ 0.3% error) than for the "3-space" model (~ 0.5% error). These calculations are shown in Table 6.

Table 6. Sage and CFD-ACE+/Fluent (P_{max}, V_{min}) and (P_{min}, V_{max}) Data

Numerical Code	Cylinder Space of "2-space" Model (Using Sage/CFD-ACE+)		Cylinder Space of "3-space" Model (Using Sage/Fluent)	
	Pressure, N/m^2			
	Max. Value @ 5.9 cm^3	Min. Value @ 160.4 cm^3	Max. Value @ 5.9 cm^3	Min. Value @ 160.4 cm^3
Sage	1,487,850	660,900	1,512,615	643,042
CFDACE+/Fluent	1,553,454	663,053	1,521,588	645,876
% Diff.	4.3	0.3	0.6	0.4
	Piston Net Work Input, W			
Sage	29.9502915		22.37000149	
CFD-ACE+/Fluent	53.24190164		34.12	
% Diff.	43.7		34.4	

From Table 6, it is noted that the maximum pressure in each domain is about 2.4 times the minimum pressure. A large disparity between Sage and CFD-ACE+/Fluent calculations of the piston net work input (~ 34.4% error) is also noted. The area under the process curve

on a pressure-volume (P-V) diagram is equal in magnitude to the work done during the expansion or compression process of a closed system. The area within the P-V diagrams, Figs. 9(a) and 9(b), indicates non-zero P-V work and heat transfer. The area is equivalent to a net piston work input because the work done by the system on the piston during the expansion process is less than the work done on the system by the piston during the compression part of the cycle. On the average, Sage and Fluent results appear to compare better for the "3-space" model.

6.2.5 Wall Heat Transfer Rate

Table 7 shows Sage and CFD-ACE+/Fluent work and heat transfer calculation results for a single cycle taken from mid 6th cycle to mid 7th cycle. Note that work and heat transfer calculations must be multiplied by two to get values for the entire domain since only one half of the domain is simulated.

Table 7. Sage and CFD-ACE+/Fluent Work and Heat Transfer Data (with the incorporation of the β weighting factor)

Code	"2-space" Domain (Using CFD-ACE+)			"3-space" Domain (Using Fluent)			
	Net Input Work, W	Heat Transfer, W		Net Input Work, W	Heat Transfer, W		
Sage	29.95	$\dot{Q}_{out}$ (HXer.)	$\dot{Q}_{in}$ (Cyl.)	22.37	$\dot{Q}_{out}$ (Regen.)	$\dot{Q}_{out}$ (HXer.)	$\dot{Q}_{in}$ (Cyl.)
		42.58	12.71		1.797E-07	37.95	15.58
CFDACE+/ Fluent	53.24	80.93	27.65	34.12	33.06	24.22	23.14

The cylinder input heat rate corresponds to a rate of cooling of the cylinder walls. The heat exchanger and regenerator output heat rates correspond to the heating rates of the heat exchanger and regenerator walls. Results indicate negligible heating of the regenerator wall when compared to the heat exchanger wall heating rates. The net work input,

$\dot{W}_{net,in} = \dot{Q}_{out} - \dot{Q}_{in}$ is confirmed by the results in Table 7. The piston action essentially pumps heat from the cylinder to the heat exchanger and regenerator. Thus with respect to the cylinder, the model acts like a "cooler" whereas with respect to the heat exchanger or the regenerator, the model acts as a "heat pump" even though the wall temperature is kept constant at 294 K.

With the addition of the regenerator, Fluent reports a considerable reduction in the cooling action in the cylinder and heat pumping action in the heat exchanger. Sage on the other hand reports a slight increase in the cooling action in the cylinder and a slight reduction in the heat pumping action in the heat exchanger. The addition of the regenerator results, on the average, in about 31% reduction in the net cycle heat loss (or input work) prediction.

The heat addition-heat rejection process described above occurs in Stirling engines also. Heat is pumped from the expansion volume of a Stirling engine to the "appendix gap" (clearance volume between the displacer piston and the cylinder) and is lost to the walls of the clearance volume. This represents a net loss of heat to the work producing portion of the Stirling engine and is called an "appendix gap pumping loss.

Figures 10(a-d) show plots of wall heat transfer rate as functions of the crank angle. Variations of the cylinder wall, heat exchanger wall and overall wall heat transfer rates in the "2-space" model are illustrated in Figs. 10(a,b). Variations of the cylinder wall, heat exchanger wall, regenerator matrix and overall wall heat transfer rates in the 3-space model are illustrated in Figs. 10(c-d). In each model, the reference piston position is at BDC ($\theta = 0^o$).

Plots of the wall heat transfer rates exhibit oscillatory behavior over the range

$0^{o} \le \theta \le 360^{o}$ in all the domains. CFD-ACE+/Fluent and Sage signals are not in phase. In the "2-space" domain, net cycle heat loss is predicted by both CFD-ACE+ (53.28 W) and Sage (29.88 W). The difference in the net cycle heat loss is about 43.9%. In the "3-space" domain, net cycle heat loss is predicted by both Fluent (34.12 W) and Sage (22.37 W). The difference in the net cycle heat loss is about 34.4%. These results are in agreement with corresponding entries in Table 7.

"2-space" model **"3-space" model**

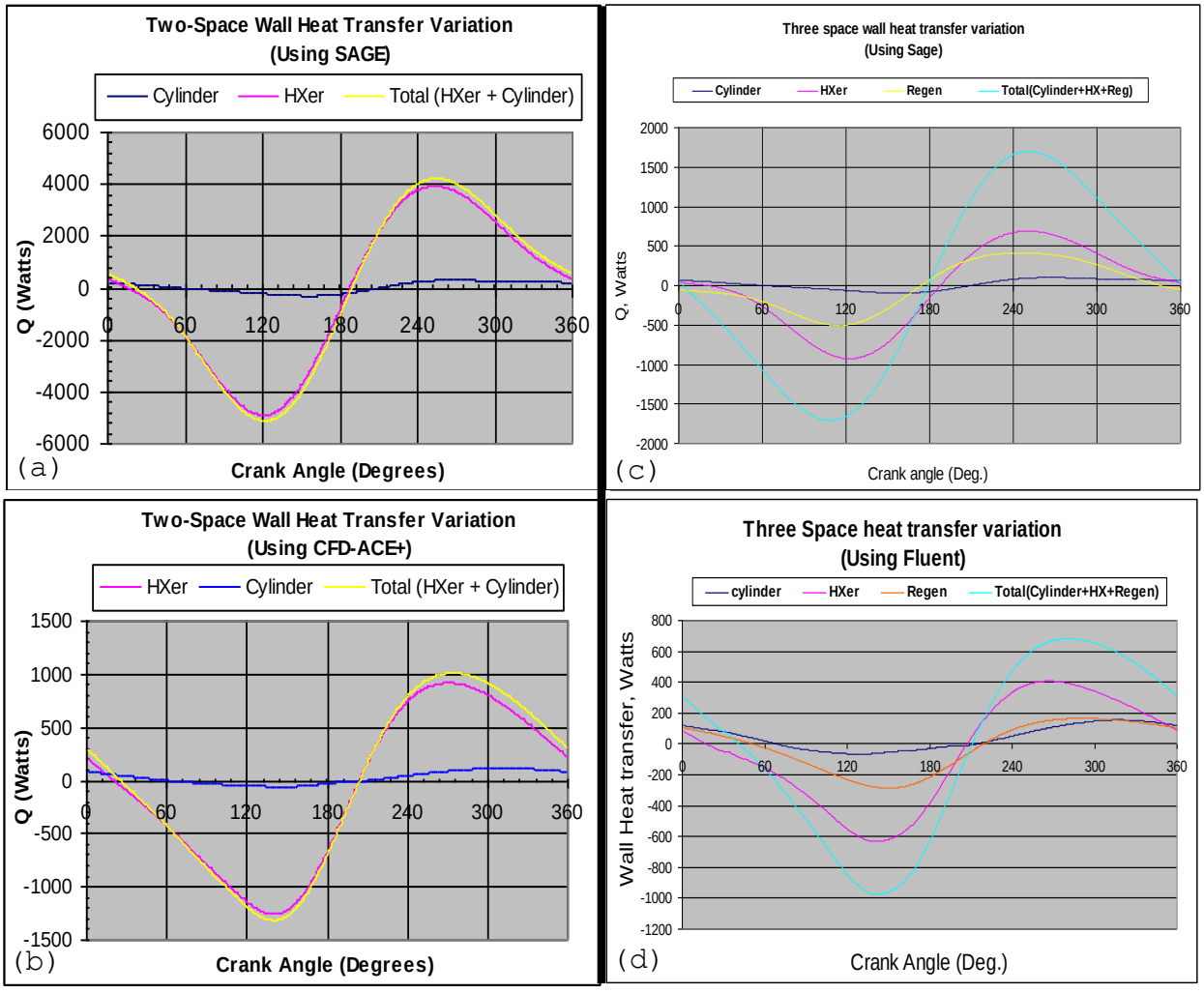

Figure 10(a-d). Wall Heat Transfer Vs. Crank Angle
(Operating Conds.: 201.7 RPM, 1.008 MPa, T_{wall} = 294 K, #tspc = 480, Grid size = 147 x 46)

6.3 CFD-ACE+ Results vs. Some Literature Results

6.3.1 Surface Heat Flux and Temperature Difference

Figures 11(a-c) illustrate the effect of the oscillating laminar flow on the heat exchanger surface heat flux in the "2-space" model. Heat flux data obtained at the entrance of the heat exchanger and at 1/16, 1/8, ¼, ½ and "end" of the heat exchanger length from the entrance are plotted against the crank angle starting at BDC. The corresponding temperature differences between the gas temperature at the radial center of the heat exchanger and the heat exchanger wall are shown in Figs. 12(a-c). Kornhauser's experimental results [25], Figs. 11(a) and 12(a), Tew's modified CAST code results [40], Figs. 11(b) and 12(b) and CFD-ACE+ results [13], Figs. 11(c) and 12(c) are presented and compared. The corresponding Fluent results of the present study of the "3-space" model, Figs. 11(d) and 12(d) are also illustrated in order to explain the effect of the regenerator if any. Note that the sign of the heat transfer in the modified CAST (Fig. 11(b)) is reversed relative to that of Kornhauser's (Fig. 11(a)). This is because in modified CAST, CFD-ACE+ and Fluent, heat transfer was defined to be positive for heat flow from the wall to the gas (opposite to the assumption made by Kornhauser). The signs in the CFD-ACE+ (Fig. 11(c)) and Fluent results (Fig. 11(d)) were reversed in order to obtain a plot which conforms with Kornhauser's plot.

The general qualitative tendencies of the experimental results (Kornhauser's) and numerical results (CAST, CFD-ACE+ and Fluent) for the heat fluxes and the temperature differences appear, for the most part, to agree well. However, there are notable differences.

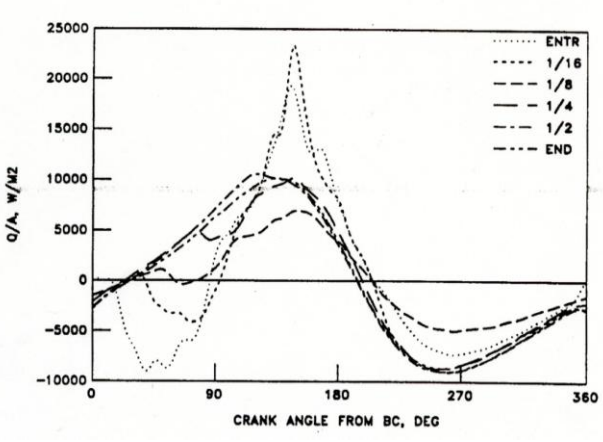

Figure 11(a). Heat flux vs. Crank angle at various positions along heat exchanger surface relative to entrance to cylinder. (Kornhauser's Experimental Data [3]: Run #10271539, 201.7 RPM, 1.008 MPa (arithmetic mean pressure), T_{wall} = 294 K).

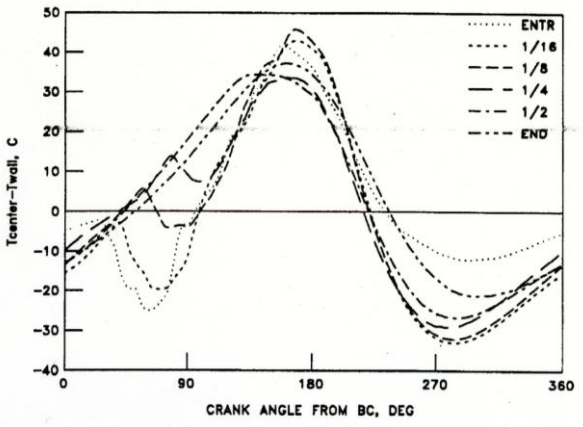

Figure 12(a). Temp. difference (T_{center} - T_{wall}) vs. Crank angle at various positions along heat exchanger surface relative to entrance to cylinder. (Kornhauser's Exptal Data [3]: Run #10271539, 201.7 RPM,1.008 MPa (arithmetic mean pressure), T_{wall} = 294 K).

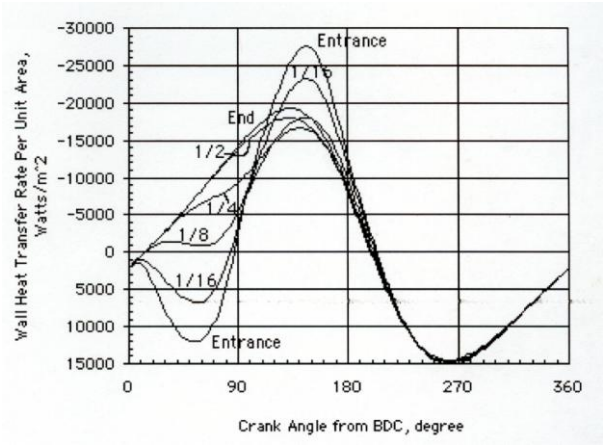

Figure 11(b). Heat flux vs. Crank angle at various positions along heat exchanger surface relative to entrance to cylinder. (Tew's Modified Cast Code Calculations [40]: 34 x 20 grids, 120 tspc.).

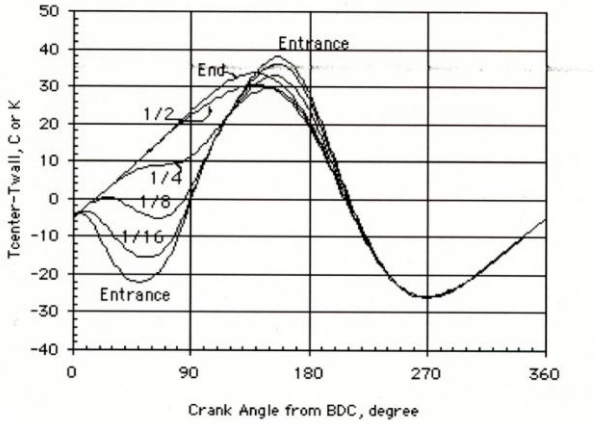

Figure 12(b). Temp. difference (T_{center} - T_{wall}) vs. Crank angle at various positions along heat exchanger surface relative to entrance to cylinder. (Tew's Modified Cast Code Calculations [40]: 34 x 20 grids, 120 tspc.).

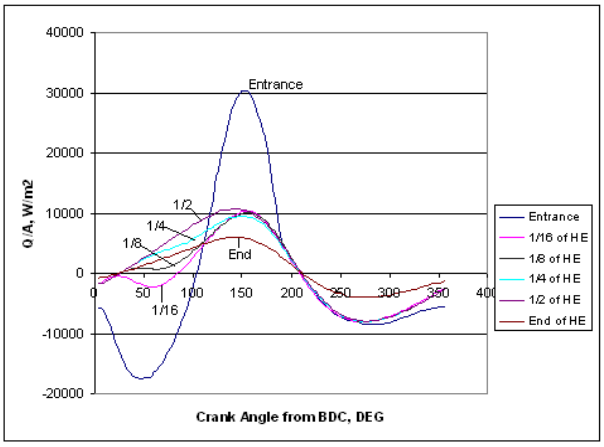

Figure 11(c). Heat flux vs. Crank angle at various positions along heat exchanger surface relative to entrance to cylinder. (CFD-ACE+ Code Calculations [21]: 34 x 20 grids, 120 tspc.)

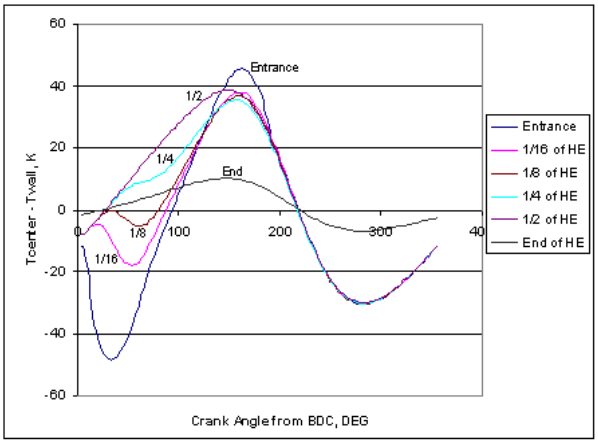

Figure 12(c). Temp. difference (T_{center} - T_{wall}) vs. Crank angle at various positions along heat exchanger surface relative to entrance to cylinder. (CFD-ACE+ Code Calculations [21]: 34 x 20 grids, 120 tspc.)

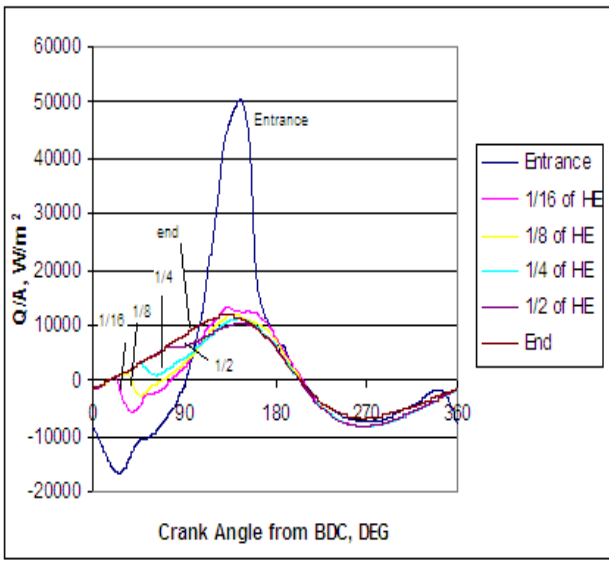

Figure 11(d). Heat flux vs. Crank angle at various positions along heat exchanger surface relative to entrance to cylinder. (Fluent Code Calculations: 34 x 20 grids, 120 tspc).

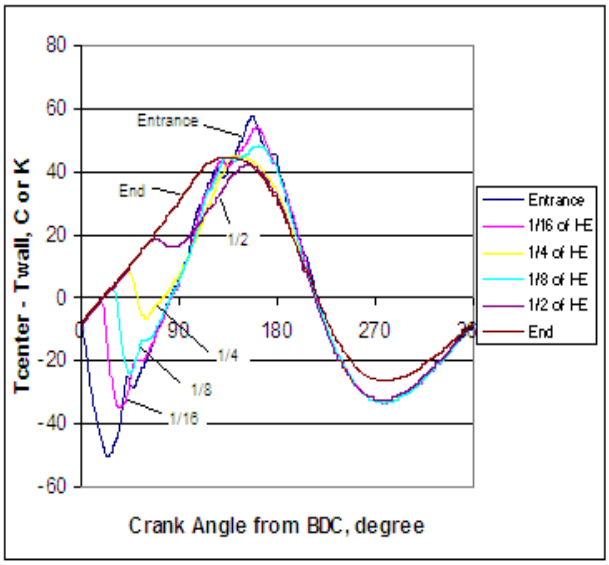

Figure 12(d). Temp. difference ($T_{center} - T_{wall}$) vs. Crank angle at various positions along heat exchanger surface relative to entrance to cylinder. (Fluent Code Calculations: 34 x 20 grids, 120 tspc).

Kornhauser's experimental heat flux results appear to exhibit some erratic variations in the heat flux plots near the heat exchanger entrance with no evident corresponding erratic variations in temperature difference. Similar erratic variations are not observed in the numerical results.

With the exception of Kornhauser's experimental results, most of the results of the heat flux and temperature difference appear insensitive to position along the heat exchanger surface during the half cycle $180^\circ \le \theta \le 360^\circ$ when flow is from the heat exchanger to the cylinder. The CAST code results are most insensitive in this crank angle range.

The magnitudes of the heat fluxes and temperature differences are also somewhat different. During the compression phase of the cycle, the maximum values for the heat flux and temperature difference are observed at the 1/16 and 1/8 of the heat exchanger length from the entrance respectively for Kornhauser's and at the entrance of the heat exchanger for Tew's CFD-ACE+'s and Fluent's results. With the exception of Kornhauser's results,

the minimum values are largely insensitive to position along the heat exchanger surface.

Table 8 illustrates the quantitative differences in the maximum and minimum heat fluxes and temperature differences at the entrance and at the end of the heat exchanger.

Table 8. Maximum and Minimum Heat Flux and Temperature Difference

Result Type	Max. and Minimum Heat Flux, W/m^2		Max. and Minimum (T_{center}-T_{wall}), K	
	HXer Entrance	HXer End	HXer Entrance	HXer End
Kornhauser's	+22,500 ≈ -10,000	≈ +10,000 ≈ -10,000	≈ +40 ≈ -35	≈ +36 ≈ -25
Modified CAST	≈ -27,500 ≈ +15,000	≈ -20,000 ≈ +15,000	≈ +37 ≈ -25	≈ +34 ≈ -25
CFD-ACE+	+30,389 ≈ -20,000	+5,952 ≈ -3,000	+46 ≈ -30	+10 ≈ -6
Fluent	+50,429 ≈ -17,200	+11,689 ≈ -6682	+58 ≈ -33	+43 ≈ -26

There are noticeable differences in the magnitudes of the heat flux and temperature difference at the heat exchanger entrance and end. The effect of the regenerator is clearly noticed at the entrance of the heat exchanger where the maximum values of the heat flux and temperature difference are elevated.

6.3.2 Temperature Contours

Temperature contour plots at 90^o before TDC where maximum piston velocity is toward the heat exchanger are illustrated in Figs. 13(a-e). Similar qualitative results are obtained in the heat exchanger space and the cylinder space using CFD-ACE+ code (Figs. 13(a-c)), the modified CAST code (Fig. 13(d)) and the Fluent code (Fig. 13(e)). It is observed that whereas in the heat exchanger space the fluid temperature increases from the wall region towards the interior, in the cylinder space the opposite trend is observed with fluid temperature decreasing as one moves into the cylinder interior from the wall region. Also, the cooler fluid at the entrance of the heat exchanger is observed to become warmer

as the fluid moves towards the end of the heat exchanger.

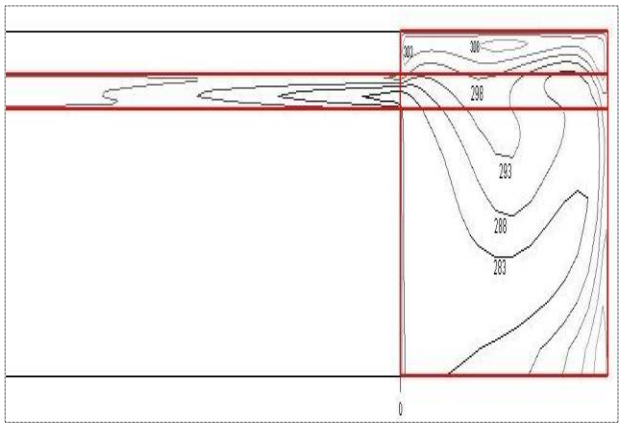

Figure 13(a). Temperature contours for Cylinder and entrance of HXer. (CFD-ACE+, 147x51grids, Δ t = 6.19E-04, (480 tspc); 90^o befor TDC; Op. Conds.: 201.7 RPM, 1.008 MPa)

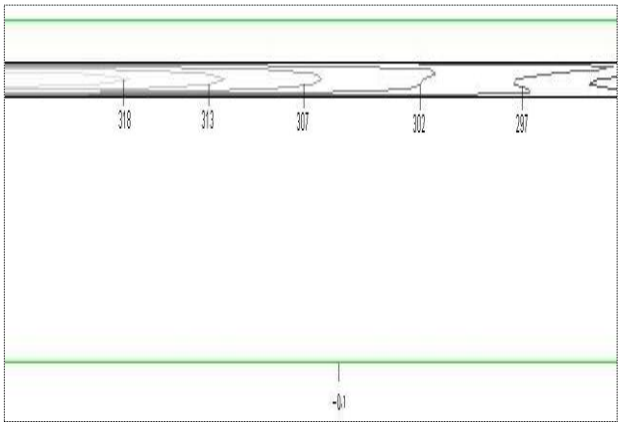

Figure 13(b). Temp. contours for middle part of Heat Exchanger (CFD-ACE+, 147x51grids, Δ t = 6.19E-04, (480 tspc); 90^o before TDC; Op. Conds.: 201.7 RPM, 1.008 MPa)

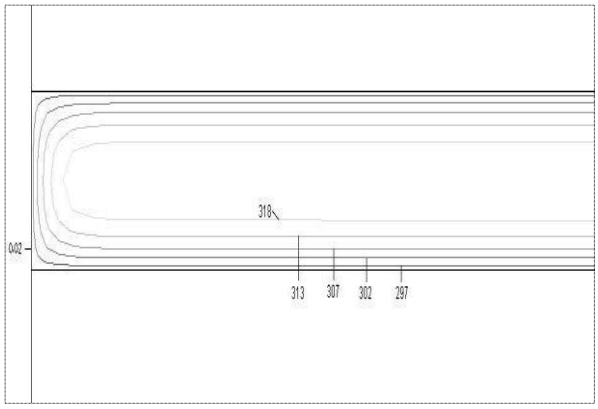

Figure 13(c). Zoom in on temp. contours for end of HXer (CFD-ACE+, 147x51grids, Δ t = 6.19E-04, (480 tspc); 90^o before TDC; Op. Conds.: 201.7 RPM, 1.008 MPa).

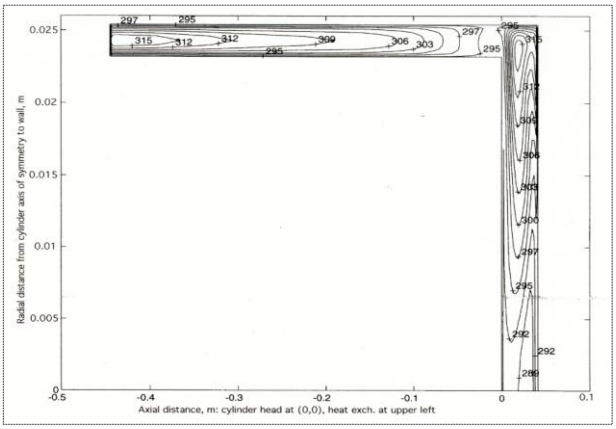

Figure 13(d). Temperature contours for entire domain (Modified CAST Run #13 with 82 x 20 grids, 960 tspc. Simulation of Kornhauser's[1] Experimental Run #10271539. Maximum Piston Velocity toward the HXer. 90^o before TDC.).

Notice that unlike in the CFD-ACE+ "2-space" model (Figs.(a-c)) and the Fluent "3-space" model (Fig. 13(e)), the outer cylinder wall is flush with the outer wall of the heat exchanger in the CAST model (Fig. 13(d)). Due to this difference in geometries, it is observed that the higher temperature contours are situated close to the upper cylinder region in CFD-ACE+ and Fluent and not at the entrance to the heat exchanger as in CAST.

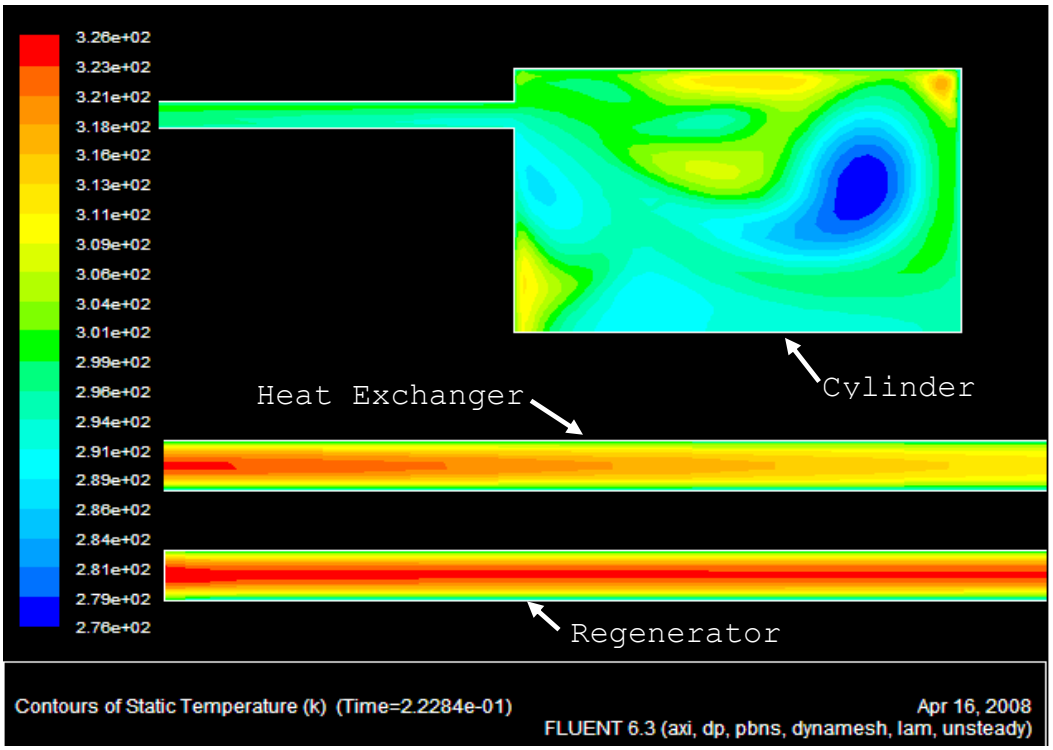

Figure : 13 (e) Temperature contours of Three Space domain (Fluent, 147x46grids Δt = 6.19E-04, (480 tspc); 90^o befor TDC; Op. Conds.: 201.7 RPM, 1.008 MPa)

As in the heat exchanger space, the fluid temperature increases from the wall region towards the interior.

6.3.3 Velocity Vectors

Figures 14(a-e) show laminar velocity vector field plots in the ("2-space" model in Figs. 14(a-d)) and "3-space" model in (Fig. 14(e)). The CAST code (Fig. 14(b)), the CFD-ACE+ code (Fig. 14(c)) and the Fluent code (Fig. 14(e)) show the fluid accelerating around the corner of the inner wall of the annulus to enter the heat exchanger. The velocity is primarily radial along the cylinder head approaching the heat exchanger. Across the exchanger entrance, as the fluid prepares to turn the corner, the velocity changes from mostly radial at the lower "corner" to mostly axial at the upper wall for the CAST model. For the CFD-ACE+ and Fluent models, because of the slight difference in geometries, the transition from radial to axial transition from radial to axial flow takes place at the lower

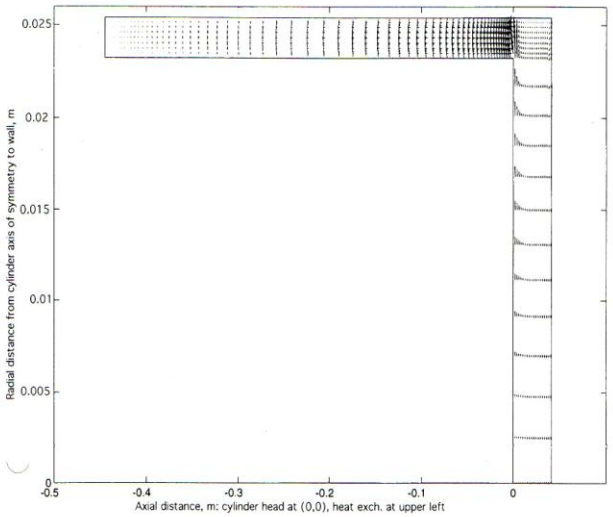

Figure 14(a). Velocity Field Plot for entire domain (Modified CAST Run #13 with 82x20 grids, 960 tspc Simulation of Kornhauser's [3] Experimental Run #10271539. Maximum Piston Velocity toward the HXer.)

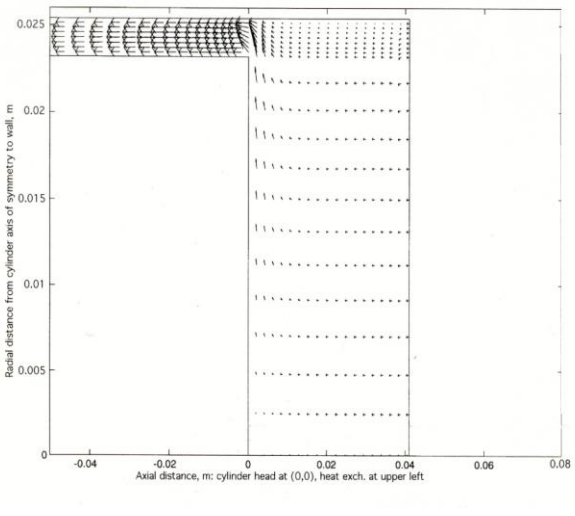

Figure 14(b). Zoom in on Velocity Field Plot at HXer Entrance (Modified CAST Run #13 with 82x20 grids, 960 tspc Simulation of Kornhauser's [3] Experimental Run #10271539. Maximum Piston Velocity toward the HXer.)

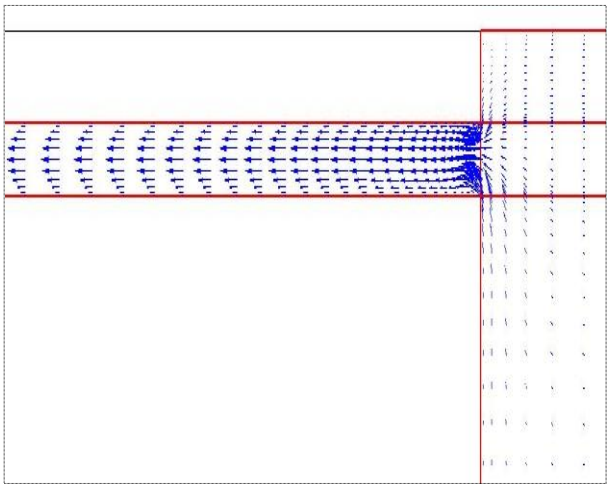

Figure 14(c). Zoom in on Velocity Field Plot at HXer Entrance (CFD-ACE+, Grid = 147x51, Δt = 6.19E-04, (480 tspc); Maximum piston velocity toward the 90° before TDC; Operating Conditions: 201.7 RPM, 1.008 MPa).

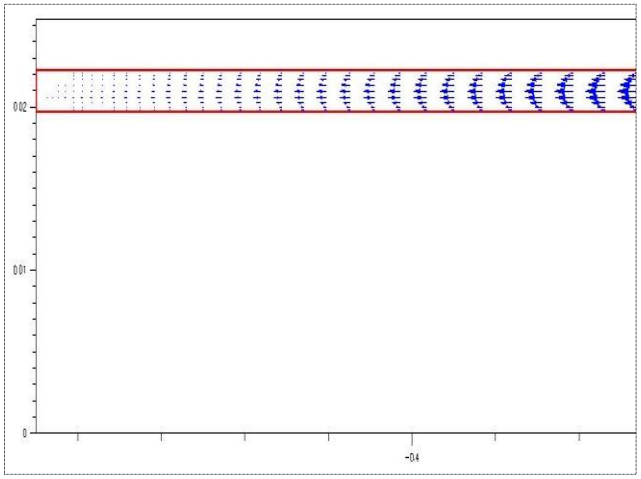

Figure 14(d). Zoom in on Velocity Field Plot at HXer End (CFD-ACE+, Grid = 147x51, Δt = 6.19E-04, (480 tspc); Maximum piston velocity toward the 90° before TDC; Operating Conditions: 201.7 RPM, 1.008 MPa).

and upper corners of the heat exchanger entrance. Mass conservation requires a substantial increase in axial velocity near the outer wall for the CAST model (Fig. 14(b)) or in the middle, away from the walls for the CFD-ACE+ (Fig. 14(c)) and Fluent (Fig.(e)) models, as the fluid enters the exchanger.

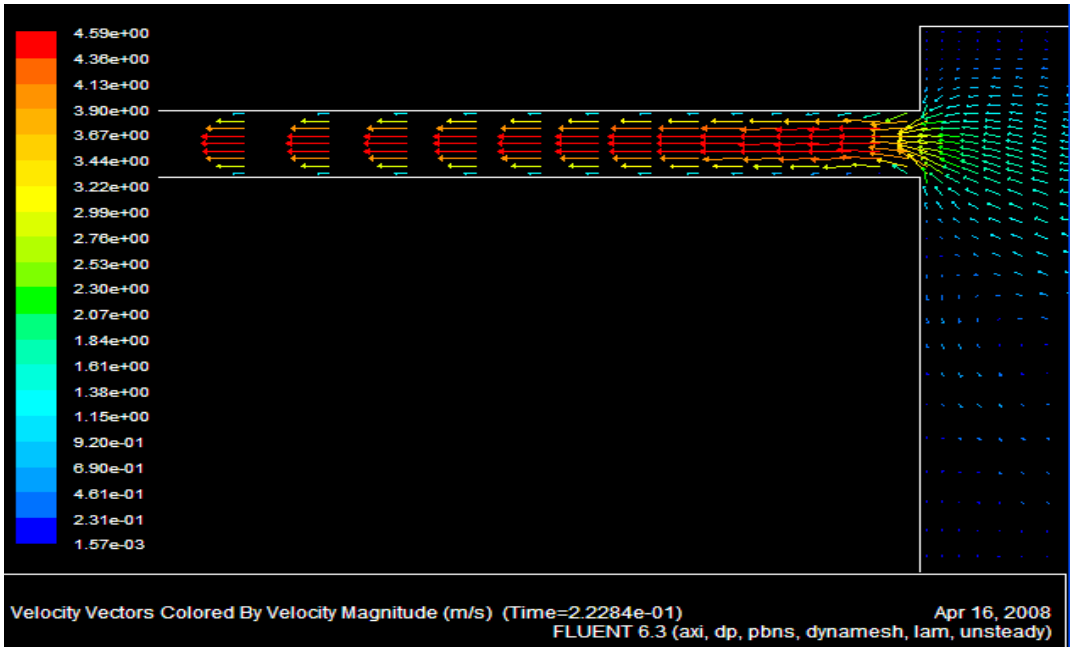

Figure 14 (e) Zoom in on velocity field plot at HXer entrance. Fluent Grid = 147x56, Δt = 6.19E-04, (480 tspc); Maximum piston velocity toward the 90^o before TDC; Operating Maximum piston velocity toward the 90^o before TDC; Operating Conditions: 201.7 RPM, 1.008 MPa).

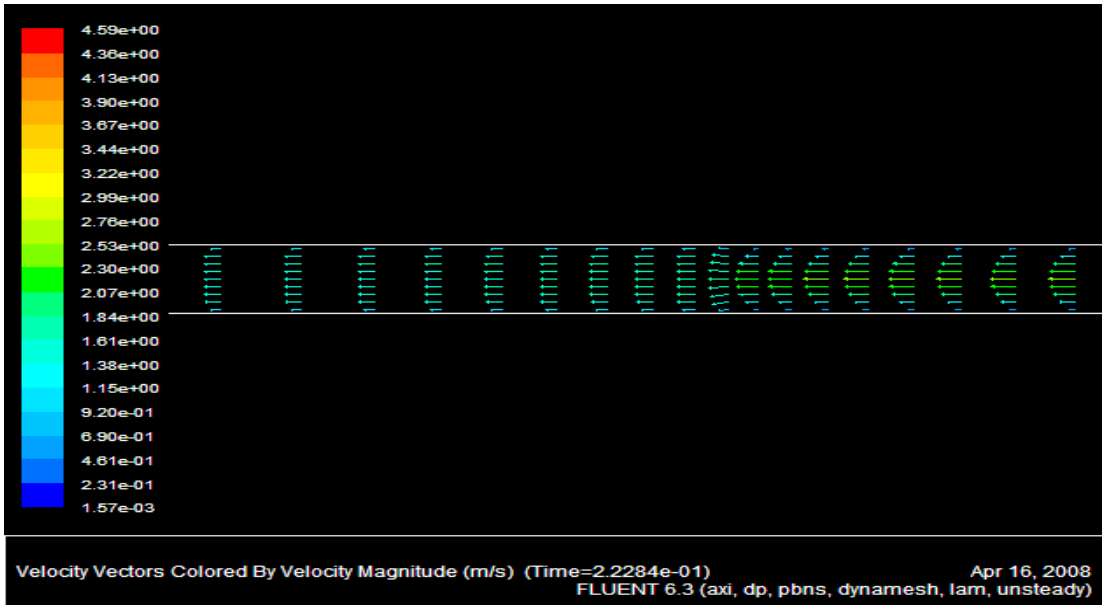

Figure 14 (f) Zoom in on velocity field plot at HXer end. Fluent Grid = 147x56, Δt = 6.19E-04, (480 tspc); Maximum piston velocity toward the 90^o before TDC; Operating Maximum piston velocity toward the 90^o before TDC; Operating Conditions: 201.7 RPM, 1.008 MPa).

Then the fluid begins to redistribute across the annulus and the axial velocity near the outer wall (CAST model) or near the inner and outer walls (CFD-ACE+ and Fluent models)

decreases.

As with the CAST results (Fig. 14(a)), CFD-ACE+ and Fluent results show that the velocity tends to zero at the dead end of the heat exchanger in the “2-space” model (Fig.14(d)) and at the end of the regenerator in the “3-space” model .

CHAPTER VII

POST PROCESSING OF NUMERICAL RESULTS

7.1 Introduction

Equations (5.34 - 5.47) clearly show that local entropy production depends functionally on the local values of heat transfer rate, temperature, pressure, density, mass-specific entropy, velocity and viscous dissipation. Thus entropy generation can be considered a derived quantity that can be computed by post-processing experimental or numerical flow fields. Equation (5.48) shows that local entropy production is also a function of availability energy loss and temperature.

7.2 Using Sage

Sage entropy generation results (external and internal) for the "3-space" domain are calculated from Eq. (5.48) using availability loss results component obtained from Sage output file viz.:

$$\dot{S}_{gen} = \frac{\text{Availability Energy Loss}}{T_L} = \frac{AEfric + AEQw + AEQx \pm |AEDiscr|}{T_0} \tag{7.1}$$

The parameters AEfric, AEQw, and AEQx are available energy losses due to flow

friction, surface heat flow and axial heat flow respectively. |AEDrcsi| is the absolute value of the discrepancy between the total available energy loss due to internal entropy generation (AEinternal = AEfric + AEQw + AEQx) and that due to external entropy generation, AEexternal. The "+" is used when it is assumed that AEexternal is greater than AEinternal and the "-"sign is used when the reverse is the case. These assumptions are arbitrary since the relative magnitudes of AEexternal and AEinternal cannot be determined apriori. A discrepancy of zero implies the total available energy loss due to internal entropy generation is equal to that due to external entropy generation.

7.3 Using Fluent

7.3.1 External Entropy Generation, $\dot{S}_{gen(ext.)}$

Closed System Analysis:

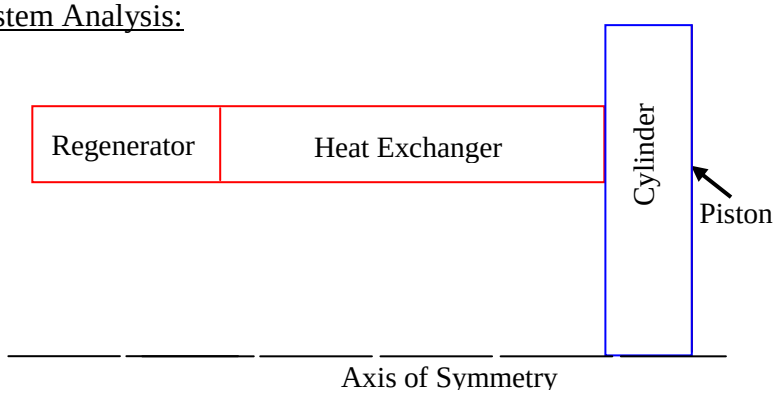

Figure 15. "Three-Space" Model Set-Up for External Entropy Generation Analysis

The "3-space" model shown in Fig. 15 above taken as a whole constitutes a closed, isothermal, non-adiabatic, reciprocating system. When viewed as a closed system for external entropy generation analysis, Eq. (5.34) for the non-porous domain and Eq.(5.40) for the porous domain are thus reduced to:

$$\text{Non-porous domain:} \quad \dot{S}_{\substack{gen,sys,cyl(ext)\\(non\text{-}porous)}} = \oint_{period} \int_{cs} \left(\frac{\bar{q}_\alpha}{T_\alpha} \cdot \hat{n}_\alpha + \frac{\bar{q}_\beta}{T_\beta} \cdot \hat{n}_\beta \right) dA\, dt \quad \geq \quad 0 \qquad (7.2)$$

Porous domain: $$\left\langle \dot{S}_{\substack{gen,sys,\,cyl(ext)\\ porous}} \right\rangle = \oint_{period} \int_{cs} \left(\varepsilon_\alpha N_k \frac{\langle \bar{q}_\alpha \rangle^\alpha}{\langle T_\alpha \rangle^\alpha} \cdot \hat{n}_\alpha + \frac{\langle \bar{q}_\beta \rangle^\beta}{\langle T_\beta \rangle^\beta} \cdot \hat{n}_\beta \right) dA\, dt \quad \geq \quad 0 \qquad (7.3)$$

in which case only the results of surface heat transfer and temperature for both the fluid and solid phases are post-processed. Note that Eq.(7.3) is used for the bounding surfaces of the regenerator. Integrated surface heat transfer rates generated each time step are exported to an Excel spreadsheet for calculation of the cyclic time integral value. Division of the cyclic integral value by the constant surface temperature completes the calculation of the external entropy generation.

Open System Analysis:

The "3-space" model can also be analyzed, by considering its separate components – regenerator, heat exchanger space and cylinder space – as open systems for which both entropy transfer components (heat and mass flow) of Eqs.(5.34) and (5.40) are now applicable. Fluent generated results of surface heat transfer, temperature, mass flow rate and mass specific entropy are post-processed for external entropy generation. In order to simplify the analysis, the "3-space" model was partitioned into five volume conditions – outer, mid and inner volume conditions in the cylinder space plus the heat exchanger and regenerator volume conditions (see Fig.16 below).

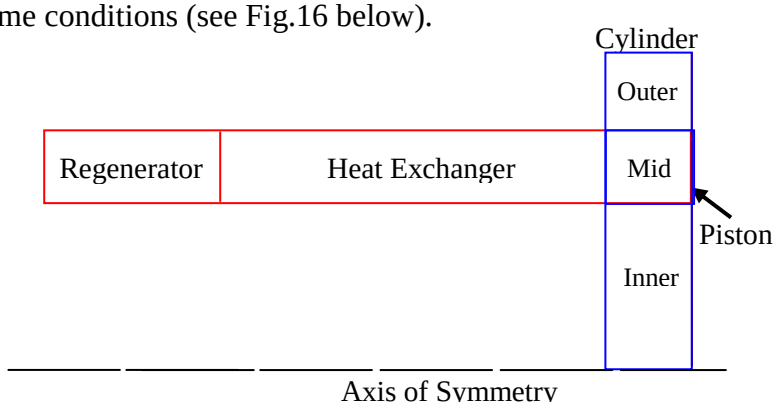

Figure 16. "Three-Space" Model Set-Up for External Entropy Generation Analysis

The external entropy generation is calculated for each volume condition with the sum of the results for the separate volume conditions yielding the total external entropy generation for the "3-space" model. The result for this open system analysis should equal the result for the closed system analysis.

If the "3-space" model is analyzed by considering its separate components as open systems, as done in this study, Fluent generated results are post-processed for the external entropy generation by using a user defined function interfaced with the Fluent solver. User defined functions can be used to post-process any Fluent generated closed or open system data. User defined functions, especially necessary for open systems, require an in-depth knowledge of Fortran concepts.

User defined functions are written in FORTRAN 90 to post-process Fluent generated surface heat transfer, temperature, velocity gradients, mass flow and mass specific entropy data. The discretized domain of interest (interior and bounding surfaces) consists of cells (interior) and short line segments called "faces" (boundary) as shown in Figure 17 below.

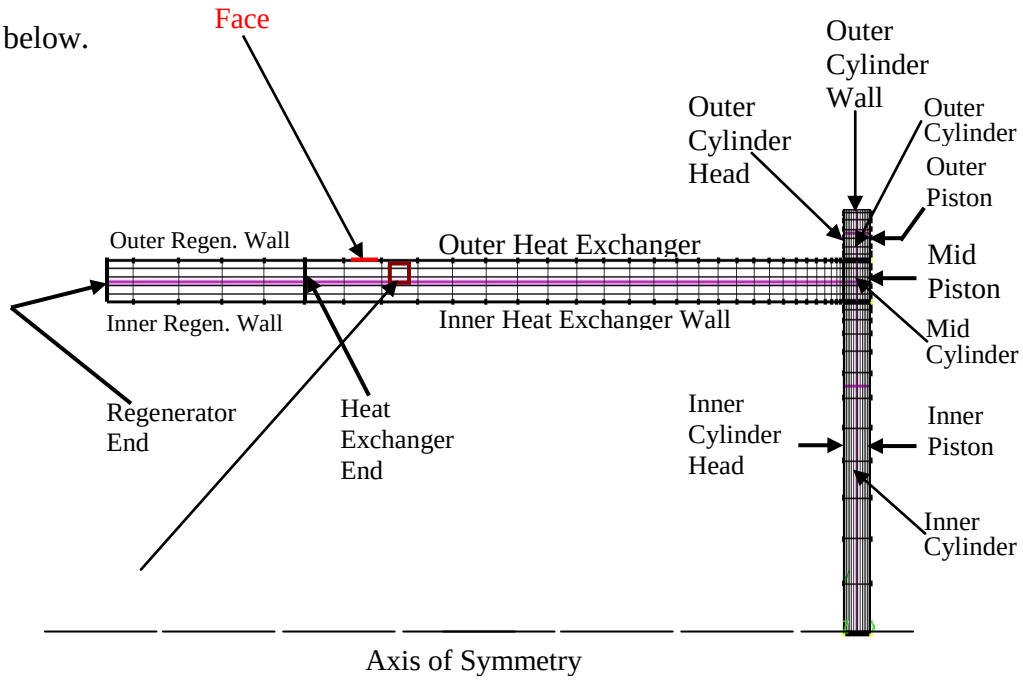

Figure 17. Discretized "Three-Space" computational domain showing "faces"

Surface heat transfer, temperature, velocity and temperature gradients, mass flow and mass specific entropy values can be obtained at cell or "face" centers except at the interface between volume conditions where data values can only be obtained at cell centers near the interface. The velocity and temperature gradient values at cell centers can either be obtained directly from the "get gradient function" module in Fluent or calculated using finite difference approximations for the non uniform grid spacing in the computational domain [39]. The summation of surface, volume and time values, implied by the integrals in Eqs. (5.34, 5.40, 5.44, 5.47) is facilitated with the use of do loops in the User Defined Functions. In order to minimize program complexity, the User Defined Functions are written to sum up the surface and volume integral values at each time step only and thereafter data is exported to an Excel spreadsheet for calculation of the cyclic time integrals. A carefully constructed algorithm is needed for implementation of Eqs. (5.34, 5.40, 5.44, 5.47).

7.3.2 Internal Entropy Generation, $\dot{S}_{gen(int.)}$

The volume conditions in the model may be further refined for calculation of internal entropy generation as shown in Figure 8 below in order to obtain a better resolution of the losses. Equations (5.44) and (5.47) are used to calculate the Internal entropy generation due to conductive heat flow and viscous dissipation are calculated for the porous region using Eq.(5.44) and internal entropy generation due to conductive heat flow, film heat transfer, viscous and inertial losses. Results of heat transfer, temperature and gradients of temperature, velocity and gradients of pressure are post-processed via user defined functions written for the "3-space" models.

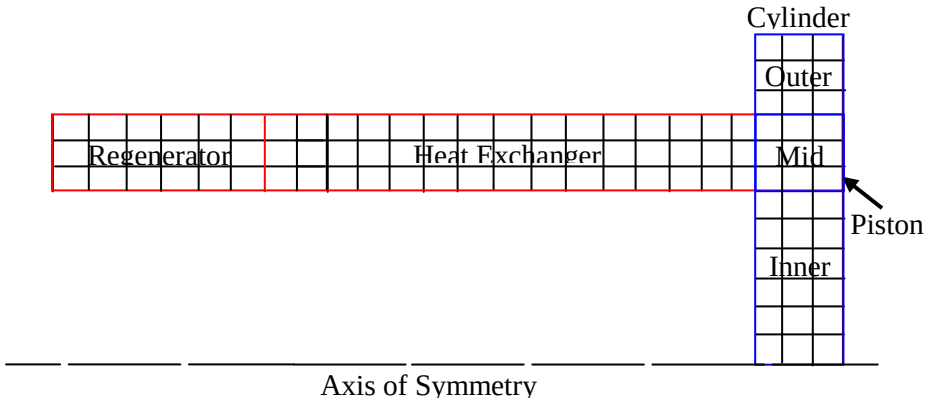

Figure 18. "Three-Space" Model Set-Up for Internal Entropy Generation Analysis

Local and global distribution of entropy generation rates due to the various system irreversibilities can be evaluated via a histogram map. Also, with the entropy generation known, the availability energy loss can be calculated using Eq.(5.47).

7.4 Entropy Generation and Availability Loss Results

The results of the post-processing analysis are shown and discussed below. Figures 19 and 20 below illustrate the results of the external and internal entropy generations for each of the sub-domains in the "2-space" and "3-space" models. Figs. 19(a,c) show the functional dependence of entropy generation on the number of cycles of piston motion and Figs. 19(b,d) show histograms of the entropy generation values characterizing the contributions of each sub-domain to the external entropy generation. Figures 20(a-d) illustrate corresponding results for the internal entropy generation.

Figs. 19(a,c) show the external entropy generation plots to be independent of the number of cycles of piston motion beyond the third cycle. The negative values for the

External Entropy Generation from "2-space" Sub-domains (CFD-ACE+)

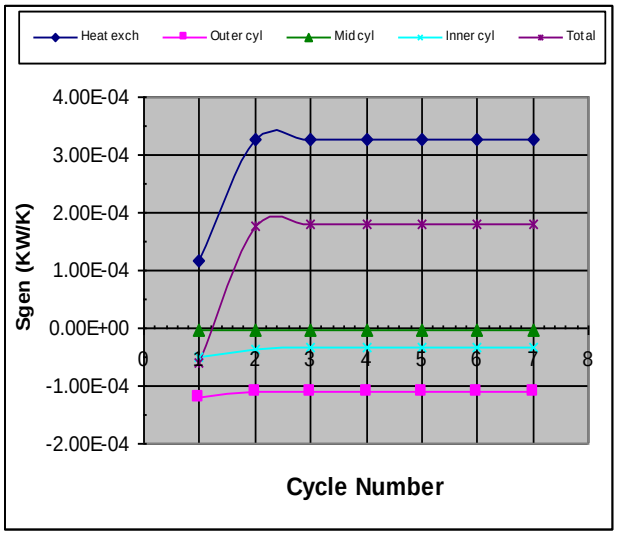

Figure 19(a). "2-space" External Entropy generation vs. Cycle No. (201.7 RPM, 1.008 MPa., T_{wall} = 294 K ; Grid size = 147 x 46, #tspc = 480).

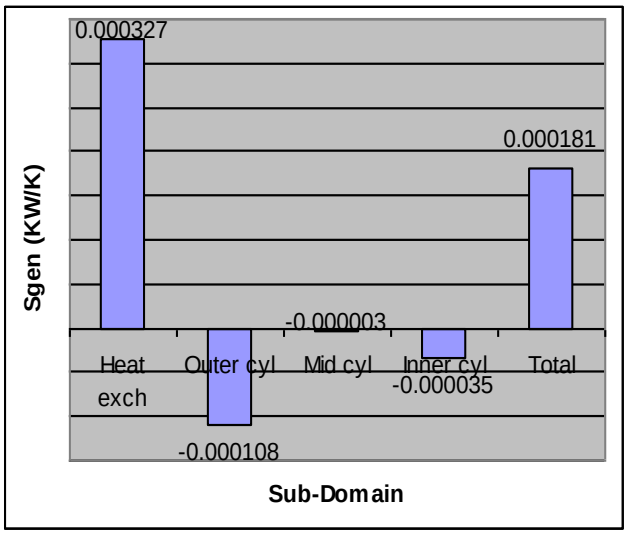

Figure 19(b). "2-space" External Entropy generation vs. Region (201.7 RPM, 1.008 MPa., T_{wall} = 294 K ; Grid size = 147 x 46, #tspc = 480).

External Entropy generation from "3-space" Sub-domains (Fluent)

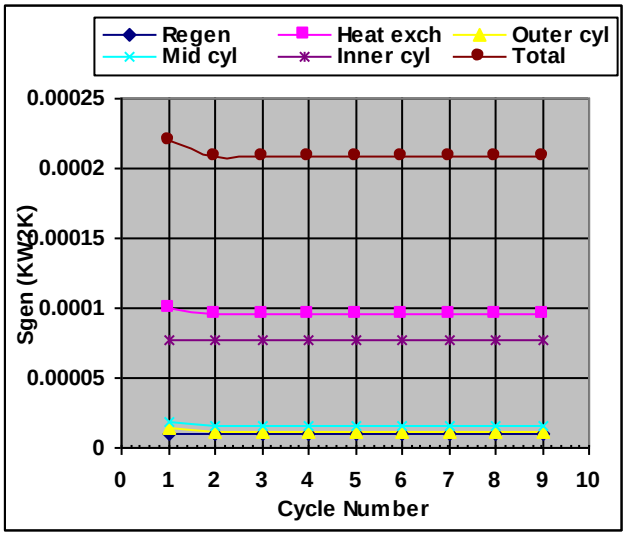

Figure 19(c). "3-space" External Entropy generation vs. Cycle No. (201.7 RPM, 1.008 MPa., T_{wall} = 294 K ; Grid size = 147 x 46, #tspc = 480).

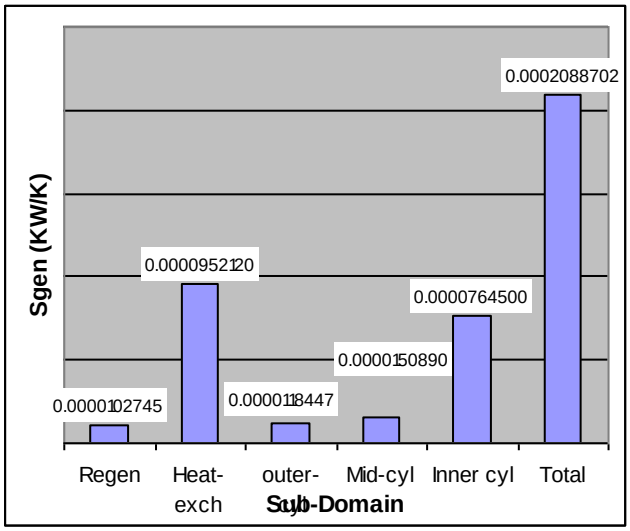

Figure 19(d). "3-space" External Entropy generation vs. Region (201.7 RPM, 1.008 MPa., T_{wall} = 294 K ; Grid size = 147 x 46, #tspc = 480).

external entropy generation in the cylinder sub-domains in the "2-space" model should be interpreted as the cylinder acting as "entropy sink". That is, these sub-domains appear to extract entropy from their surroundings (due to heat entering the cylinder in these sub-domains).

Internal Entropy Generation in "2-space" Sub-domains (CFD-ACE+)

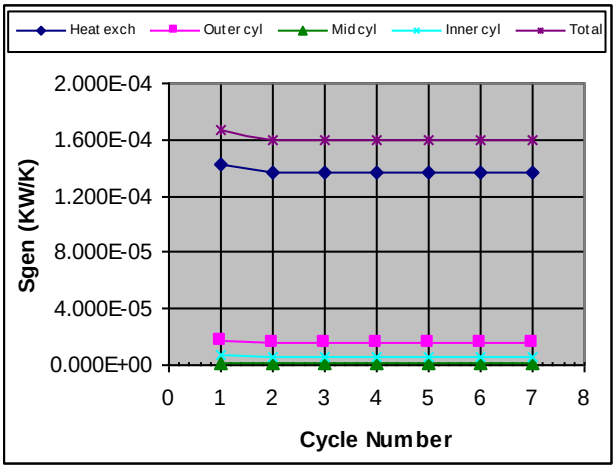

Figure 20(a). "2-space" Internal Entropy generation vs. Cycle No. (201.7 RPM, 1.008 MPa., T_{wall} = 294 K ; Grid size = 147 x 46, #tspc = 480).

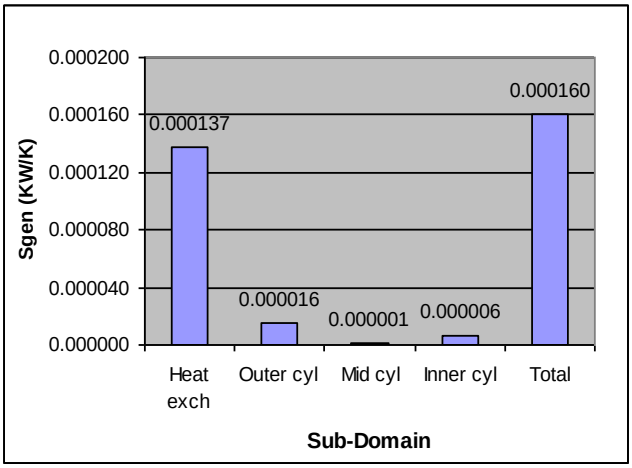

Figure 20(b). "2-space" Internal Entropy generation vs. Region (201.7 RPM, 1.008 MPa., T_{wall} = 294 K ; Grid size = 147 x 46, #tspc = 480).

External Entropy generation from "3-space" Sub-domains (Fluent)

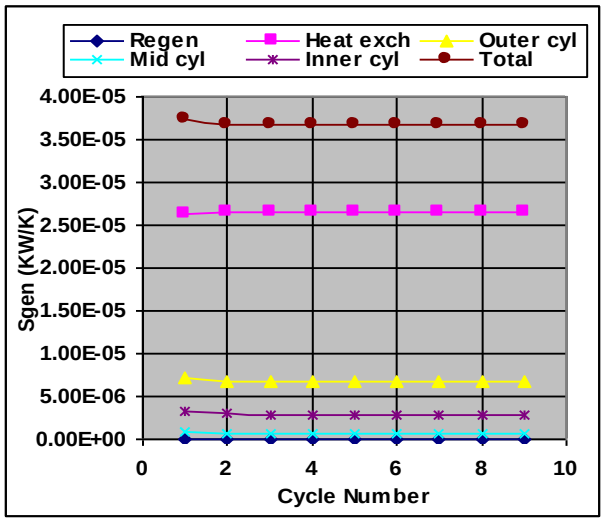

Figure 20(c). "3-space" Internal Entropy generation vs. Cycle No. (201.7 RPM, 1.008 MPa., T_{wall} = 294 K ; Grid size = 147 x 46, #tspc = 480).

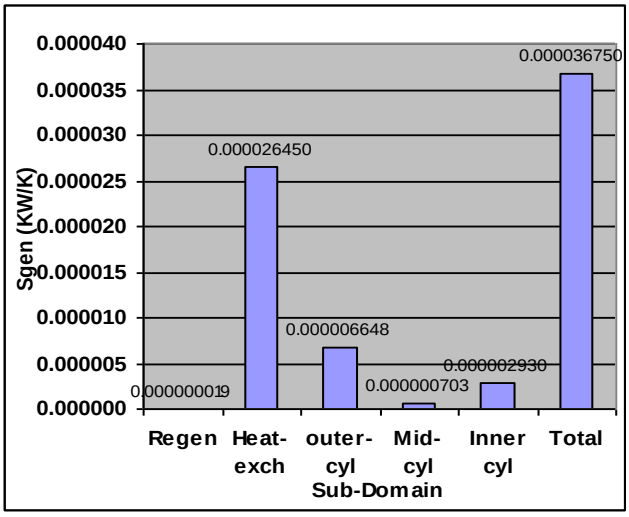

Figure 20(d). "3-space" Internal Entropy generation vs. Region (201.7 RPM, 1.008 MPa., T_{wall} = 294 K ; Grid size = 147 x 46, #tspc = 480).

Figs. 20(a,c) show the internal entropy generation plots to be independent of the number of cycles of piston motion one cycle earlier than does the external entropy generation plots. The heat exchanger is observed to contribute more to the total external entropy generation than it does to the total internal entropy generation. In the "2-space" model, the heat exchanger's contribution exceeds the total external entropy generation by

about 81% (see Fig. 19(b)) but falls short by about 54% in the “3-space” model. The heat exchanger’s contribution to the total internal entropy generation falls short by about 14% and 28% in the “2-space” (Fig. 20(b)) and “3-space” (Fig. 20(d)) models respectively. A clear inference from these plots is that the major sub-domain contribution to entropy generation is from the heat exchanger.

Of the three cylinder’s sub-domains, the outer cylinder’s contribution to the entropy generation is most significant in the “2-space” domain (external or internal) and “3-space” domain (internal). The inner cylinder’s contribution to the external entropy generation is most significant in the “3- space” domain. When taken as a whole, the cylinder’s and regenerator’s contributions to both external and internal entropy generations are minimal compared to the heat exchanger’s contribution.

Figure 17 shows the distribution of entropy generation inside the “2-space” and “3-space” models. The impact of the entropy generation due to conductive heat transfer, fluid friction and mass transfer on the efficiency of the models is quantified. Under the specified condition (201.7 RPM, 1.008 MPa., T_{wall} = 294), relatively higher losses are experienced in the heat exchanger. This is followed by losses in the outer cylinder and inner cylinder. Contributions from the mid-cylinder are very negligible. The heat exchanger’s conductive heat transfer has the most impact on the model efficiency followed by outer and inner cylinder conductive heat transfer. Contributions to the entropy generation due to viscous dissipation, mass transfer and conductive heat transfer are very negligible. The relatively high losses in the heat exchanger support the extensive effort in the Stirling community to reduce the pressure drop in the regenerator which is a form of heat exchanger. In compact-heat-exchanger passages for example, improvements

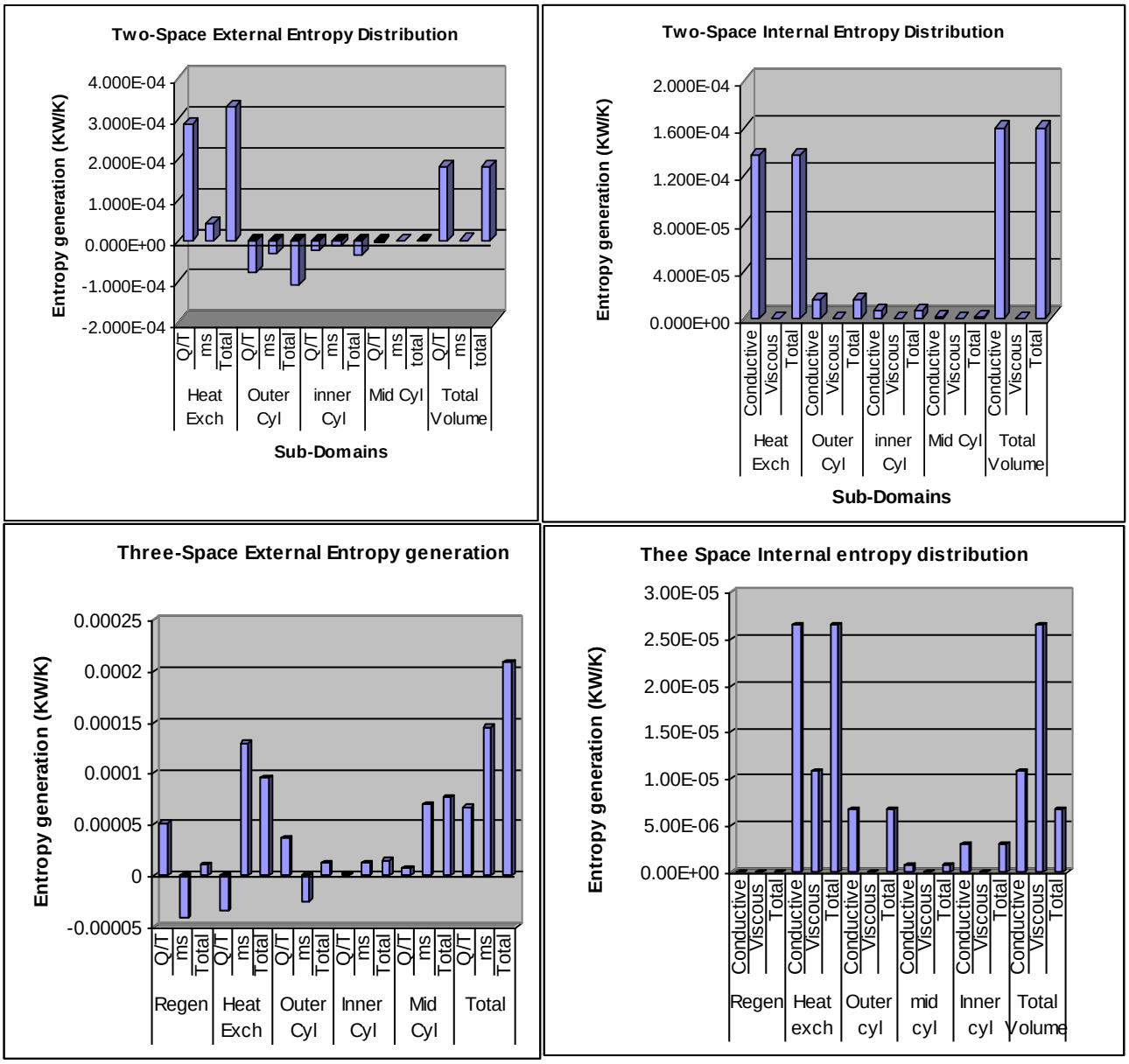

Figures 21. External and Internal Entropy Distribution in the "2-space" and "3-space" Models (201.7 RPM, 1.008 MPa., T_{wall} = 294 K ; Grid size = 147 x 51, #tspc = 480, at Opt. Cycle = 6).

can be made in the constructive details of the channels (channel shape and aspect ratio, curvature of the return channels, etc.), the actual temperature differences between the cold and hot fluids, the surface finishing, and the type of materials used.

Tables 9 and 10 illustrate entropy generation and availability loss results obtained for the "2-space" and "3-space" models respectively. For the "2-space" model, all CFD-ACE+

Table 9: Entropy Generation and Availability Loss Results (Sage vs. CFD-ACE+)

"2-space" (Cylinder + Heat Exchanger)				
Sub-Domain	Sage (T_{wall} = 294 K)		CFD-ACE+: V2004 (Alpha version) (201.7RPM, 1.008 MPa., T_{wall} =294K,) (Grid size = 147X51, #tspc = 480, Opt. Cycle = 6)	
	Internal	External	Internal	External
	Entropy Generation (KW/K)			
Heat Exchanger	0.0000706900	0.0000653500	0.00013700	0.000327000
Cylinder	0.00002245	0.00002198	0.000023000	-0.000146000
Total	0.0000931400	0.00008733	0.00016000	0.00018100
Available Energy Loss (KW)				
Heat Exchanger	0.02120649	0.01960549	0.0402950	0.096142
Cylinder	0.00673410	0.00659400	0.006793	-0.042866
Total	0.02794059	0.02619949	0.047088	0.053276
AEDiscr	0.00174110		0.0061880	
Sub-Domain	|%Difference| between Internal and External Entropy Generation (or AE Loss)			
Heat Exchanger	8.0		58.0	
Cylinder	2.0		116.0	
Total	7.0		12.0	
	|%Difference| between Sage and CFD-ACE+ Results			
	Internal		External	
	Entropy	AE Loss	Entropy	AE Loss
Heat Exch.	48.4	47.4	80.0	79.6
Cylinder	2.4	0.9	115.1	115.4
Total	41.8	40.7	51.8	50.8

results, with the exception of the external entropy generation and external availability energy loss results for the cylinder, are greater than corresponding Sage results. For the "3-space" model (Table 10 below), whereas the internal entropy generation and internal availability energy loss results reported by Fluent are less than corresponding results reported by Sage, the reverse is the case for external entropy generation and external

Table 10: Entropy Generation and Availability Loss Results (Sage vs. Fluent)

"3-space" (Cylinder + Heat Exch. + Regenerator)				
Sub-Domain	Sage (T_{wall} = 294 K)		Fluent (201.7RPM, 1.008 MPa., T_{wall} =294K,) (Grid size = 147X51, #tspc = 480, Opt. Cycle = 6)	
	Internal	External	Internal	External
	Entropy Generation (KW/K)			
Regenerator	0.0000067568	0.0000064611	0.0000000192	0.0000102745
Heat Exchanger	0.0000352724	0.0000313046	0.00002645	0.000095212
Cylinder	0.00002669	0.00002270	0.000010281	0.0001033873
Total	0.0000687192	0.00006046	0.00003675	0.00020887
Available Energy Loss (KW)				
Regenerator	0.002251	0.00215253	0.0000051835	0.00275
Heat Exchanger	0.01012557	0.00898657	0.0067493	0.02429
Cylinder	0.0076174	0.0064784	0.00262335	0.02638
Total	0.08855057	0.01759663	0.0093776	0.0533
AEDiscr	0.07095394		0.0439224	
Sub-Domain	|%Difference| between Internal and External Entropy Generation (or AE Loss)			
Regenerator	4.0		100.0	
Heat Exchanger	11.0		72.0	
Cylinder	15.0		90.0	
Total	8.0		82.0	
	|%Difference| between Sage and Fluent Results			
	Internal		External	
	Entropy	AE Loss	Entropy	AE Loss
Regenerator	99.7	99.7	37.1	21.7
Heat Exch.	25.0	33.3	67.1	63.0
Cylinder	61.5	65.5	78.0	75.4
Total	46.5	89.4	71.0	67.0

availability energy loss results. Calculation of the percentage differences between internal and external results of entropy and availability energy loss are based on the assumption that external results are more accurate since the calculation of the integral heat transfer

rates are more dependable. With Sage, it does not seem to matter what the basis for calculation of the percentage differences is. Calculation of the percentage differences between Sage and the multi-dimensional (multi-D) codes (CFD-ACE+ and Fluent) are based on the assumption that results generated by multi-D codes are more accurate since they are more suited to handle multi-D flow situations. Availability energy losses in the heat exchanger are greater than in the cylinder. The least losses are reported in the regenerator. The numerical errors reflected by the discrepancies between the internal and external entropy generation (or availability energy losses) indicate that Sage does a better job than the multi-D codes in satisfying the entropy generation accounting principle which require that the two methods of calculating for the entropy generation should give the same answer.

The internal calculations errors for entropy and AE loss calculations between Sage and the multi-D codes are noted in general to be smaller than the corresponding external calculations errors. The exceptions are the errors reported in the regenerator. The great disparities in the percentage differences between Sage and the multi-D codes results of entropy and AE loss may possibly be due to the inability of the Sage 1-D code to accurately account for temperature and velocity gradients caused by flow separations from walls where there are changes in flow area as for example, between the cylinder and the heat exchanger in the “2-space” and “3-space” models. Sage 1-D flow is assumed to immediately adjust to the wall boundaries through all geometrical changes in area and can only approximately account for the effect of flow separations, vortex formation, etc. where there are changes in flow area.

CHAPTER VIII

CONCLUSIONS AND RECOMMENDATIONS

An overview of the Stirling engine, a discussion of the computer models of the modified MIT "2-space" test rig leading to the "3-space" model which includes a regenerator, the effect of the regenerator on the Sage "2-space" to "3-space" modeling, theoretical development of the thermodynamic loss models, discussion of the numerical simulation results, post-processing of the numerical simulation results and entropy generation/availability energy loss results for the "2-space" and "3-space" models have been provided.

The following conclusions can be drawn from the results of this study which sought to evaluate the effect of adding a regenerator to the MIT "2-space" test rig and to characterize the irreversibilities related to heat transfer, mass flow and viscous friction occurring in the modified MIT test rig via entropy generation:

1) The incorporation of the work term weighting factor, based on calibration with an adiabatic-gas-spring model, significantly improved energy balances for Fluent modeling of non-adiabatic gas springs. As expected, the Sage code does a poorer job validating energy conservation than Fluent in the "3-space" model.

2) The predicted mean temperature in the cylinder was almost 5% lower than predicted by Sage, but in the heat exchanger was about 1.1% higher than predicted by Sage. The Fluent mean pressure prediction was about 1.5% higher than predicted by Sage in the cylinder and in the heat exchanger --meaning the initial pressure needed to be adjusted downward by about that percentage.

3) The temperature profiles recorded by Fluent in the cylinder space of the "3-space" model vary, depending on point location and whether the location is stationary or moving.

4) Fluent predicts flow vortices close to end of compression but Sage cannot because of its uniform flow assumption.

5) Fluent's pressure profiles in the cylinder space of the "3-space" model are insensitive to stationary or moving spatial coordinates and are almost symmetric with the Sage pressure profile over the crank angle range $0^o \leq \theta \leq 360^o$ with peak pressure values predictably occurring very close to the end of the compression cycle.

6) In going from the cylinder space to the heat exchanger space of the "3-space" model, Sage predicts a large pressure drop. Fluent predicts no pressure drop.

7) The pressure-volume diagrams for the "2-space" and "3-space" models look qualitatively similar.

8) Plots of Sage and CFD-ACE+/Fluent results for the heat transfer rate in the "2-space" model are qualitatively similar with minimal cylinder wall heat transfer rate contribution in the "3-space" model.

9) Beyond the initial cycle, external entropy generation is insensitive to the number of cycles of piston motion.

10) Sage and CFD-ACE+/Fluent predictions of availability loss and external entropy generation are in much better agreement for the "2-space" than for the "3-space" model.

11) The comparison of the Fluent calculations with experimental data and other numerical results from the literature showed good qualitative agreement between Fluent predictions and the experimental data, however there were some disagreements in magnitudes of the heat exchanger heat fluxes and temperature differences. Overall, the Fluent calculations show good promise.

12) The inclusion of the regenerator resulted in a reduction in the minimum and maximum pressure and work-input values in the cylinder with the exception of the increase in Sage maximum pressure.

13) Addition of the regenerator elevates the cylinder space temperatures at stationary points especially at points close to the midpoint of the cylinder clearance volume (x = 0.001374 m) and piston top center position (x = 0.002747 m).

14) The presence of the regenerator does appear to decrease the maximum temperature recorded in the heat exchanger of the "2-space" model by ~ 11 K, and increase the minimum temperature by ~ 2 K and to shift the maximum and minimum temperature values from near the end of the heat exchanger to near the heat exchanger entrance during a cycle.

15) The addition of the regenerator helps to improve the pressure profile correspondence with Sage result in both the heat exchanger and cylinder spaces and to reduce the 2-D peak pressure values in both the cylinder and heat exchanger domains.

16) With the addition of the regenerator, Fluent reports ~ 16% reduction in the cooling action in the cylinder but a considerable (~ 70%) reduction in the heat pumping action in the heat exchanger. A 19% reduction in the net cycle heat loss (or input work) is noted. Sage on the other hand reports ~ 23% increase in the cooling action in the cylinder and ~ 11% reduction in the heat pumping action in the heat exchanger. An 8% reduction in the net cycle heat loss (or input work) is noted.

17) The incorporation of the regenerator tended to reduce the error between the 1-D and 2-D code predictions.

18) The effect of the regenerator is clearly noticed at the entrance of the heat exchanger where the maximum values of the heat flux and temperature difference are elevated.

19) The heat exchanger provides the major sub-domain contribution to entropy generation. Thus the heat exchanger heat transfer has the most impact on the "3-space" model efficiency followed by outer and inner cylinder heat transfer. Viscous dissipation throughout the entire "3-space" domain and mid-cylinder mass transfer and conductive heat transfer contribute minimally to the model's efficiency.

20) In both the "2-space" and "3-space" models the two methods of accounting for the entropy generation (external and internal) appear insensitive to the number of cycles of piston motion beyond the third cycle.

21) The multi-D codes do not satisfy the accounting principle as well as Sage.

Typically neglected and often viewed as superfluous, the second law of thermodynamics remains an esoteric and mysterious subject [20] particularly in computational analysis of thermo-fluid systems. When properly applied, the second law of thermodynamics has proven to be a very powerful tool in the optimization of complex thermodynamic systems. Loss analysis using entropy-generation rates due to heat and fluid flow is a relatively new technique for assessing component performance. It offers a deep insight into the flow phenomena, allows a more exact calculation of losses than is possible with traditional means involving the application of loss correlations and provides an effective tool for improving performance. Designers will know the cumulative amount of all losses computed locally in the flow domain. Entropy generation maps can be produced, and designers can use them by scanning them to detect critical areas (locations in which entropy generation is higher than its integral average value over the entire flow field). By considering the local values of entropy generation rates due to thermal and viscous dissipation, designers can generate a thermodynamically better design by simply trying to avoid these critical areas or re-computing them after a design modification has been introduced to assess local and global effects of the design change. Our understanding of loss mechanisms is however far from complete. Although numerical predictions are valuable in predicting the heat transfer and flow structure, there are difficulties in predicting the loss accurately. This is due to errors in predicting the boundary layers, transition as well as due to false entropy generation due to numerical dissipation. This work provides a point of reference for incorporation of loss post-processors into Stirling engine numerical codes. The incorporation of a loss post-processor in Stirling engine numerical codes, it is believed, will facilitate the optimization of Stirling engine performance.

BIBLIOGRAPHY

1. Ahern, J. E., 1980, The Exergy Method of Energy Systems Analysis, Wiley, New York.

2. Amiri, A., and Vafai, K., "Transient Analysis of Incompressible Flow through a Packed Bed," Int. J. Heat Mass Transfer, Vol. 41, pp. 4259-4279, 1998.

3. Bejan, A. A study of entropy generation in fundamental convective heat transfer, ASME J. Heat Transfer 101 (1979) 718-725.

4. Bejan, A. 1997. Advanced Engineering Thermodynamics, Second Edition, John Wiley & Sons, Inc.

5 Bejan, A., Entropy Generation Minimization: The Method of Thermodynamic Optimization of Finite-Time Systems and Finite-Time Processes, CRC Press, Boca Raton, NY, 1996

6. Bejan A., 1982, Entropy Generation through Heat and Fluid Flow, Wiley, New York.

7. Bejan, A., "Second-law analysis in heat transfer and thermal design," Adv. Heat Transfer 15 (1982) 1-58.

8 Cengel, Y. A. and Boles, M. A., Thermodynamics, an Engineering Approach, 5th. ed., The McGraw-Hill Companies, Inc., 2006.

9 Chafe, J.N., "A Study of Gas Spring Heat Transfer in Reciprocating Cryogenic Machinery," Ph.D. Thesis, Dept. of Mech. Eng., Massachusetts Institute of Technology, Cambridge, MA, 1988.

10. Currie, T.C. and Carscallen, W.E. Simulation of trailing edge vortex shedding in a transonic turbine cascade. ASME Paper No. 96-GT-483, 1996.

11 Denton, J.D., 1993. Loss mechanisms in turbomachines. ASME Paper No.93-GT-435.

12. Drost, M. K., Zaworski, J.R., A review of second law analysis techniques applicable to basic thermal science research, ASME, AES 4 (1988) 7-12.

13. Ebiana, A.B., Savadekar, R.T, Vallury, A., "2nd Law Analysis of Sage and CFD-ACE+ Models of MIT Gas Spring and "Two-Space" Test Rigs", Proceedings of 2nd. International Energy Conversion Engineering Conference. Aug 16—Aug 19, 2004, Providence, Rhode Island.

14 Ebiana, A.B., Praveen Gidugu, "Theoretical Basis for 3-D Stirling Engine Loss Model", NASA Grant #NNC05AA24A Project Status Report, 2006.

15. Ebiana, A.B., Savadekar, R.T., Patel, K.V., A., "Entropy Generation/Availability Energy Loss Analysis inside MIT Gas Spring and 'Two-Space' Test Rigs," Proceedings of 3rd. International Energy Conversion Engineering Conference. Aug 15—Aug 18, 2005, San Francisco, California.

16. Faulkner, H.B., "An Investigation of Instantaneous Heat Transfer During Compression and Expansion in Reciprocating Gas Handling Equipment," Ph.D. Thesis, Dept. of Mech. Eng., Massachusetts Institute of Technology, Cambridge, MA, 1983.

17. Gedeon, D., 1999. Sage Pulse Tube Model-Class Reference Guide, Gedeon Associates.

18. Gedeon, D., Sage User's Guide, 3rd.ed., (Gedeon Associates, 16922 South Canaan Road, Athens, OH 45701), 1999.

19. R. Gordon Campbell, Foundations of Fluid Flow Theory, Addison-Wesley Publishing Company, Inc., Reading, Massachusetts, 1973.

20. H. Grad, "The Many Faces of Entropy". Communications on Pure and Applied Mathematics, vol. XIV, pp. 323-354, 1961.

21. H. Reader, G. T, and Hooper, C., 1983,"Stirling Engines", University Press, Cambridge.

22. Hamaguchi, K., Hiratsuka, Y. and Miyabe, H., "Effects of Regenerator Size Change on the Stirling Engine Performance", Proceedings of the 26th IECEC, (1991).

23. Harvey, J. P., "Oscillatory Compressible Flow and Heat Transfer in Porous Media – Application to Cryocooler Regenerators", Georgia Institute of Technology Ph.D., 2003.

24 Hofman, K.A., Chiang, S.T., Computational Fluid Dynamics for Engineers Volume II, Engineering Education System, 1993, pp. 15.

25. Kornhauser, Alan A. "Gas-Wall Heat Transfer During Compression and Expansion", Ph.D. Thesis, Dept. of Mech. Eng., Massachusetts Institute of Technology, Cambridge, MA, 1989.

26 Krane, R. J., ed., 1995, Thermodynamics and the Design, Analysis, and Improvement of Energy Systems 1995, AES-Vol. 35, ASME, New York.

27. Lee, K.P. and Smith, J.L. Jr., "Influence of Cyclic Wall-to-Gas Heat Transfer in Cylinder of the Valved Hot-Gas Engine", Proceedings of the 13th. Intersociety Energy Conversion Engineering Conference, Paper No 789195, 1978.

28. Michels, A.P.J., "The Philips Stirling Engine: A study of its efficiency as a function of operating temperatures and working fluids", Proceedings of the 11th IECEC, (1976).

29. Minkowcyz, W.J., Haji-Sheikh, A. and Vafai, K., "On Departure from Local Thermal Equilibrium in Porous Media due to a Rapidly Changing Heat Source: The Sparrow Number," Int. J. Heat Mass Transfer, Vol. 42, pp. 3373-3385, 1999.

30. Mralidhar, K. and Suzuki, K., "Analysis of Flow and Heat Transfer in a Regenerator Mesh using a Non-Darcy Thermally Non-Equilibrium Model," Int. J. Heat Mass Transfer, Vol. 44, pp. 2493-2504, 2001.

31. Narusawa, U., The second-law analysis of mixed convection in rectangular ducts, Heat Mass Transfer 37 (2001) 197-203.

32. Paoletti, S., Rispoli, F., Sciubba, E., Calculation of exergetic losses in compact heat exchanger passages, ASME AES 10 (1989) 21-29.

33. Quintard, M. and Whitaker, S. 1996. Transport in chemically and mechanically heterogeneous porous media. I: Theoretical development of region-averaged equations for slightly compressible flow. Advances in Water Resources, Vol. 19, No. 1, 29-47.

34 Recktendwald, G. W., "A Study of Heat Transfer between the Walls and Gas Inside the Cylinder of a Reciprocating Compressor," University of Minnesota Ph.D. Thesis, 1989.

35 Rupesh T. Savadekar, "2nd Law Analysis of Sage and CFD-ACE+ Models of MIT 'Two-Space' Test Rig", M.S. Thesis, Department of Mechanical Engineering, Cleveland State University, Cleveland, OH 44115.

36 Sahin, A. Z., Second law analysis of laminar viscous flow through a duct subjected to constant wall temperatures, J. Heat Transfer 120 (1980) 76-83.

37. Simon, T., "Contributions to Regenerator Modeling," Presentation for Regenerator Modeling Panel Discussion, 2nd International Energy Conversion Engineering Conference, Providence, RI, August 18, 2004.

38. Singh, C., Tathgir, R.G., and Muralidhar, K., "Comparison of 1-equation and 2-equation Models for Convective Heat Transfer in Saturated Porous Media, "The Institution of Engineers (India) Journal, Vol. 84, MC 3, pp. 104-113, October 2003.

39. Tannehill, J.C., Anderson, D.A. and Pletcher, R.H., Computational Fluid Mechanics and Heat Transfer, Taylor & Francis, 2nd. ed., Hemisphere Publishing Corporation, 1984.

40 Tew, R.C. Jr., "Two-Dimensional Compressible Non-Acoustic Modeling of Stirling Machine Type Components", Doctor of Engineering Thesis, Dept. of Mech. Eng., Cleveland State University, Cleveland, OH, 2000.

41. Tew, R.C. Jr., "Overview of Stirling Regenerators (Porous Media) CFD Modeling Problems," Presentation for Workshop on Convective Heat Transfer in Porous Media, Hosted by NASA Glenn Research Center, North Olmsted, OH, April 28-29, 2004.

42 Tew, R.C., et al, "Overview 2004 of NASA-Stirling Convertor CFD Model Development and Regenerator R&D Efforts", in proceedings of Space Technology and Applications International Forum (STAIF 2005), Albuquerque, NM February 2005.

43. Tew, R., Simon, T., Gedeon, D., Ibrahim, M. and Rong, W. "An Initial Non-Equilibrium Porous-Media Model for CFD Simulation of Stirling Regenerators", Prepared for 4th. International Energy Conversion Engineering Conference, San

Diego, CA, June 26-29, 2006.

44. Thieme, L.G. and Schreiber, J.G., NASA GRC Stirling Technology Overview, " Proceedings of the Space Technology Applications international Forum (STAIF-2003), Albuquerque, NM, edited by M.S. El-Genk, American Institute of Physics, Melville, NY, 2003, AIP CP-654, pp. 613-620, also as NASA/TM--2003-212454, 2003.

45 Thompson, K .W., Lecture Series in Computational Fluid Dynamics, NASA TM 100010, August 1987.

46 Whitaker, S. 1996. The Forchheimer equation: a theoretical development. *Transport in Porous Media*, Vol. 25, Kluwer Academic Publishers, Netherlands, 27-61.

47. Whitaker, S. 1999, *The method of volume averaging*, Kulwer Academic Publishers, Netherlands.

Appendix

/*Program for describing the piston motion*/

```
#include"udf.h"
DEFINE_CG_MOTION(piston, dt, vel, omega, time, dtime)
{
real AMPLITUDE=0.0381;
real pi=3.1415926535879;
vel[1]=0;
omega[0]=0;
omega[1]=0;
vel[0]= (AMPLITUDE*(2*pi/0.29712)*cos((2*pi/0.29712)*time+(1.5*pi)));
}
```

/*Program for matching the dual cell grids and also for inputting heat transfer between solid and fluid phases in the regenerator*/

```
# include "udf.h"

/*************** Dual cell approach explanation starts
*****************************************
```

The user needs to provide the dual cell mesh. Dual cell mesh does not have to be on top of each other. A distance is allowed but not rotation. The code will figure out the distance automatically and the user only needs to push a button to match them. Another button is provided for the user to check the matching. The user needs to provide dual cell zone ID in pair. After that, two macroes are created for easy access to dual cell information.

For the matching information, it will be saved automatically to the data file. So, when you read in the case/data the matching information will be read in as well.

Note that you will need a fluent6.1 to run this.

Note that when you read the case and data back in. You do NOT need to match the dual cell again because the matching information is saved automatically to the data file. Unpon reading the case/data in, the matching information will be there agaion. But you might want to check the matching just to make sure everything is all right.

Input explanation:

static int dual_cell_zone_ID[][2]={{12, 14}, {13, 4}, {-1, -1}}; Provide dual cell cell zone ID in pair. In this example, 12 and 14 are dual cell zone; 13 and 4 are dual cell zone. The final pair is a flag and please keep it.

DUAL_CELL(c,t) Macro allow you to find dual cell for a given cell and thread
DUAL_CELL_THREAD(t) Macro allow you to find dual cell zone thread for a given cell and thread

Limitation:

The program works for both 2d and 3d. But it has not been tested for 2d axisymmetric geometry though.

```
/************************************ Dual cell approach explanation ends ************************************/


#defineDUAL_CELL(c,t)
matching_info_of_cell_zone[ID_to_matching_index_ji_j(THREAD_ID(t))][ID_to_matching_index_ji_i(THREAD_ID(t))].dual_cell[c]
#defineDUAL_CELL_THREAD(t)
matching_info_of_cell_zone[ID_to_matching_index_ji_j(THREAD_ID(t))][ID_to_matching_index_ji_i(THREAD_ID(t))].dual_thread

/********************************** dual cell user input starts ***********************************/


/* Dual cell cell zone ID */
static int dual_cell_zone_ID[][2]={{65534, 2},{-1, -1}};

/********************************** dual cell user input ends ***********************************/

struct matching
{
 int cell_zone_ID;
 int dual_cell_zone_ID;
 Thread * thread;
 Thread * dual_thread;
 cell_t * dual_cell;
 int no_of_cells;
 real displacement[ND_ND];

} (* matching_info_of_cell_zone)[2];

static int check_maching_info(void)
{
 int i, j, no_of_pairs;
 Domain *domain;
```

```
 domain=Get_Domain(1);

 i=0;
 while(dual_cell_zone_ID[i][0]>0)
   {
    i++;
   }
 no_of_pairs=i;

 for(j=0; j<no_of_pairs; j++)
   {
    for(i=0; i<2; i++)
      {
       if(matching_info_of_cell_zone[j]+i==NULL)
         {
          Message0("\n\nNo data in the matching info struct yet!\n\n");
          return 0;
         }

       if(matching_info_of_cell_zone[j][i].thread!=Lookup_Thread(domain,
dual_cell_zone_ID[j][i]))
          {
           Message0("\n\nNo matching yet--You will need to match it before checking\n\n");
           return 0;
          }
      }
   }
 return 1;
}

static int ID_to_matching_index_ji_j(int ID)
{
 int i, j, no_of_pairs;

 i=0;
 while(dual_cell_zone_ID[i][0]>0)
   {
    i++;
   }
 no_of_pairs=i;

 for(j=0; j<no_of_pairs; j++)
   {
    for(i=0; i<2; i++)
      {
       if (matching_info_of_cell_zone[j][i].cell_zone_ID==ID)
         {
```

```
        return j;
          }
      }
    }
  Message0("\nNo dual cell for the given ID  - aborting!!\n");
  exit(0);
}

static int ID_to_matching_index_ji_i(int ID)
{
  int i, j, no_of_pairs;

  i=0;
  while(dual_cell_zone_ID[i][0]>0)
    {
     i++;
    }
  no_of_pairs=i;

  for(j=0; j<no_of_pairs; j++)
    {
     for(i=0; i<2; i++)
       {
        if (matching_info_of_cell_zone[j][i].cell_zone_ID==ID)
          {
           return i;
          }
       }
    }
  Message0("\nWrong ID - aborting!!\n");
  exit(0);
}

static cell_t f_find_dual_cell(struct matching * cell_zone_matching, cell_t cell, real *
displacement)
{
  Thread * thread;
  Thread * dual_thread;
  cell_t mirror_cell, c;
  real distance, min_distance, dis_vec[ND_ND], x1[ND_ND], x2[ND_ND];

  min_distance=1e20;

  thread=cell_zone_matching->thread;
  dual_thread=cell_zone_matching->dual_thread;

  begin_c_loop(c, dual_thread)
```

```
 {
  C_CENTROID(x1, c, dual_thread);
  C_CENTROID(x2, cell, thread);
  NV_V(x1, -=, displacement);

  NV_VV(dis_vec, =, x1, -, x2);

  distance=NV_MAG(dis_vec);

  if(distance<min_distance)
    {
     mirror_cell=c;
     min_distance=distance;
    }
 }
end_c_loop(c, dual_thread)

return mirror_cell;
}


static void find_CG(int cell_zone_ID, real * CG)
{
 cell_t c;
 Thread * thread;
 real vx[ND_ND], x[ND_ND], volume, t_volume;
 Domain *domain;

 domain=Get_Domain(1);

 thread=Lookup_Thread(domain, cell_zone_ID);

 NV_S(vx,=,0);
 t_volume=0;
 begin_c_loop(c, thread)
   {
    C_CENTROID(x, c, thread);
    volume=C_VOLUME(c, thread);

    t_volume+=volume;

    vx[0]+=volume*x[0];
    vx[1]+=volume*x[1];

    #if RP_3D
    vx[2]+=volume*x[2];
    #endif
```

```
  }
 end_c_loop(c, thread)

 NV_VS(CG, =, vx, /, t_volume);
}

static void find_displacement(real * displacement, int cell_zone_ID, int
dual_cell_zone_ID)
{
 real CG_cell_zone[ND_ND], CG_dual_cell_zone[ND_ND];

 find_CG(cell_zone_ID, CG_cell_zone);
 find_CG(dual_cell_zone_ID, CG_dual_cell_zone);

 NV_VV(displacement, =, CG_dual_cell_zone, -, CG_cell_zone);
}


static void initialization(void)
{
 int i, j, no_of_pairs;
 Domain *domain;

 domain=Get_Domain(1);

 /* Allocate memory for  matching_info_of_cell_zone */

 i=0;
 while(dual_cell_zone_ID[i][0]>0)
   {
    i++;
   }
 no_of_pairs=i;

 if((matching_info_of_cell_zone=(struct matching (*)[2])calloc(no_of_pairs,
2*sizeof(struct matching)))==NULL)
   {
    Message0("\nInsufficient memory--aborting\n");
    exit(0);
   }

 /* Initialize  matching_info_of_cell_zone */

 for(j=0; j<no_of_pairs; j++)
   {
    for(i=0; i<2; i++)
      {
```

```
      matching_info_of_cell_zone[j][i].cell_zone_ID     =dual_cell_zone_ID[j][i];

matching_info_of_cell_zone[j][i].dual_cell_zone_ID=dual_cell_zone_ID[j][i==0?1:0];
      matching_info_of_cell_zone[j][i].thread                    =Lookup_Thread(domain,
dual_cell_zone_ID[j][i]);
      matching_info_of_cell_zone[j][i].dual_thread               =Lookup_Thread(domain,
dual_cell_zone_ID[j][i==0?1:0]);
      matching_info_of_cell_zone[j][i].no_of_cells
=THREAD_N_ELEMENTS(matching_info_of_cell_zone[j][i].dual_thread);
      find_displacement(matching_info_of_cell_zone[j][i].displacement,
matching_info_of_cell_zone[j][i].cell_zone_ID,

matching_info_of_cell_zone[j][i].dual_cell_zone_ID);


      if((matching_info_of_cell_zone[j][i].dual_cell=(cell_t *)
          calloc(matching_info_of_cell_zone[j][i].no_of_cells,sizeof(cell_t)))==NULL)
        {
         Message0("\nInsufficient memory--aborting\n");
         exit(0);
        }
      }
   }
}

/* This function will match dual cell
Note that you will have to initialize the fluid flow in order to use the function */

DEFINE_ON_DEMAND(matching_dual_cell)
{
 cell_t c;
 int i, j, no_of_pairs;

 if (!Data_Valid_P ())
   {
      Message0("\n\nNo cell centroid data--please initialize the fluid flow and try
again!!!\n\n");
      return;
   }

 initialization();

 /* Matching.  From the given cell and cell zone matching info, a mirror cell will be
found and the
 index saved into dual_cell */

 i=0;
```

```
 while(dual_cell_zone_ID[i][0]>0)
  {
   i++;
  }
 no_of_pairs=i;

 for(j=0; j<no_of_pairs; j++)
  {
   for(i=0; i<2; i++)
     {
      begin_c_loop(c, matching_info_of_cell_zone[j][i].thread)
        {

matching_info_of_cell_zone[j][i].dual_cell[c]=f_find_dual_cell(matching_info_of_cell_z
one[j]+i,c,matching_info_of_cell_zone[j][i].displacement);
        }
      end_c_loop(c, matching_info_of_cell_zone[j][i].thread)
     }
  }

 /* Print out dual cell info */
/*
 for(j=0; j<no_of_pairs; j++)
  {
   for(i=0; i<2; i++)
     {
      Message0("\nCell                zone                ID:                %5d\n",
matching_info_of_cell_zone[j][i].dual_cell_zone_ID);
      begin_c_loop(c, matching_info_of_cell_zone[j][i].thread)
        {
         Message0("%5d %5d\n", c, matching_info_of_cell_zone[j][i].dual_cell[c]);
        }
      end_c_loop(c, matching_info_of_cell_zone[j][i].thread)

      Message0("\n");
     }
  }*/

 Message0("\nMatching is complete. You may want to check the matching as well.\n");
}

DEFINE_ON_DEMAND(print_matching)
{
 cell_t c;
 int i,j, no_of_pairs;

 if(!check_maching_info())
```

```
  {
   Message0("\nCheck failed!!!  You need to match the dual cell first.\n\n");
   return;
  }

 i=0;
 while(dual_cell_zone_ID[i][0]>0)
  {
   i++;
  }
 no_of_pairs=i;

 for(j=0; j<no_of_pairs; j++)
  {
   for(i=0; i<2; i++)
    {
     Message0("ID:%5d dual cell zone ID:%5d\n",
matching_info_of_cell_zone[j][i].cell_zone_ID,
matching_info_of_cell_zone[j][i].dual_cell_zone_ID);

     Message0("  cell    dual cell\n");
     begin_c_loop(c, matching_info_of_cell_zone[j][i].thread)
      {
       Message0("%5d %5d\n", c, matching_info_of_cell_zone[j][i].dual_cell[c]);
      }
     end_c_loop(c, matching_info_of_cell_zone[j][i].thread)

     Message0("number of cells: %5d\n", matching_info_of_cell_zone[j][i].no_of_cells);

     #if RP_3D
     Message0("displacement:(%f %f %f)\n",
matching_info_of_cell_zone[j][i].displacement[0],
                matching_info_of_cell_zone[j][i].displacement[1],
                matching_info_of_cell_zone[j][i].displacement[2]);
     #endif

     #if RP_2D
     Message0("displacement:(%f %f)\n",
matching_info_of_cell_zone[j][i].displacement[0],
                matching_info_of_cell_zone[j][i].displacement[1]);
     #endif

     Message0("\n");
    }
  }
}
```

```
DEFINE_ON_DEMAND(check_dual_cell_matching)
{
 real distance, max_distance, dis_vec[ND_ND], x1[ND_ND], x2[ND_ND];
 cell_t c;
 Domain *domain;
 int i,j, no_of_pairs;
 int same_index;

 domain=Get_Domain(1);

 if(!check_maching_info())
   {
    Message0("\nCheck failed!!!  You need to match the dual cell first.\n\n");
    return;
   }

 if (!Data_Valid_P ())
   {
      Message0("\n\nNo cell centroid data--please initialize the fluid flow and try
again!!!\n\n");
      return;
   }

 i=0;
 while(dual_cell_zone_ID[i][0]>0)
   {
    i++;
   }
 no_of_pairs=i;

 /* Checking one to one correspondance */

 for(j=0; j<no_of_pairs; j++)
   {
    for(i=0; i<2; i++)
      {
       begin_c_loop(c, matching_info_of_cell_zone[j][i].thread)
        {

if(matching_info_of_cell_zone[j][i==0?1:0].dual_cell[matching_info_of_cell_zone[j][i].
dual_cell[c]]!=c)
          {
           Message0("\n\nChecking failed to find one to one correspondance!!\n\n");
           return;
          }
        }
```

```
      end_c_loop(c, matching_info_of_cell_zone[j][i].thread)
     }
   }

/*  Checking the cell index */

same_index=0;
for(j=0; j<no_of_pairs; j++)
  {
   for(i=0; i<2; i++)
     {
      begin_c_loop(c, matching_info_of_cell_zone[j][i].thread)
       {
        if(matching_info_of_cell_zone[j][i].dual_cell[c]!=c)
          {
              same_index=1;
              break;
          }
       }
      end_c_loop(c, matching_info_of_cell_zone[j][i].thread)
     }
  }

/* Check max dual cell distance */

max_distance=0;
for(j=0; j<no_of_pairs; j++)
  {
   for(i=0; i<2; i++)
     {
      begin_c_loop(c, matching_info_of_cell_zone[j][i].thread)
      {
        C_CENTROID(x1, c, matching_info_of_cell_zone[j][i].thread);
        C_CENTROID(x2,                    matching_info_of_cell_zone[j][i].dual_cell[c]
,matching_info_of_cell_zone[j][i].dual_thread);
        NV_VV(dis_vec, =, x1, -, x2);

        distance=NV_MAG(dis_vec);

        if(fabs(distance-
NV_MAG(matching_info_of_cell_zone[j][i].displacement))>max_distance)
          {
           max_distance=fabs(distance-
NV_MAG(matching_info_of_cell_zone[j][i].displacement));
          }
       }
      end_c_loop(c, matching_info_of_cell_zone[j][i].thread)
```

```
    }
  }

 if(same_index==1)
  {
   Message0("\nChecking is successful BUT failed to find the same index for dual cells\n");
  }
 else
  {
   Message0("\nChecking is successful AND finds the same index for dual cells\n");
  }
 Message0("The max distance between dual cell after displacement considered is:%12.4e\n", max_distance);
}

DEFINE_RW_FILE(writer, fp)
{
 int i, j, no_of_pairs;
 cell_t c;

 Message0("\nWriting matching data to data file...\n");

 if(!check_maching_info())
  {
   Message0("\nWriting matching data to data file failed!! You need to match the dual cell first.\n");
   return;
  }

 i=0;
 while(dual_cell_zone_ID[i][0]>0)
  {
   i++;
  }
 no_of_pairs=i;

 for(j=0; j<no_of_pairs; j++)
  {
   for(i=0; i<2; i++)
    {
     fprintf(fp, "%5d %5d\n", matching_info_of_cell_zone[j][i].cell_zone_ID, matching_info_of_cell_zone[j][i].dual_cell_zone_ID);

     begin_c_loop(c, matching_info_of_cell_zone[j][i].thread)
      {
       fprintf(fp, "%5d %5d\n", c, matching_info_of_cell_zone[j][i].dual_cell[c]);
```

```
        }
      end_c_loop(c, matching_info_of_cell_zone[j][i].thread)

      fprintf(fp, "%5d\n", matching_info_of_cell_zone[j][i].no_of_cells);

      #if RP_3D
      fprintf(fp, "%f %f %f \n", matching_info_of_cell_zone[j][i].displacement[0],
                          matching_info_of_cell_zone[j][i].displacement[1],
                          matching_info_of_cell_zone[j][i].displacement[2]);
      #endif

      #if RP_2D
      fprintf(fp, "%f %f \n", matching_info_of_cell_zone[j][i].displacement[0],
                        matching_info_of_cell_zone[j][i].displacement[1]);
      #endif

      fprintf(fp, "\n");
     }
   }
}

DEFINE_RW_FILE(reader, fp)
{
 int i, j, no_of_pairs;
 cell_t c;
 int dummy;
 Domain * domain;

 domain=Get_Domain(1);

 Message0("\nReading matching data from data file...");

 initialization();

 i=0;
 while(dual_cell_zone_ID[i][0]>0)
   {
    i++;
   }
 no_of_pairs=i;

 for(j=0; j<no_of_pairs; j++)
   {
    for(i=0; i<2; i++)
      {
       fscanf(fp, "%d %d\n", &(matching_info_of_cell_zone[j][i].cell_zone_ID),
                         &(matching_info_of_cell_zone[j][i].dual_cell_zone_ID));
```

```
      matching_info_of_cell_zone[j][i].thread                    =Lookup_Thread(domain,
matching_info_of_cell_zone[j][i].cell_zone_ID);
      matching_info_of_cell_zone[j][i].dual_thread=Lookup_Thread(domain,
matching_info_of_cell_zone[j][i].dual_cell_zone_ID);

      begin_c_loop(c, matching_info_of_cell_zone[j][i].thread)
        {
         fscanf(fp, "%d %d\n", &dummy, matching_info_of_cell_zone[j][i].dual_cell+c);
        }
      end_c_loop(c, matching_info_of_cell_zone[j][i].thread)

      fscanf(fp, "%d\n", &(matching_info_of_cell_zone[j][i].no_of_cells));

      #if RP_3D
      fscanf(fp, "%f %f %f \n", matching_info_of_cell_zone[j][i].displacement+0,
                          matching_info_of_cell_zone[j][i].displacement+1,
                          matching_info_of_cell_zone[j][i].displacement+2);
      #endif

      #if RP_2D
      fscanf(fp, "%f %f \n", matching_info_of_cell_zone[j][i].displacement+0,
                         matching_info_of_cell_zone[j][i].displacement+1);
      #endif
     }
   }

 Message0("\n\nMatching info is read from the data file. You may want to check the
matching as well.\n");
}

/*************************************************************************
**********************************

  User needs to supply heat transfer coefficient and unit area per unit volume.

  For porous meda, a few things that the user needs to pay attention that I can think of

  1) you need to modify the density as the solid in the model does not have porosity built
in.
  2) For the same reason, when considering velocity for heat transfer coefficient
calcuation,
     caution must be exercised.

*************************************************************************
**********************************/
```

```
/*Energy equation input for fluid region in the porous zone (i.e. alpha region)*/
DEFINE_SOURCE(energy_source_fluid, c, t, dS, eqn)
{
real volume;
real volume_integral=6.7212804E-05;
real temperature_fluid;
real temperature_fluid_integral=0;
real temperature_fluid_volume_average;
real h=10;
real temperature_solid;
real temperature_solid_integral=0;
real temperature_solid_volume_average;
real porosity=0.9;
real field_factor=0.1;
real source3;
real source;
real density_fluid;
real enthalpy_fluid;
real pressure_fluid;
real internal_energy;
real internal_energy_integral=0;
real internal_energy_derivative_volume_average;
real density_volume_average;
real density_integral=0;
real density_fluid_prev_timestep;
real density_derivative_integral=0;
real density_derivative_volume_average;
real internal_energy_derivative_integral=0;
real internal_energy_volume_average;
real source1;
real enthalpy_fluid_integral=0;
real velocity_fluid_x_gradient;
real velocity_fluid_y_gradient;
real velocity_gradient_integral=0;
real Nk=7.12;
real K=0.152;
real gradient_temperature_integral=0;
real gradient_temperature_volume_average;
real source2;
real velocity_derivative_volume_average;
real enthalpy_fluid_volume_average;
real gradient_temeprature_volume_average;

/*begin_c_loop(c,t)
```

```
{*/
   volume=C_VOLUME(c,t);
        /*volume_integral+=volume;
}
end_c_loop (c,t)*/

/* calculation of volume averaging of density 1st term*/
  density_fluid=C_R(c,t);
  density_integral+=(density_fluid*volume);
  density_volume_average=(density_integral/(porosity*volume_integral));
/* Calculation of volume average of internal engergy*/
  enthalpy_fluid=C_H(c,t);
 /*Message0("enthalpy of the fluid is %g\n", enthalpy_fluid);*/
  pressure_fluid=C_P(c,t);
  internal_energy=(enthalpy_fluid-(pressure_fluid/density_fluid));
  internal_energy_integral+=(internal_energy*volume);
 /*Message0("internal energy of the fluid is %g\n", internal_energy);*/

internal_energy_volume_average=(internal_energy_integral/(porosity*volume_integral));
  C_UDSI(c,t,0)=(internal_energy_volume_average*density_volume_average);
  /* Time derivative of UDSI first term*/
  C_UDMI(c,t,0)=((C_UDSI(c,t,0)-C_UDSI_M1(c,t,0))/0.000619);
  source1=C_UDMI(c,t,0);
 /* Calculation of volume average of enthalpy*/
  enthalpy_fluid_integral+=(enthalpy_fluid*volume);
  enthalpy_fluid_volume_average=(enthalpy_fluid_integral/(porosity*volume_integral));
 /* volume average of velocity*/
  velocity_fluid_x_gradient=C_U_G(c,t)[0];
  velocity_fluid_y_gradient=C_U_G(c,t)[1];

velocity_gradient_integral+=((velocity_fluid_x_gradient+velocity_fluid_y_gradient)*vol
ume);

velocity_derivative_volume_average=(velocity_gradient_integral/(porosity*volume_inte
gral));
  /* calculation of volume averaging of temperature of fluid*/
  temperature_fluid=C_T(c,t);
  /*Message("temperature of the fluid1 at each cell = %g\n", temperature_fluid);*/
  temperature_fluid_integral+=(temperature_fluid*volume);
  /*Message0("temperature of the fluid is %g\n", temperature_fluid_integral);*/

temperature_fluid_volume_average=(temperature_fluid_integral/(porosity*C_UDMI(c,t,
6)));
  /*Message("temperature of the fluid1 = %g\n", temperature_fluid_volume_average);*/
  C_UDSI(c,t,1)=C_T_G(c,t)[0];
  C_UDSI(c,t,2)=C_T_G(c,t)[1];
  C_UDMI(c,t,1)=C_UDSI_G(c,t,1)[0];
```

```
  C_UDMI(c,t,2)=C_UDSI_G(c,t,2)[1];
  gradient_temperature_integral+=((C_UDMI(c,t,1)+C_UDMI(c,t,2))*volume);

gradient_temeprature_volume_average=(gradient_temperature_integral/(porosity*volum
e_integral));

source2=((density_volume_average*velocity_derivative_volume_average*enthalpy_fluid
_volume_average)-(Nk*K*gradient_temeprature_volume_average));
  /* calculation of volume averaging of temperature of solid*/
  temperature_solid=C_T(DUAL_CELL(c,t),DUAL_CELL_THREAD(t));
  /*Message("temperature of the solid1 at each cell = %g\n", temperature_solid);*/
  temperature_solid_integral+=(temperature_solid*volume);
  /*Message0("temperature of the solid is %g\n", temperature_solid_integral);*/

temperature_solid_volume_average=(temperature_solid_integral/(field_factor*volume_i
ntegral));
  /*Message("temperature of the solid1 = %g\n", temperature_solid_volume_average);*/
  source3=(h*(temperature_solid_volume_average-temperature_fluid_volume_average));
     source=(source1+source2);
Message("energy input to fluid zone= %g\n", source);

 return source;
}
```